ADDIS ABABA UNIVERSITY

ADDIS ABABA INSTITUTE OF TECHNOLOGY

SCHOOL OF CIVIL AND ENVIRONMENTAL ENGINEERING

Numerical Investigation of the Effect of Aerodynamic and Seismic Load Interaction on the Stability of Land-Based Wind Turbine Towers

A Thesis in Structural Engineering

By Gossaye Mathewos

GSR/0272/13

June 13, 2023 G.C

Addis Ababa, Ethiopia

Advisor: Dr. Bedilu Habte

A Thesis Submitted in Partial Fulfillment of the Requirements for the Degree of Master of Science in Civil Engineering

The undersigned have examined the thesis entitled '**Numerical Investigation of the Effect of Aerodynamic and Seismic Load Interaction on the Stability of Land-Based Wind Turbine Towers**' presented by **Gossaye Mathewos**, a candidate for the degree of Master of Science and hereby certify that it is worthy of acceptance.

Dr. Bedilu Habte	_____	_____
Advisor	Signature	Date
Dr. Abrham Gebre	_____	_____
Internal Examiner	Signature	Date
Dr. Esayas G/Yohannes	_____	_____
External Examiner	Signature	Date
Dr. Abrham Gebre	_____	_____
Chairperson	Signature	Date

UNDERTAKING/DECLARATION

I certify that research work titled “Numerical Investigation of the Effect of Aerodynamic and Seismic Load Interaction on the Stability of Land-Based Wind Turbine Towers” is my own work. The work has not been presented elsewhere for assessment. Where material has been used from other sources it has been properly acknowledged / referred.

_____

Gossaye Mathewos

ABSTRACT

Wind energy is one form of renewable energy and the utilization of wind energy is rapidly growing worldwide due to its abundance. Wind turbines are a feasible, cost-effective, and durable source of wind energy, and ensuring their safety is essential for proper service life operation to protect the investment. The installation of wind turbines in seismic regions is growing to meet renewable energy demand around the world, and analyzing the stability of wind turbines in these regions is critical. This research analyzes the effect of aerodynamic and seismic load interaction on the stability of land-based horizontal axis wind turbine towers built in seismic areas. The methodology implemented to conduct this study is a decoupling approach to analyze the effect of wind loads and seismic loads independently and combine results obtained from ANSYS Workbench 2022. A reliable finite element model is established by validating modal analysis results with experimental values. Then, global responses such as top tower displacement and second order (P-Δ) effect, and local responses such as maximum Von Mises stress and eigenvalue buckling analysis of wind turbine towers were conducted. Earthquake loads are found to be dominant loads compared to wind loads for all wind turbines and earthquake-induced emergency shutdown condition is found to be the most critical operation condition for all wind turbines. In addition, the second-order (P-Δ) effect from analysis of wind turbine towers shows that 1.5MW and 5MW wind turbine towers are significantly affected, but P-Δ is negligible for 65kW wind turbine. Moreover, a 1.5MW wind turbine has higher top tower displacement and maximum Von Mises stress compared to a 5MW wind turbine which is due to the effect of the shell property of the tower and the weight of wind turbines. Furthermore, the characteristics of the acceleration vs time records are also found to have a significant effect on the response behavior of the turbines rather than the magnitude and distance earthquake records are measured from the source alone. This study emphasizes the need to consider the impact of the second order (P-Δ) effect for the design of 1.5MW and 5MW wind turbines to avoid structural stability failure.

ACKNOWLEDGMENTS

First of all, I would like to thank Almighty God for giving me the strength and ability to undertake this study.

I would like to express my deep and sincere gratitude to my Advisor, Dr. Bedilu Habte, who guided me throughout this research. His support, patience, motivation, and comments are highly vital through all stages completed during this study.

I would also like to thank my family for their continuous support, encouragement, and prayers to complete this research.

Finally, I wish to extend my special thanks to my colleague Mr. Teshome Debessa for his technical support during this study.

TABLE OF CONTENTS

LIST OF TABLES

LIST OF FIGURES

CHAPTER ONE: INTRODUCTION

1.1 Background of the Research

Energy is the capacity or power to do the work. There are two forms of energy available which are renewable and non-renewable. Non-renewable forms of energy like fossil fuels have a lion's share of energy consumption around the world, which exists in limited amounts. Exploiting these limited resources results in significant depletion and their adverse environmental effects have led to the need for other forms of energy. Thus, the utilization of renewable forms of energy is becoming a reliable solution to these problems. Wind energy is one form of renewable energy which is growing rapidly around the world since it is available abundantly and environmentally friendly [1].

Recent scientific and cultural interest has focused heavily on wind turbines as a practicable, affordable, and long-lasting source of wind energy. Based on the axis of rotation, there are two different types of wind turbines: vertical-axis wind turbines and horizontal-axis wind turbines. Horizontal-axis wind turbines are more efficient than vertical-axis wind turbines, which only have a 30% efficiency. Vertical-axis wind turbines are simpler, more affordable, and simpler to build. Currently, the installation of horizontal-axis wind turbines is a common practice around the world. To prevent failure due to strength and stability, adequate design and analysis of wind turbines that are subjected to various loads, such as aerodynamic and seismic loads, are required. A detailed investigation is needed, particularly for the stability of wind turbines erected in earthquake zones. To prevent catastrophic collapse, it is crucial to understand how the combination of earthquake and wind loads impacts the stability of the structures. This study examines the interplay between aerodynamic and seismic loads and how it affects the stability of land-based, horizontal-axis wind turbines constructed in seismic regions.

1.2 Statement of the Problem

Wind turbines are practicable, affordable, and long-lasting sources of wind energy that have inspired researchers to have an interest in this area. Ensuring the safety of wind turbines is essential for the proper service life operation and to protect the investments made for the construction of these structures. However, these structures are vulnerable to different types of failure and of these types of failure, stability failure is the most dangerous which could result in the partial or full collapse of wind turbines. Currently,

the installation of wind turbines in seismic regions is growing to meet renewable energy demand by different nations, and analyzing the stability of wind turbines in these regions is critical to minimize failure. Thus, it is highly important to determine how aerodynamic and seismic load interaction affects the stability of the wind turbine to avoid catastrophic failure. This research focuses on analyzing the impact of aerodynamic and wind load interaction on the stability of land-based horizontal-axis wind turbines, which are built in seismic areas.

1.3 Objectives of the Research

1.3.1 General objective

The main goal of this research is to study the effect of aerodynamic and seismic load interaction on the stability of land-based horizontal-axis wind turbine towers of different sizes subjected to different aerodynamic conditions and ground motions.

1.3.2 Specific objectives

- To develop reliable finite element models by using a finite element software.
- To study the structural responses of the wind turbine tower with respect to top displacement, Von Mises stress and eigenvalue buckling due to wind and earthquake load interaction for different operating conditions.
- To assess the impact of aerodynamic and seismic load interaction on the structural stability of the wind turbine towers.

1.4 The scope and Limitation of the Study

This research addresses the numerical investigation of the effect of Aerodynamic and Seismic Load Interaction on the Stability of Land-Based 65kW, 1.5MW, and 5MW wind turbine towers. The scope of this study is limited to an assessment of the effect of aerodynamic and seismic load interaction on the stability of land-based wind turbine towers with selected wind load variation and earthquake load. The model of wind turbines is developed by approximating the geometry and material properties of wind turbines, and by considering the base of the wind turbine as fixed. The analysis is made by using finite element software which is validated for the analysis of wind turbines. Selected wind load and ground motion are applied to the developed model to determine the response behavior of the wind turbine tower.

In this study, the soil-structure interaction has not been considered. Furthermore, because of the high amount of time needed to simulate the model in the software, the mesh size used in the study was limited.

1.5 Organization of the Research

The study is organized into six chapters; the first chapter is a general introduction describing the background of the research, a statement of the problem, the objectives of the study, and the scope and limitation of the study. A review of relevant literature is presented in Chapter 2. Chapter 3 describes a methodology implemented for determining the impact of aerodynamic and earthquake load interaction on the stability of land-based wind turbine towers. In addition, Chapter 4 focuses on the modelling and analysis of wind turbines. Results and discussions from Modelling and Analysis are discussed in Chapter 5. Finally, the conclusions and recommendations of the study are included in Chapter 6.

CHAPTER TWO: LITERATURE REVIEW

2.1 Introduction

Shortage of fossil fuels which are conventional sources of nonrenewable forms of energy, major environmental threats, and the urgent need for energy in expanding new economies of developing countries have all contributed to the expansion of the use of renewable energy technologies. Currently, wind energy is the most mature and affordable [2]. Wind energy is crucial to secure and enhancing global energy by decreasing reliance on fossil fuels that are vulnerable to price and supply instability.

Since wind energy doesn't emit any CO_2, it has no impact on the greenhouse effect. Because it requires a lot of labor, wind energy supports a large number of jobs. Wind energy can be coupled with a diesel engine to reduce fuel consumption in distant places or areas with a shaky grid. It can also be utilized to charge batteries. Additionally, in coastal regions with low freshwater demand, like the Middle East, wind turbines may be utilized to desalinate water. In windy areas, the cost of producing electricity is comparable to the cost of using more conventional production techniques, including coal-fired power stations. However, the cost of land, interest rates, and last but not least the amount of wind that can be found at a particular location all have an impact on the cost of producing electrical energy [3].

Investments in the renewable energy sector have shown big rewards for green recovery around the world. Analysis from International Renewable Energy Agency (IRENA) shows that every investment in sustainable energy pays-off from three to seven-fold [4]. Thus, it is important to build back better and proper energy transition from non-renewable forms of energy into renewable forms of energy in order to achieve net zero CO_2 emission.

The worldwide wind sector experienced the biggest year-over-year growth compared to prior years in 2020, according to the Global Wind Report 2021. Since more than 93GW of wind energy was added in 2021 despite disruption from global difficulties like COVID-19, the wind sector has demonstrated tremendous resilience. 86.9GW were installed in the worldwide onshore market, a 59% increase from 2019. To attain the net zero objectives outlined by the United Nations (UN) by the year 2050, however, around 180 GW must be deployed annually globally [5].

Variations in wind speed must be estimated to determine the power generation capacity of wind turbines. Weibull probability distribution, which describes different mean wind speeds occurring at the site during a period of time, is used to best describe fluctuation in wind speed (wind turbulence) at a certain location. Wind turbulence strongly affects the power output of wind turbines. Strong fluctuation of wind may create high dynamic fatigue loads acting on the turbine which may affect the durability of the structures or may result in failure [6].

Wind gust, which is a sudden increase in wind speed in a relatively small interval of time, may change wind speed, turbulence, and wind shear significantly. Thus, rotor balance should be kept while sustaining the power output of the wind turbine generators due to sudden wind gusts requiring a relatively rapid change of the pitch-angle of the blades [7].

The magnitude of power a wind turbine produces depends on the wind's velocity. Wind turbines begin to operate when the cut-in wind speed reaches 3m/s. Until the rated wind speed is attained, the energy produced by a wind turbine at this point is proportional to a third power of the wind speed. With the aid of stall-regulation or pitch-control devices, the power is constant from the rated wind speed up to 25m/s. In order to prevent heavy mechanical stresses on the turbine components when the wind speed reaches 25m/s, they are typically brought to a stop or emergency shutdown. The term "cut-out wind speed" refers to this wind speed [8]. Figure 2.1 shows the power curve which shows the characteristics of wind speed vs. power output.

Depending on its ability to generate power and the rotor design used, wind turbines come in a variety of sizes and types. The average capacity of wind turbine machines was initially somewhere between 30 and 50 kW, but it quickly increased. Several very big prototypes were created at the same time as part of numerous national projects focused on utility-scale power. The German Growian, Danish Nibe, British LS-1, and US MOD series were examples of megawatt-scale devices [9].

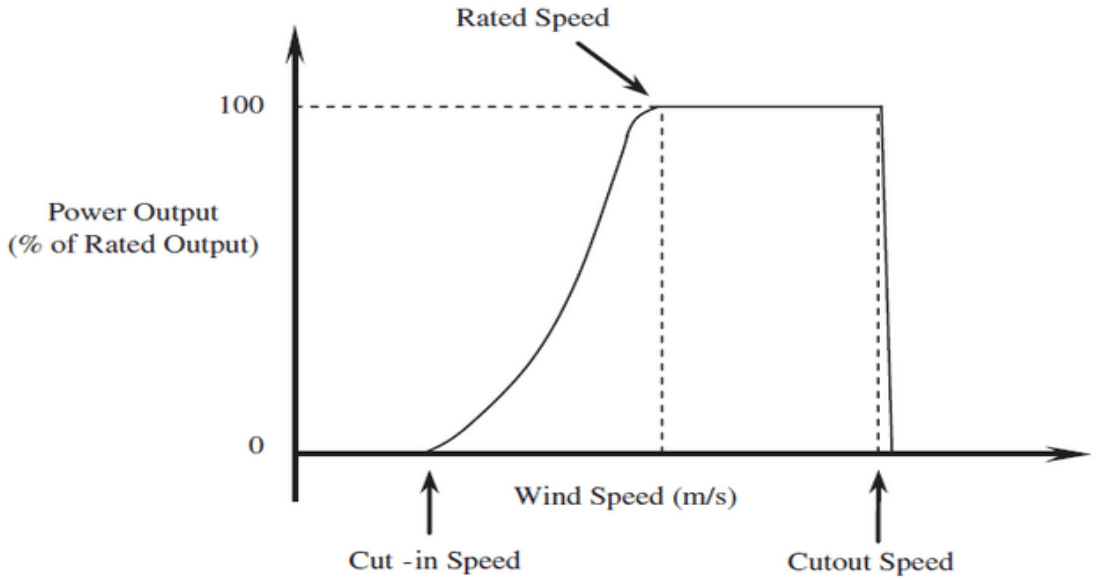

Figure 2.1: Typical wind turbine power curve [10]

The U.S.A expects the energy supply of the country's needs from wind energy will be 20% by 2030 which is higher than the current electrical energy generation from wind turbines by 10%. Different types of wind turbines are fabricated by various companies to meet the wind energy demands of citizens including small-scale wind turbines (10 to 100 kW), utility-scale wind turbines (1 to 5 MW), and large wind turbines for wind farms (50 to 500 MW) [11].

The country's entire usable wind energy potential is estimated to be over 1,350 GW per the Ethiopian electric power report [12]. Nevertheless, despite the enormous capacity of this energy system, Ethiopian wind farm construction is still in its early phases. For both technological and financial reasons, wind zones with a wind density of 300W/m^2 and a wind speed of 6.5m/s or above are suitable for grid-based energy generation. With a combined installed power capacity of 324 MW, the Ashegoda, Adama I, and Adama II wind farms are currently complete and integrated into the grid [13].

2.2 Classification of wind turbines

2.2.1 Classification of wind turbines based on axis of rotation of rotor

Depending on the rotor working principles, modern wind turbines are divided into two categories which are horizontal-axis wind turbines (HAWT) and vertical-axis wind turbines (VAWT) [14].

A. Vertical axis wind turbines (VAWT)

Traditional water wheels allow water to enter tangentially, perpendicular to the wheel's axis of rotation. Wind turbines with vertical axes are made to behave appropriately toward the air. Despite the fact that in theory, such a concept would also function with a horizontal-axis, it requires a more intricate design that hardly match the level of efficiency of a propeller-type turbine. The main benefits of these wind turbines are the ground-mounted generator and gearbox, which are both conveniently accessible and do not need a yaw mechanism. A significantly lower overall level of efficiency, the need to completely disassemble the turbine only to change the main bearing, and the placement of the rotor very near to the land surface where there is little wind are drawbacks.

B. Horizontal axis wind turbines (HAWT)

HAWT is commonly installed type of wind turbine in use today around the world. In fact, all grid-connected commercial wind turbines are today designed with propeller-type rotors mounted on a horizontal-axis on top of a vertical tower. In contrast to the mode of operation of the vertical-axis turbines, the horizontal-axis turbines need to be aligned with the direction of the wind, thereby allowing the wind to flow parallel to the axis of rotation.

Upwind and downwind rotors are distinguished in relation to horizontal-axis wind turbines. Upwind rotors possess the advantage of slightly preventing the wind shading impact caused by the presence of the tower because they are subjected to the wind in front of the vertical tower. To keep the rotor axis aligned with the direction of the wind, upwind rotors require a yaw mechanism. On the tower's lee side, downwind rotors are installed. The fluctuating wind power caused by the rotor passing through the tower's wind shadow, which increases fatigue loads, is a significant drawback of this design. To prevent the rotor blades from touching the tower, upwind rotors must be very rigid, whereas downwind rotors can be more flexible. The downwind rotors suggest potential weight reductions and could lessen the stresses placed on the tower. Upwind rotors are found on the great majority of wind turbines in use currently.

2.2.2 Classification of wind turbines based on location of construction

Onshore wind farms, which are substantial installations of wind turbines located on land, and ***offshore wind farms***, which are installations located in bodies of water, are the two main "types" of wind energy used today [15].

The history of onshore (land-based) wind turbine development is extensive. Onshore turbines have a number of benefits, including less expensive foundations, simpler electrical grid integration, less expensive tower construction and turbine installation, and easier access for maintenance and operation. Because of presence of higher offshore wind potential in terms of wind intensity and consistency, offshore wind turbines have advanced more quickly than onshore ones since the 1990s. Compared to an identical turbine built onshore, an installed offshore wind turbine can produce more power and run more hours per year. Furthermore, environmental regulations are more relaxed offshore than they are onshore. For instance, offshore wind turbine noise is no longer a concern.

2.3 Components or elements of HAWT

HAWT is commonly installed type of wind turbine in use today which typically consists of three blades. A typical wind turbine consists of a tower, nacelle which contains most elements of the turbine inside and rotor as shown in Figure 2.2. Three blades are connected to the rotor hub, and the hub is connected to the gearbox through main shaft of the turbine. The rotor of the wind generator is connected to the output shaft of the gearbox. The gear is used to increase the slow rotating speed of the rotor hub to the desired high rotating speed of the generator rotor. The pitch-control system helps each blade, which is pitched individually, to optimize the angle of attack of the blade for allowing a higher energy production in normal operation and for protecting the turbine components from damage in emergency shut-down situations. With the feedback information such as measured instantaneous wind direction and speed from the wind vane, the yaw control system provides the yaw orientation control for ensuring the turbine is constantly against the wind [16].

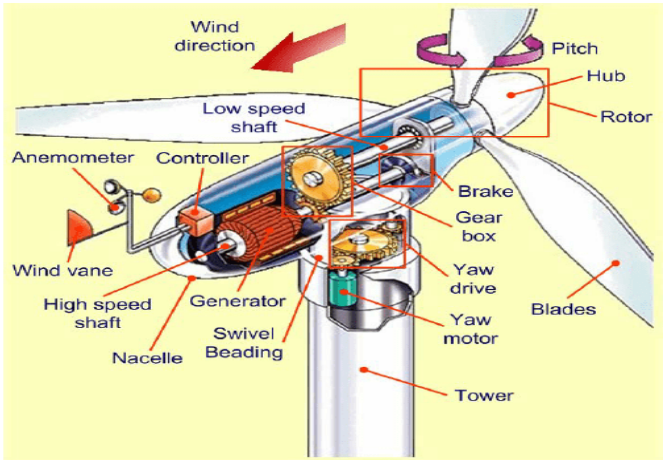

Figure 2.2: Components of a typical horizontal-axis upwind wind turbine [17]

2.4 Action effects on wind turbine towers of HAWT

Wind turbines are practicable, affordable, and long-lasting sources of wind energy that have inspired researchers to have an interest of study in this area. Gwon 2011 [18], discussed action effects on wind turbine towers which includes wind loads (drag and lift force), inertia loads (that result from gravity, rotation, vibration, or gyroscopic effects), functional loads (from transient operation conditions of turbine such as braking, yawing, transmitting power to generator) and other loads from environment sources such as wave, current, ice and earthquake.

Research shows that depending on the operational state of the turbine there is variation in extreme loads, which cannot be considered for simplified models described in the wind turbine guidelines [19]. Of particular concern for turbine structures is ensuring that the turbine tower does not fail during simultaneous earthquake and wind action. However, modeling approaches used by previous researchers that include wind dynamics [20 21] cannot directly predict tower failure because they rely on a simple linear multi-body dynamics representation of the turbine structure. Investigations of varying detail have been conducted to directly consider tower buckling and failure, but most have ignored the wind dynamics and operational states of the turbine [22 23 24]. Figures 2.3 and 2.4 show that tower failure which was caused by earthquake forces that led the wind turbines to completely collapse.

Figure 2.3 (left): Turbine tower failure occurred in Japan

Figure 2.4 (Right): Wind turbine tower and blade failure obtained from web-link [25].

2.5 Materials used for HAWT

Wind energy covers roughly 10% of the world's total energy consumption and being renewable form of energy will only make it essential to realize the ever-growing potential of this sector around the world. In order to remain competitive with existing technologies, the optimization of wind turbine efficiency is crucial and dictated by engineering design complemented by judicious choice of materials. Additionally, the materials should be long-lasting, environmentally friendly, and economical in terms of production so as not to offset the positive environmental impact and economic advantages of wind energy.

The tower is one of major components of wind turbine which supports the nacelle and rotor blades and it is made of tubular steel (which is conical in shape with linear variation of diameter with height of the tower), concrete, or steel lattice. The materials must be strong and stiff to withstand harsh environmental conditions and extreme winds.

Fibrous materials are characterized by the fact that they are significantly longer than they are wide. The exceptional strength and stiffness of fibers make them excellent candidates for turbine blade materials, where the long fibers provide longitudinal stiffness when aligned parallel along the blade length. Fibers are often brittle and can snap easily, so they are not used alone as a material but as additive reinforcements. Thus, Composite materials remain the most practical and prevalent choice for turbine blades [26].

2.6 Existing Guidelines for design of wind turbines

One of the wind turbine design guidelines is the Guidelines for Design of Wind Turbines by Risø-DNV 2002. It provides the foremost implicit specifications. In this guideline, the turbine is represented by a simplified model in which concentrated mass (sum of the mass of the rotor, nacelle, and a quarter of the tower) is applied at the center on the top of a tower. The frequency-domain analysis with a specific response spectrum is implemented to determine the load set up due to the ground motion [27].

Another guideline is the Germanischer Lloyd (GL 2003) guidelines which recommend that either local building codes should be applied or in the absence of specific provisions, the American Petroleum Institute (API) recommendations are to be used. The analysis of ground motion induced loads in this guideline is dependent on the interaction of aerodynamic loads and seismic acceleration with a recurrence period of 475 years [28]. Seismic load is to be combined with standard aerodynamic load conditions in a load combination with a load factor equal to one. Eurocode 8 provides earthquake consideration provisions for building structures [29].

The International Electro-Technical Commission (IEC 2005) guidelines are also one of the guidelines which indicate that the design level earthquake is prescribed as a 475-year return period event and the action loads must be applied with the maximum operating loads or emergency shutdown loads with factor of safety of one. A simplified estimate of the seismic load is provided in Annex C of this guideline, which suggests the use of a design response spectrum from local building code adjusted to a damping ratio of 1% to find the design response acceleration based on the first natural frequency of the tower [30]. Guidelines like IEC (2005) or GL (2003) use linear combinations for considering extreme seismic and operational loads together and they use load factors of one for operational and earthquake load interactions. However; there are no suggestions on the methods to deal with the effect of non-linearity or buckling of the components of the turbine in the three guidelines discussed previously.

A document that provides recommended practices for the design and permitting of large wind turbine support structures has been published as a result of a methodical effort by a joint committee that was appointed by the American Wind Energy Association (AWEA) and the American Society of Civil Engineers (ASCE) [31]. This document offers instructions for calculating earthquake loads for big wind turbines while taking into

account the standards for the relevant U.S. building codes and the industries indicated above. It is advised to add the operational and seismic loads together in absolute terms with a load factor of 0.75. Spectral response acceleration parameters should be based on the damping ratio of 1% while idled and damping ratio of 5% while the wind turbine is operating normally. Seismic ground motion values are calculated from ASCE 7-10 [32]. In the ASCE/AWEA publication, non-linear responses are first discussed. It is mentioned that a method for buckling analysis that takes into account geometric and material non-linearity with flaws in the shell's initial shape would be acceptable, but no further information is given.

2.7 Stability of wind turbine tower

The buckling resistance of the wind turbine tower, including the second-order effect, is connected to its stability. Both overall (or global) buckling and local buckling are common mechanisms of buckling failure for steel members. The two modes' differences are shown in Figure 2.5. A member's longitudinal axis may be deformed or buckled to indicate global buckling. The strength of the cross-section is weakened by the buckling of a cross-sectional component in local buckling, which does not distort the member's axis [33]. Therefore, proper care should be given to wind turbine verification during design and analysis to prevent stability failure that causes the structure to fail prematurely. Eurocode 3 provides procedures for checking the stability of steel structures including the second-order effect [34].

Wind turbine blade and tower failures could be due to the decay of the turbines, repetitive/cyclic loads; some are due to material stiffness and defects during production stage; and lastly, some are new failure modes related to the increased rotor size and equally increasing hub heights [35]. The delivery of long steel tower is a challenge in itself since parts of the tower are moved and connected to the site.

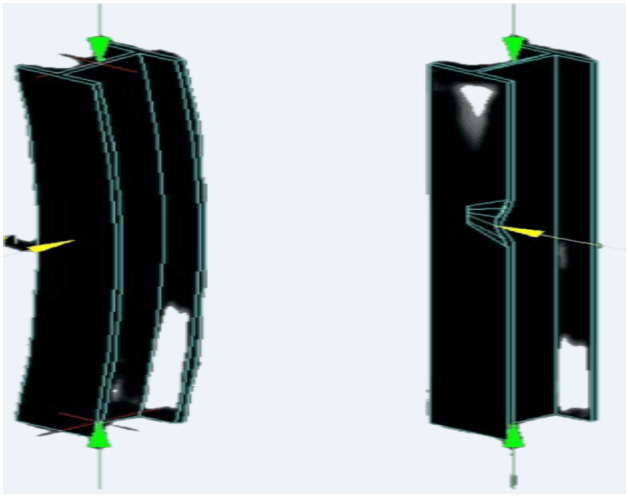

Figure 2.2: Global buckling (left) and Local buckling (right)

The collapse of the wind turbine tower is a serious type of failure in these structures. Thus, there will be huge economic loss from investment in these structures due to either the overall collapse or partial failure of the tower. A statistical study on the causes failure in wind turbines shows that tower damage accounted for 25%, and blade failure accounted for 75% [36].

According to Kim 2002, a horizontal axis wind turbine tower modeled as a cylindrical shell structure could collapse due to whole or partial buckling, which is the most common type of failure in the wind turbine tower. Buckling analysis of the wind turbine tower is important to calculate critical load and design the structure with better capability. Buckling in the wind turbine tower is not only related to action load but also to its geometry (shell structure) [37].

Congxin Yang et al 2012 studied the buckling of a 2.5MW horizontal-axis wind turbine tower tube by theoretical analysis and numerical simulation (ANSYS software) and found that axial and lateral loads are main contributors to buckling of wind turbine tower, bending moment also has effect on the buckling of tower and the effect of due to wind load in extreme conditions should also be considered [38]. However, their study is limited to Global buckling and wind loading effect only.

Chou and Tu (2011) [39] and Chou et al. (2013) [40] studied the reason behind the collapse of wind turbine tower and the damage to the rotor blade due to typhoon Jangmi in Taiwan in 2008. The study found that inadequate strength and low quality of bolts of the wind turbine were the causes of the failure of the tower due to extreme winds. Chou

et al. 2013 investigated a composite blade damaged due to typhoon and showed that the blade failed at a wind speed of 53.4m/s by delamination and cracking, although it was expected to resist forces up to tip wind speed of 80m/s.

Song Xi et al 2013 studied elastic stability or the buckling of the conical tower of a 1.5 MW wind turbine by using numerical simulation (ANSYS software) under combined action of concentrated load and gravity load. Results showed that the use of a finite element models is feasible in engineering applications. From the mode shapes of buckling analysis, it was seen that for the tower with a doorway, the doorway is a weak position where local buckling occurs [41].

In Asareh 2015, the collapse of a turbine tower due to buckling was investigated for a range of wind speeds and seismic intensities. He came to the conclusion that the tower would collapse in weaker earthquakes if the applied wind loading was close to the turbine's rated wind speed [42].

The buckling investigation of a 10 MW offshore wind turbine (OWT) subjected to wind-wave-earthquake loadings was conducted by Yangtian Yan et al in 2021. They discovered that the fore-aft wind, wave, and current loads significantly influence the seismic responses of the OWT and cause severe buckling [43]. However, there is a need for research into the stability of wind turbines in conditions of variable size, operation, and loading.

2.8 Previous studies on modelling and analysis of wind Turbines

Researchers are now able to take into account the significance of earthquake load for an operational wind turbine thanks to the development of current computational techniques. Early studies by Bazeos et al. [44] and Lavassas et al. [45] focus on the tower's loading when considering the seismic loading of wind turbines. These streamlined models for prototype 450kW and 1MW turbines with 38m and 44m tall steel towers intended for installation in Greece consider the top tower components (nacelle and rotor) to be a concentrated mass. According to the authors, earthquake design may become crucial in areas with greater seismic risk and unfavorable soil properties.

Witcher [46] presented an overview of the GH Bladed [47] seismic module for a 2MW upwind turbine with an 80m blade diameter and 60m tower height and considers the response of the structure under three different operation conditions. The significance of

time-domain analysis and the effects of aerodynamic damping was emphasized in his work. Prowell et al. [48] conducted experimental work on a 65kW Nordtank wind turbine using the large high-performance outdoor shake table test available at the University of California at San Diego. Earthquake motions were applied in two horizontal directions and the modal characteristics and dynamic behavior of this turbine were obtained. Their study emphasizes the importance of considering seismic effect increases as the turbines grow in size. Ishihara and Sawar [49], and Haenler et al [50] also investigated the impact of wind dynamics and earthquake loads using simplified models.

An 80m tall 1.65MW wind turbine steel tower with diameter to thickness (d/t) ratios ranging from 105 to 278 was the subject of an incremental dynamic analysis by Nuta et al. [51] using a suite of earthquake records representing North American seismic activity, including Los Angeles and Western Canada. By doing incremental dynamic analysis and taking into account various intensity measures, damage measures, and damage states, the authors created fragility curves. The 5-MW offshore platform's seismic fragility analysis by Kim et al. [52] also took into account soil-pile interactions by utilizing the characteristics of the soil profiles. The damage criteria utilized in fragility analysis to determine the likelihood of failure were stress at yielding, permissible stress, displacement at yielding, and allowable deformation. However, aerodynamic loading was not taken into account in these two studies.

Hua Wei et al. 2011 studied the aerodynamic strength of the 1MW wind turbine tower by using the finite element method (ANSYS software) and the result showed that the aerodynamic load has higher impact on the tower’s displacement along the wind speed, and the maximum Von Mises stress of the tower becomes larger after taking into account the influence of aerodynamic load [53].

Wei Chen 2014 studied static and modal analysis of large horizontal-axis wind turbines by using the finite element method (ANSYS software) and found overall maximum stress of the tower does not always observed at the base. The thickness and the load of the wind turbine tower should be considered, and there would be no resonance of the wind turbine in normal operation conditions [54].

Chun-you Zhang and Xiaoqiang Wu 2014 studied the static and dynamic response of the 1.5MW wind turbine tower by using finite element analysis and found that through

modal analysis of the tower of the wind turbine there will be no resonance during normal operation the tower. Furthermore, they suggested operation condition of a wind turbine is complex and needs to consider many factors, such as temperature, ice, lightning, and earthquake [55].

In 2015, Atul Sudhakar Patil assessed the 1.65MW wind turbine tower's response to earthquake and high-velocity wind loading events. Using the finite element method and fragility analysis, the performance was evaluated using a probabilistic methodology (ANSYS software). He observed that the most important limit state to take into account when building the wind turbine tower system is foundation overturning. The near-fault earthquake loading poses the greatest threat to the stability of wind turbine structures in the event of an earthquake [56].

Using finite element analysis, Asareh 2015 performed a fragility analysis of a 5-MW NREL wind turbine taking into account the interaction of wind and earthquake loads. ABAQUS is used to scale and choose the earthquake ground motion for simulation on the finite element model. In each time step, various wind speeds are also chosen and applied to the model's blade elements as aerodynamic loads. The final step is fragility analysis, which reflects the non-linear behavior of the turbine tower under various loading situations and evaluates tower failure and buckling analysis using nonlinear models. This analysis makes use of various intensity measures, engineering demand factors, and damage states. The coupling method of load application for simulation was used to carry out the investigation [57].

A thorough examination of the dynamic earthquake response of a 1.5MW steel tower that was modeled as a nearly cylindrical shell structure was conducted by Sadowski et al. (2017) [58]. Then, 10 near-fault and 10 far-fault earthquake ground motions were chosen as representative examples. The creation of a very unstable plastic hinge under earthquake excitations revealed the tower to have significant rigidity. In comparison to far-fault earthquakes without these characteristics, the overall reaction was much more destructive during near-fault earthquakes with pulse-like effects and high vertical accelerations.

A probabilistic framework was created by Alberto Maria et al. in 2017 [59] with the goal of estimating the likelihood that the supporting structures for horizontal-axis wind turbines may break under the influence of wind and seismic activity. Where independent

aerodynamic and seismic responses are estimated in the time-domain, uncoupled analysis was performed since nonlinearities were possible. In a probabilistic framework, the study presents some findings related to the structural response investigation of a 5MW land-based HAWT subject to aerodynamic and earthquake loads.

Pradin Suinyal 2017 [60] investigated the response behavior of wind turbines of different sizes under different types of earthquakes. A 65kW, 1MW, and 5MW wind turbines are selected for analysis due to earthquakes loads. ANSYS Workbench 16.2 was used to develop models and runs the analysis. Parametric study with respect to size, damping ratio, base acceleration direction, and earthquake types was performed. However, this study does not include aerodynamic analysis and operation conditions of wind turbines.

Muhsen Awad 2017 [61] studied nonlinear dynamic analysis of wind turbine towers subject to design wind and seismic loads by considering different combination scenarios and developed a new model called HWAT for analysis and the local buckling effect was included in his study. He also addressed the geometric and material non-linear effects that result from the extreme loads that a wind turbine is subjected to under the failure loads. Jian Fan et al 2018 [62] studied the collapse analysis of wind turbine towers under the coupled effects of wind and near-field earthquakes. It developed a model for analysis using collapse probability with peak ground acceleration considering global and local deformation for a wind turbine with a 60m hub height.

CHAPTER THREE: METHODOLOGY

3.1 Modelling of Wind Turbines for Earthquake Analysis

There are two different types of models that are used for analyzing seismic effect of wind turbines. The first type of model is called the simple model which is mainly based on the tower by accounting for the mass of the nacelle and rotor as a point mass at the top of the tower and the second type of model is called the full system model which describes the full turbine including the nacelle and rotor with some level of detail. Simplified models are recommended by both Risø-DNV guidelines [63] and International Electrotechnical Commission (IEC) guidelines Annex C [64]. The simplified model considers the turbine as a single degree of freedom (SDOF) system and it is not reliable for analysis of wind turbines beyond first mode of the tower. In contrast, the full system models consider the turbine as a multiple degree of freedom (MDOF) system. Full system models are more complex than simple models. Full system models consider different scenario to earthquake risk, including wind loads and operating conditions.

There are two types of domains used for analysis of wind turbines in full system models which are frequency domain and time domain. Frequency-domain methods are typically favored in design due to their ease of implementation. Time-domain analyses have a higher computational demand and are often used in the analysis of wind turbines. Time-domain analyses are increasingly being used in the wind turbine industry. Full system models are evaluated using two methods. The first one is a combined modal and multi-body dynamics formulation to simulate the dynamic behavior of the turbine in the time domain. The structural dynamics of the wind turbine are represented using limited-degree-of-freedom modes. This approach is less time-consuming than the second approach which is the finite element (FE) approach. For a more detailed analysis that could consider non-linearities and stress analysis through different components of the system, the FE method is recommended. This study used finite element software (ANSYS Workbench 2022) for analysis of the stability of wind turbines due to aerodynamics and seismic load interaction.

3.2 Analysis of Wind Turbines

3.2.1 Seismic Analysis of Wind Turbines

Seismic analysis of wind turbine structures is structural analysis and calculation of the response due to earthquakes. The analysis of wind turbine loading associated with ground motions is critical due to the increasing of the installation of wind turbines in earthquake active zones. The approach taken for such analysis is generally based on codified methods that have been developed for the assessment of seismic loads acting on buildings.

3.2.1.1 Equation of Motion and Numerical Method for Seismic Analysis

A finite difference method is used by discretization of time over the history of dynamic action and reaction in order to obtain a solution to the time-dependent (dynamic) problem.

For a single degree of freedom (SDOF) system, the dynamic equation of the motion of a spring-damper-mass system is:

$$M\,\ddot{u}(t) + C\,\dot{u}(t) + K\,u(t) = F^a \qquad (1)$$

Where, M, C and K are mass, damping and stiffness respectively

$\ddot{u}(t), \dot{u}(t), u(t)$ are acceleration, velocity and displacement respectively

F^a is the applied force

Similarly, for a multi-degree of freedom (MDOF), the dynamic equation can be represented as:

$$[M]\{\ddot{u}(t)\} + [C]\{\dot{u}(t)\} + [K]\,\{u(t)\} = \{F^a\} \qquad (2)$$

Where, [M], [C] and [K] are mass, damping and stiffness matrices respectively

$\{\ddot{u}(t)\}, \{\dot{u}(t)\}, \{u(t)\}$ are nodal acceleration, velocity and displacement

respectively

$\{F^a\}$ is the applied force vector

Ground acceleration during earthquakes varies irregularly to such an extent that the analytical solution of the equation of motion is not easy to determine that is tedious and time consuming.

Therefore, numerical methods are necessary to determine the structural response. The solution of differential equations (1 and 2) has to be determined for selected time steps from the beginning of the earthquake load in order to calculate the response over the total time of a seismic load. This method of solving the above equations of motion is called the numerical method of dynamic response.

Although the analytical solution of non-linear structures necessitates acceleration and the second derivative of displacement is not to be a smooth function, the solutions obtained by these approaches are presumed to be smooth. Therefore, only single-step algorithms are used to solve this form of acceleration discontinuity.

In order to solve structural dynamic problems for both blast and earthquake stress, Newmark created a family of single-step integration techniques known as the Newmark time integration approach. ANSYS Workbench 2022 frequently uses this method to solve equation (2) described previously. A finite difference method for the time interval of Δt is used for analysis by this approach as shown below:

$$\{\dot{u}_{n+1}\} = \{\dot{u}_n\} + [(1-\delta)\{\ddot{u}_n\} + \delta\{\ddot{u}_{n+1}\}]\,\Delta t \quad (3)$$

$$\{u_{n+1}\} = \{u_n\} + \{\dot{u}_n\}\,\Delta t + [(\tfrac{1}{2}-\alpha)\{\ddot{u}_n\} + \alpha\{\ddot{u}_{n+1}\}]\,\Delta t^2 \quad (4)$$

Where, α and δ are the Newmark's integration variables

$\{u_n\}$, $\{\dot{u}_n\}$, $\{\ddot{u}_n\}$ are nodal displacement, velocity and acceleration vectors respectively at time t_n

$\{u_{n+1}\}$, $\{\dot{u}_{n+1}\}$, $\{\ddot{u}_{n+1}\}$ are the nodal displacement, velocity and acceleration vector respectively at time t_{n+1}

Here in this equation $\Delta t = t_{n+1} - t_n$

The governing equation (2) can be written at time t_{n+1} to calculate $\{u_{n+1}\}$ as follows

$$[M]\{\ddot{u}_{n+1}\} + [C]\{\dot{u}_{n+1}\} + [K]\{u_{n+1}\} = \{F_{n+1}{}^a\} \quad (5)$$

Rearranging equations (4) and (5) as follows to find the value of $\{u_{n+1}\}$:

$$\{\ddot{u}_{n+1}\} = a_0(\{u_{n+1}\} - \{u_n\}) - a_2\{\dot{u}_n\} - a_3\{\ddot{u}_n\} \quad (6)$$

$$\{\dot{u}_{n+1}\} = a_5\{\dot{u}_n\} - a_6\{\ddot{u}_n\} - a_7\{\ddot{u}_{n+1}\} \quad (7)$$

Where; $a_0 = \frac{1}{\alpha \Delta t^2}$ $a_2 = \frac{1}{\alpha \Delta t}$ $a_3 = \frac{1}{2\alpha}$ - 1

$a_5 = \frac{\Delta t}{2}\left(\frac{\delta}{\alpha} - 2\right)$ $a_6 = \Delta t\,(1-\delta)$ and $a_7 = \delta \Delta t$

$\{\ddot{u}_{n+1}\}$ in equation (3) can be substituted in equation (4), and then the equations for $\{\ddot{u}_{n+1}\}$ and $\{\dot{u}_{n+1}\}$ are substituted in equation (5) to give:

$$(a_0[M] + a_1[C] + [K])\{u_{n+1}\} = \{F^a_{n+1}\} + [M](a_0\{u_n\} + a_2\{\dot{u}_n\} + a_3\{\ddot{u}_n\}) + [C](a_1\{u_n\} + a_4\{\dot{u}_n\} + a_5\{\ddot{u}_n\}) \quad (8)$$

Where; $a_1 = \frac{\delta}{\alpha \Delta t}$ $a_4 = \frac{\delta}{\alpha}$ - 1

The Newmark's integration variables related to the input are:

$$\alpha \geq \frac{1}{4}\left(\frac{1}{2} + \delta^2\right)^2 \quad \text{and} \quad \delta \geq \frac{1}{2} \quad (9)$$

According to Zienkiewicz & Taylor 1977 [65], equation (9) have been modified by introducing parameter γ as shown in equation (10). γ is the amplitude decay factor. If $\gamma \geq 0$, the solutions of equation (5) are stable.

$$\alpha = \frac{1}{4}(1+\gamma)^2 \quad \text{and} \quad \delta = \frac{1}{2} + \gamma \quad (10)$$

One of the parameters δ in equation (9), can be used to modify the amount of numerical dissipation. The Newmark approach, however, is unable to maintain the second-order precision at lower frequency modes because δ > 1/2. Numerical damping does not exist in the Newmark implicit approach (constant average method, particularly δ = 1/2 and α = 1/4), which is second-order accurate and unconditionally stable. The higher frequencies of the structure may cause unacceptable amounts of numerical noise if additional sources of numerical damping are not added, as this lack of damping can be undesired (Hughes, 1987) [66]. The generalized HHT-α [67] method, which sufficiently dampens out an erroneous high-frequency response by introducing adjustable numerical dissipation in higher frequency modes, is implemented by the ANSYS program to get around the shortcomings of the Newmark family approaches.

The generalized HHT-α method uses the following equation to determine unknowns:

$$[M]\{\ddot{u}_{n+1-\alpha m}\} + [C]\{\dot{u}_{n+1-\alpha f}\} + [K]\{u_{n+1-\alpha f}\} = \{F^a_{n+1-\alpha f}\} \quad (11)$$

Where;

$$\{\ddot{u}_{n+1-\alpha m}\} = (1-\alpha_m)\{\ddot{u}_{n+1}\} + \alpha_m\{\ddot{u}_n\},$$

$$\{\dot{u}_{n+1-\alpha f}\} = (1-\alpha_f)\{\dot{u}_{n+1}\} + \alpha_m\{\dot{u}_n\},$$

$\{u_{n+1-\alpha f}\} = (1-\alpha_f)\{F^a_{n+1}\} + \alpha_f F^a_n$ and

$\{F^a_{n+1-\alpha f}\} = (1-\alpha_f)\{F^a_{n+1}\} + \alpha_f\{F^a_n\}$

The generalized HHT-α method uses the finite difference approximation equations and equation (11) in the finite difference form gives:

$$(a_0[M] + a_1[C] + (1-\alpha_f)[K])\{u_{n+1}\} = (1-\alpha_f)\{F^a_{n+1}\} + \alpha_f\{F^a_n\} - \alpha_f[K]\{u_n\} + [M](a_0\{u_n\} + a_2\{\dot{u}_n\} + a_3\{\ddot{u}_n\}) + [C](a_1\{u_n\} + a_4\{\dot{u}_n\} + a_5\{\ddot{u}_n\}) \quad (12)$$

Where;

$a_0 = \frac{1-\alpha m}{\alpha \Delta t^2}$ $a_1 = \frac{(1-\alpha f)\delta}{\alpha \Delta t}$ $a_2 = a_0\Delta t$ $a_3 = \frac{1-\alpha m}{2\alpha} - 1$ $a_4 = \frac{1-\alpha f}{\alpha} - 1$

$a_5 = (1-\alpha f)\left(\frac{\delta}{2\alpha} - 1\right)\Delta t$

HHT-α method is unconditionally stable and second order accurate if the variables meet the following conditions [68]:

$$\delta = \frac{1}{2} - \alpha m + \alpha_f \qquad \alpha \geq \frac{1}{2}\delta \qquad \text{and} \qquad \alpha_m \leq \alpha_f \leq \frac{1}{2} \quad (13)$$

Where; $\alpha_m \leq 0$

3.2.1.2 Modal Analysis

Modal analysis is performed using ANSYS Workbench 2022, for seismic analysis of developed finite element models as discussed in chapter three of this study, in order to verify that the first two natural frequencies are acceptable. Performing modal analysis is important to proceed to time history analysis in this study.

Therefore, before doing any other dynamic analysis, it is crucial to undertake a modal analysis first. The calculation of eigenvalues and eigenvectors is referred to as mode extraction. ANSYS Workbench offers a number of modal analysis techniques, including Block Lanczos, Subspace, Reduced, Damped (Full), QR Damped, and others. The default solver for most applications is the quick and reliable ***Block Lanczos method***.

The frequency domain process known as the Block Lanczos method is used to examine the modal characteristics of the structures. The Block Lanczos approach is acknowledged as a more potent tool for the extraction of a large number of Eigen pairs in large-scale structural mechanics issues because a bigger number of Eigen pairs is frequently required for seismic analysis. The Eigenvectors are solved using the Lanczos algorithm in this approach.

3.2.1.3 Transient Response (Time-History) Analysis

Transient structural analysis is used to determine the response behavior of a structure under the action of time-dependent loading. There are two methods in ANSYS Workbench for transient structural analysis which are direct integration method and modal superposition method.

Direct Integration Method is a step-by-step integration method which does not require determination of the mode shapes and natural frequencies. The direct integration method can be used for both linear and non-linear analyses. However; the main drawback of this method is that it requires more computational resources compared to the modal superposition method. This method also produces a large number of outputs, which requires a large-processing effort to perform all the necessary design checks as a function of time.

Modal Superposition Method uses modal equations of motion which are a reduced form of the equations of motion for different modes of vibration. The main advantage of the modal superposition method over the direct step method is that it is faster and requires fewer computational resources. Thus, this method is a more reliable method for performing linear or mildly non-linear dynamic analysis.

Modal superposition method is used to perform seismic analysis of wind turbine towers in this research due to aforementioned advantages.

3.2.1.4 Damping Calculation

The amount of energy dissipated in a vibrating structure that puts it to rest is known as damping. The amplitude of a vibrating body that has been dampened decreases over time. Important damping is the quantity of damping known as Cc determines an equilibrium condition devoid of oscillation. The expression "damping ratio" is another

term for a dimensionless number ξ which is defined as the ratio of actual damping to critical damping.

$$\xi = \frac{Actual\ Damping}{Critical\ Damping} = \frac{C}{Cc} \quad (14)$$

ANSYS workbench allows the utilization of the Rayleigh damping methods in which mass-proportional damping and stiffness-proportional damping are considered first:

$$[C_1] = \alpha\ [M] \text{ and } [C_2] = \beta\ [K] \quad (15)$$

Where the constants α and β have units s^{-1} and s, known as mass and stiffness damping coefficients respectively.

In order to construct a classical damping matrix somewhat consistent with the experimental value, damping is assumed to be a linear combination of damping associated with the mass and stiffness matrix:

$$[C] = \alpha\ [M] + \beta\ [K] \quad (16)$$

The damping ratio for the n^{th} mode of such a system is

$$\xi n = \frac{\alpha}{2\omega n} + \frac{\beta}{2}\omega n \quad (17)$$

The coefficients α and β can be determined from specific damping ratios ξ_i and ξ_j for the i^{th} and j^{th} modes, respectively.

$$\alpha = \frac{2\omega i\omega j}{\omega i^2 - \omega j^2}(\omega i - \omega j)\ \xi \quad (18)$$

$$\beta = \frac{2}{\omega i^2 - \omega j^2}(\omega i - \omega j)\ \xi \quad (19)$$

Where, ω_i and ω_j represent the natural circular frequency of the i^{th} and j^{th} modes respectively. α is mass coefficient and β is stiffness coefficient.

3.2.1.5 Characteristics of Selected Earthquake Loads for Analysis

The seismic analysis of wind turbines in this paper employs the use of the nonlinear dynamic time-history approach. It is necessary to choose earthquake recordings so that a nonlinear dynamic time-history analysis can be carried out. The quantity of energy input to the structure is largely influenced by earthquake history rather than structural characteristics.

When evaluating seismic loads and effects for analysis, a variety of elements are taken into account, including proximity to the earthquake source, seismic risk level, local soil characteristics, and structural characteristics including structural frequency, structural ductility, and structural damping.

The difference between near-field and far-field effects is determined by the distance from the epicenter and fault of an earthquake. When this distance is between 20 and 60 km, earthquake engineering refers to the near-field, whereas the far-field refers to a greater distance [69]. When compared to far-field earthquakes, which have greater frequencies, near-field earthquakes accelerate faster and have a smaller frequency range. Seismographs from such earthquakes often show protracted pulse durations of high ranges at the beginning of earthquake records, particularly when they exhibit progressive direction effects. Additionally, this study used far-field ground motions recorded from distances above 90 km as well as near-field ground motions reported from distances above 20 km.

Over the past three decades, a large number of ground motion time histories have been compiled. For this investigation, data were taken from the Consortium of Organizations for Strong Motion Observation Systems (COSMOS) website [70]. Using the COSMOS ground motion database, actual acceleration records are obtained. This database offers baseline corrected acceleration records for two horizontal and one vertical component, which are used for wind turbine analysis. For this investigation, 12 earthquake acceleration records were used. For cases involving near-fault and far-fault, six records for each were taken into consideration. The earthquake year, magnitude, and reporting station are all listed in each record. It should be noted that all of these records were chosen from soils of the same type (type-II soil) in order to be consistent with site circumstances. So, the soil-structure interaction is negligible in this study.

The logarithm of the wave amplitude recorded by seismographs is used to calculate the magnitude of an earthquake. Magnitude is measured on the Richter Scale using both whole integers and decimal fractions. Strong earthquakes are defined as those with a magnitude more than 6, moderate earthquakes with a magnitude between 5 and 6 whilst weak earthquakes are those with a magnitude between 4 and 5. Only earthquakes with magnitudes of roughly 4.5 or higher can be detected by sensitive seismographs worldwide [71].

In this work, analysis or simulation was conducted using two earthquake records from each of the three earthquake classifications—weak, moderate, and strong. The Landers, Loma Prieta, Dillon, Anza, Gilroy, and volcano earthquakes' acceleration records were used in this study. All three components of the accelerations record—two horizontal components and one vertical component—were used to analyze the real impact of these earthquakes on the structure. As a result, the structure was first exposed to the effects of each horizontal component individually (X and Z), then concurrently to both horizontal components (XZ), and finally to the combined effects of the two horizontal and one vertical component (XYZ). In Appendix A, a graph of these records' acceleration vs. time is plotted.

Table 3.1: Characteristics of the Earthquake loads used to perform analysis (Normal Component (Z direction))

Code Name	*Earthquake Name*	*Year*	*Station measured from*	*Distance from source (Km)*	*Magnitude (Mw)*	*Peak Ground Acceleration (cm/s^2)*
EL1	Landers	1992	Desert Hot Springs, California	23.1	7.3	-151.028
EL2	Landers	1992	Wrightwood, California	121.1	7.3	-37.569
ELP1	Loma Prieta	1989	Agnew, CA, Agnews State Hospital	21	7.0	157.60
ELP2	Loma Prieta	1989	Olema, CA, Point Reyes Ranger Station	106.8	7.0	100.20
ED1	Dillon	2005	Dillon, MT - Univ of Montana-Western	22.8	5.6	125.00
ED2	Dillon	2005	Bozeman, MT - Montana State Univ	117.3	5.6	-8.00
EA1	Anza	2005	Chihuahua Valley, CA	24.1	5.2	-52.00
EA2	Anza	2005	Chino Hills Hwy 71	117.9	5.2	-11.28
EG1	Gilroy	2002	Hollister, CA City Hall	23.1	4.9	-21.30
EG2	Gilroy	2002	San Francisco, CA - Golden Gate Bridge	121.6	4.9	8.40
EV1	Volcano	2003	Pahala, Hawaii Is, HI Ka`u Hospital	31.3	4.6	35.10
EV2	Volcano	2003	Waimea, Fire Station	90.9	4.6	-16.80

Table 3.2: Characteristics of the Earthquake loads used to perform analysis (Parallel component (X direction))

Code Name	*Earthquake Name*	*Year*	*Station measured from*	*Distance from source (Km)*	*Magnitude (Mw)*	*Peak Ground Acceleration (cm/s^2)*
EL1	Landers	1992	Desert Hot Springs, California	23.1	7.3	167.449
EL2	Landers	1992	Wrightwood, California	121.1	7.3	-46.470
ELP1	Loma Prieta	1989	Agnew, CA, Agnews State Hospital	21.0	7.0	163.10
ELP2	Loma Prieta	1989	Olema, CA, Point Reyes Ranger Station	106.8	7.0	-157.90
ED1	Dillon	2005	Dillon, MT - Univ of Montana-Western	22.8	5.6	-91.10
ED2	Dillon	2005	Bozeman, MT - Montana State Univ	117.3	5.6	-7.10
EA1	Anza	2005	Chihuahua Valley, CA	24.1	5.2	-39.00
EA2	Anza	2005	Chino Hills Hwy 71 & Eucalyptus	117.9	5.2	-11.73
EG1	Gilroy	2002	Hollister, CA - City Hall Annex	23.1	4.9	19.70
EG2	Gilroy	2002	San Francisco, CA - Golden Gate Bridge	121.6	4.9	-7.40
EV1	Volcano	2003	Pahala, Hawaii Is, HI Ka`u Hospital	31.3	4.6	22.90
EV2	Volcano	2003	Waimea, Hawaii Is, HI	90.9	4.6	18.40

Table 3.3: Characteristics of the Earthquake loads used to perform analysis (upward/vertical component (Y direction))

Code Name	*Earthquake Name*	*Year*	*Station measured from*	*Distance from source (Km)*	*Magnitude (Mw)*	*Peak Ground Acceleration (cm/s^2)*
EL1	Landers	1992	Desert Hot Springs, California	23.1	7.3	-163.735
EL2	Landers	1992	Wrightwood, California	121.1	7.3	28.047
ELP1	Loma Prieta	1989	Agnew, CA, Agnews State Hospital	21	7.0	82.20
ELP2	Loma Prieta	1989	Olema, CA, Point Reyes Ranger Station	106.8	7.0	55.40
ED1	Dillon	2005	Dillon, MT - Univ of Montana-Western	22.8	5.6	-61.60
ED2	Dillon	2005	Bozeman, MT - Montana State Univ	117.3	5.6	4.20
EA1	Anza	2005	Chihuahua Valley, CA Private Residence	24.1	5.2	-42.00
EA2	Anza	2005	Chino Hills Hwy 71 & Eucalyptus	117.9	5.2	4.97
EG1	Gilroy	2002	Hollister, CA - City Hall Annex	23.1	4.9	19.00
EG2	Gilroy	2002	San Francisco, CA - Golden Gate Bridge	121.6	4.9	3.30
EV1	Volcano	2003	Pahala, Hawaii Is, HI Ka`u Hospital	31.3	4.6	-17.60
EV2	Volcano	2003	Waimea, Hawaii Is, HI, Fire Station	90.9	4.6	7.30

Earthquake loads are included as both vertical and horizontal accelerations applied as uniaxial excitation input in the form of time history accelerations at the tower base. The responses that are studied from the applied accelerations are displacement at the top of the tower and the maximum stress of the wind turbine tower.

3.2.2 Aerodynamic Analysis of Wind Turbines

The wind turbines are installed at the location where there are reliable wind resources available. Such a locations are mostly away from the cities and are inhabited areas.

Once the appropriate wind velocity is determined, wind pressure and force are calculated for the tower and blades. The wind velocities are calculated by assuming the power law model for wind distribution. The rated value of wind speed is assigned as the speed at hub height and a value of 0m/s is given at the base of the tower. The wind velocity values are obtained using the equation for the power law equation from ASCE 7-05. This equation is as follows:

$$\frac{\bar{u}(z)}{\bar{u}(z_{ref})} = \left(\frac{z}{z_{ref}}\right)^n \quad (20)$$

Where $\bar{u}(z_{ref})$ is the wind velocity at reference height, z_{ref} is the reference height, z is the height for the desired wind velocity, $\bar{u}$ is the desired wind velocity and n = 1/7 for Exposure C.

The velocity pressures are then calculated along the tower using the available equation from ASCE 7-05 as follows:

$$q_z = 0.613 K_z K_{zt} K_d V^2 I \ (Nm^2) \quad (21)$$

Where K_d = 0.85 for the Main Wind Force Resisting System (MWFRS), Kzt = 1.0, Kz = 1.187 (22.6m), 1.561 (84m), 1.774 (154m) for Exposure C, I = 5% wind turbulence intensity and ρ = 1.225 kg/m^3 for air density.

In order to create a trend line that may be used to calculate the wind forces acting on the blades, the plot of pressure against the tower height is used. Values are based on a gust speed of three seconds measured at 33 feet above the ground in Exposure C in accordance with ASCE 7-16 (10) Section 26.5.1.

There were 14 different wind loads that were taken into consideration, with wind speeds ranging from 1 m/s to 75 m/s. A Weibull distribution for various wind speeds is taken into account, and 14 samples are then randomly chosen in accordance with the distribution available. This technique will guarantee that the selection is biased and that the majority of the data are centered around the turbine's rated wind speed. The wind distribution of each wind turbine is depicted in Figure 3.1 for the corresponding rated wind speed.

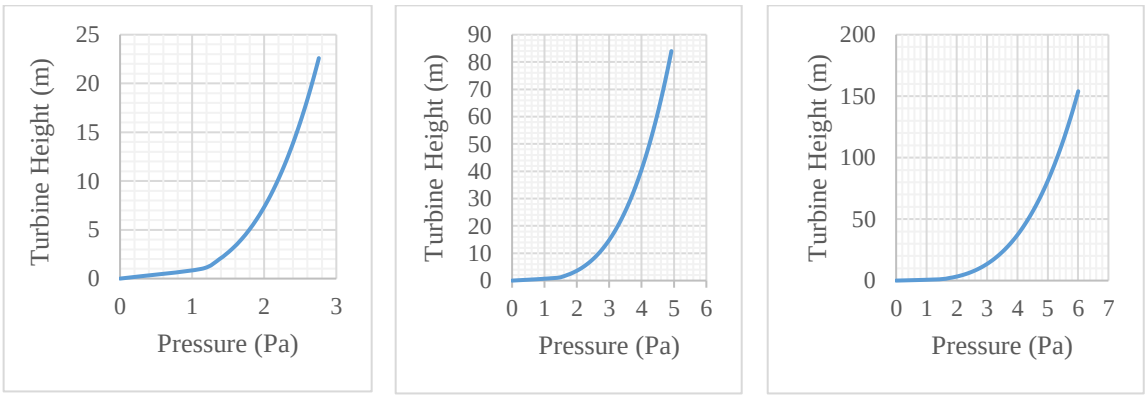

(a) (b) (c)

Figure 3.1: Wind shear distribution of the tower using Weibull probability distribution method for (a) 65kW wind turbine (b) 1.5MW wind turbine and (c) 5MW wind turbine

3.2.2.1 Wind Turbine Loads

The location and meteorological conditions are major factors which affect the flow wind. Thus, this random flow of wind is measured by wind speed and it is used to determine forces and stresses in wind turbines from finite element analysis.

Aerodynamic, gravitational, inertia and operational loads are most common types loads in the wind turbine. Figure 3.2 shows different types of loads in a typical wind turbine.

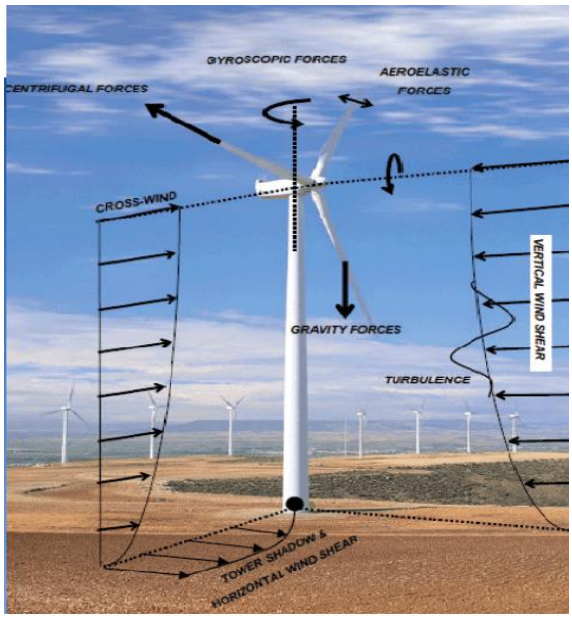

Figure 3.2: Forces in a typical wind turbine [72]

3.2.2.1.1 Aerodynamic/wind loads

Wind loads in wind turbines are created due to movement of air along the tower and blades. There are two types of aerodynamic loads along the blades which are lift force and drag force. Lift force is when the direction of air flow is perpendicular to the movement of blades whereas drag force is when air flow is parallel to the movement of blades. Thus, lift force is significant in operation condition of wind turbine otherwise drag force is the dominant force. Drag force on a tower is calculated as:

$$F_D = 0.5\,\rho\,C_D\,A\,V^2 \qquad (22)$$

Where C_D is an aerodynamic drag coefficient and A is a projected area vertical to the flow.

3.2.2.1.2 Gyroscopic Loads

These types of loads are created due to movement of the rotor of wind turbine towards the direction of wind flow using yaw driver to keep the turbine operational with good efficiency. A large gyroscopic moment will be induced in the wind turbine during fast rotation of yaw and this moment is also called pitching moment. For active yaw mechanism, the rate of rotation is low in horizontal-axis wind turbine so gyroscopic forces can be neglected. However, for passive yaw mechanism, gyroscopic forces are significant and they should be considered for design and analysis of wind turbines.

The sudden rotation of the rotor during change in direction of airflow creates extraordinary moment on the rotor blades. This is one of the reasons that the passive yaw mechanism is applied in downwind rotors that are not installed anymore around the world.

3.2.2.1.3 Wind Turbulence

The turbulence of the wind is the fluctuation of the airflow in a small-time interval which acts as a dynamic load in wind turbines. Large wind fluctuation creates fatigue in wind turbine blades which in turn could result in reduction of the durability of wind turbine blades. Wind is considered to be the average of wind speed that varies in a certain time interval. The variation in wind speed is three dimensional. However, only one dimensional (in longitudinal direction) fluctuation is considered during modeling for turbulence. This is due to the difficulty in modeling for two-dimensional turbulence.

The main parameter in turbulence is intensity which measures sudden changes in wind speed over short intervals:

$$I = \frac{\sigma_u}{\bar{u}} \qquad (23)$$

Where $\bar{u}$ is mean wind velocity and σ_u is the standard deviation ration at the same point and averaged over same period of time.

3.2.2.2 Computational Fluid Dynamics (CFD) Analysis

Wind flow is analyzed by using fluid dynamics. Computational Fluid Dynamics (CFD) is a numerical method which is used to predict fluid flow, heat transfer and chemical reactions in complex systems.

There are three fundamental principles in fluid dynamics which are principle of mass, Newton's second law (momentum) and energy conservation.

3.2.2.2.1 Mass conservation

The conservation of mass means that the rate of mass flow into a fluid element (volume) equals to the rate of increase of mass in the fluid element (volume), therefore for a compressible fluid:

$$\frac{\partial \rho}{\partial t} + div\,(\rho \boldsymbol{u}) = 0 \qquad (24)$$

Where ρ is density of the fluid and **u** is the velocity vector in Cartesian coordinates.

And the density of an incompressible fluid, such as liquid, is constant ($\frac{\partial \rho}{\partial t} = 0$), so:

$$div\, u = 0 \Rightarrow \frac{\partial u}{\partial x} + \frac{\partial v}{\partial y} + \frac{\partial w}{\partial z} = 0 \qquad (25)$$

Where u, v and w are the velocity components of **u**.

3.2.2.2.2 Newton's second law (momentum conservation)

Newton's second law declares that the rate of change of momentum equals to force summation on the fluid particles. The equations of momentum in three directions can be determined by considering the stresses in terms of the pressures on a control volume.

Therefore, the momentum equation in x, y and z components equals to:

$$\frac{\partial(\rho u)}{\partial t} + div\,(\rho u \boldsymbol{u}) = \frac{\partial(-p+\tau_{xx})}{\partial x} + \frac{\partial \tau_{yx}}{\partial y} + \frac{\partial \tau_{zx}}{\partial z} + S_{Mx} \qquad (26)$$

$$\frac{\partial(\rho v)}{\partial t} + div\,(\rho v \boldsymbol{u}) = \frac{\partial(-p+\tau_{yy})}{\partial y} + \frac{\partial \tau_{xy}}{\partial x} + \frac{\partial \tau_{zy}}{\partial z} + S_{My} \qquad (27)$$

$$\frac{\partial(\rho w)}{\partial t} + div\,(\rho w \boldsymbol{u}) = \frac{\partial(-p+\tau_{zz})}{\partial z} + \frac{\partial \tau_{xz}}{\partial x} + \frac{\partial \tau_{yz}}{\partial y} + S_{Mz} \qquad (28)$$

Where S_{Mx}, S_{My} and S_{Mz} are body forces.

3.2.2.2.3 Energy equation

The energy equation is adopted from the first law of thermodynamics. Hence, energy equation is:

$$\frac{\partial \rho i}{\partial t} + div(\rho i \boldsymbol{u}) = -p\,div\,\boldsymbol{u} + div(k\,grad\,T) + \tau_{xx}\frac{\partial u}{\partial x} + \tau_{yx}\frac{\partial u}{\partial y} + \tau_{zx}\frac{\partial u}{\partial z} +$$

$$\tau_{xy}\frac{\partial v}{\partial x} + \tau_{yy}\frac{\partial v}{\partial y} + \tau_{zy}\frac{\partial v}{\partial z} + \tau_{xz}\frac{\partial w}{\partial x} + \tau_{yz}\frac{\partial w}{\partial y} + \tau_{zz}\frac{\partial w}{\partial z} + S_i \qquad (29)$$

Where i is the internal energy, T is the temperature, k is the thermal conductivity, p is the pressure, u, v and w are the velocity components of **u** and S_i is a new source term $S_i = S_E - \mathbf{u}S_k$ which S_E is a source of energy and S_k is a mechanical (kinetic) energy source. Thus, the equation of energy for compressible fluids like air will be:

$$\frac{\partial \rho h_0}{\partial t} + div(\rho h_0 \boldsymbol{u}) = div(k\,grad\,T) + \frac{\partial p}{\partial t} + \frac{\partial(u\tau_{xx})}{\partial x} + \frac{\partial\left(u\tau_{yx}\right)}{\partial y} + \frac{\partial(u\tau_{zx})}{\partial z} +$$

$$\frac{\partial(v\tau_{xy})}{\partial x} + \frac{\partial(v\tau_{yy})}{\partial y} + \frac{\partial(v\tau_{zy})}{\partial z} + \frac{\partial(w\tau_{xz})}{\partial x} + \frac{\partial(w\tau_{yz})}{\partial y} + \frac{\partial(w\tau_{zz})}{\partial z} + S_h \qquad (30)$$

Where h_o is the specific total enthalpy and S_h is an enthalpy energy source.

3.2.2.3 Turbulence Modeling in ANSYS Fluid Flow CFX

Turbulent flow is a type of fluid (gas or liquid) flow when the velocity and other properties of the fluid fluctuate in all directions. Fluid flow in general is turbulent including air movements. Using the Navier– Stokes equations for a turbulent flow is extremely difficult due to the time-dependent, non-linear and three-dimensional

equations. Hence, the Reynolds Averaged Navier-Stokes Equation (RANS) is the most widely used for calculating industrial flows. Navier-Stokes equations are shown below:

$$\frac{\partial(\rho u)}{\partial t} + div(\rho u \boldsymbol{u}) = -\frac{\partial p}{\partial x} + div(\mu\ grad\ u) + S_{Mx} \qquad (31)$$

$$\frac{\partial(\rho v)}{\partial t} + div(\rho v \boldsymbol{u}) = -\frac{\partial p}{\partial y} + div(\mu\ grad\ v) + S_{My} \qquad (32)$$

$$\frac{\partial(\rho w)}{\partial t} + div(\rho w \boldsymbol{u}) = -\frac{\partial p}{\partial z} + div(\mu\ grad\ w) + S_{Mz} \qquad (33)$$

There are three most common types of turbulence models in a finite element analysis and these are k - ε model, k - ω model and Shear-Stress Transport (SST) model. This section presents the equations used for respective solvers in these models.

3.2.2.3.1 Standard k — ε model

The considered model for the free stream fluid is the k — ε model which has one equation for the turbulent kinetic energy, k, and one equation for the turbulent dissipation rate, ε. Hence, the turbulent viscosity of this model can be obtained from the below equation:

$$\mu_t = \frac{\rho C_\mu k^2}{\varepsilon} \qquad (34)$$

Where C_μ is a dimensionless constant, k and ε are determined by the following equations:

$$\frac{\partial(\rho k)}{\partial t} + div(\rho k U) = div\left[\left(\mu + \frac{\mu_t}{\sigma_k}\right) grad\ k\right] + P_k - \rho\varepsilon \qquad (35)$$

$$\frac{\partial(\rho \varepsilon)}{\partial t} + div(\rho \varepsilon U) = div\left[\left(\mu + \frac{\mu_t}{\sigma_\varepsilon}\right) grad\ \varepsilon\right] + \frac{\varepsilon}{k}(C_{\varepsilon 1} P_k - C_{\varepsilon 2}\rho\varepsilon) \qquad (36)$$

P_k is the turbulence production and δ_k, δ_ε, $C_{\varepsilon 1}$ and $C_{\varepsilon 2}$ are constants and equal to:

$$\delta_k = 1;\ \delta_\varepsilon = 1.3;\ C_{\varepsilon 1} = 1.44;\ C_{\varepsilon 2} = 1.92$$

3.2.2.3.2 Standard k — ω model

This model is suitable for calculating the turbulence near the wall. The k — ω model is based on model transport equations for the turbulence kinetic energy, k, and the specific dissipation rate, ω. These values are derived from the equations below:

$$\frac{\partial(\rho k)}{\partial t} + div(\rho k \boldsymbol{U}) = div\left[\left(\mu + \frac{\mu_t}{\sigma_k}\right) grad\ k\right] + P_k - \beta' \rho k \boldsymbol{\omega} \qquad (37)$$

$$\frac{\partial(\rho \boldsymbol{\omega})}{\partial t} + div(\rho \boldsymbol{\omega} \boldsymbol{U}) = div\left[\left(\mu + \frac{\mu_t}{\sigma_\omega}\right) grad\ \omega\right] + \alpha \frac{\boldsymbol{\omega}}{k} P_k - \beta \rho \boldsymbol{\omega^2} \qquad (38)$$

δ_k, δ_w, α, β and β' are constants and equal to:

$\delta_k = 1$, $\delta_w = 2$, $\alpha = 5/9$; $\beta = 0.075$; $\beta' = 0.09$

Therefore, the turbulent viscosity of this model is:

$$\mu_t = \rho \frac{k}{\omega} \qquad (39)$$

The advantage of this method is using the low-Reynolds number near the wall and easier modeling which gives us more accurate and more robust results but the disadvantage of this method is high sensitivity to the free-stream conditions.

3.2.2.3.3 Shear-Stress Transport (SST) model

The SST model is based on the k-ω model and has the same automatic wall treatment. This model is mixing the best properties of k-ω model and k-ε model which means around the near-wall region using the k-ω model and in free-stream flow using the k-ε model in order to get better results. This model is used in this research.

3.2.2.4 Fluid Structure Interaction

Fluid-structure interaction (FSI) is system which represents the effects of fluid on the deformation of solid geometry and vice-versa. There are two types of FSI which are one-way FSI and two-ways FSI. The result obtained from computational fluid dynamics (CFD) analysis is used to calculate forces on the structure due to aerodynamics and these forces are applied as a load to the mechanical analysis, and if the result has passed back to CFD then it is called two-way FSI otherwise is called one-way FSI.

The one-way FSI allows computational fluid dynamics (CFD) and finite element analysis (FEA) solvers to be run independently whereas in two ways FSI, both solvers have to be run at the same time because the results are transferred between CFD and FEA for each step until overall equilibrium is reached among the Mechanical application solution and ANSYS CFX solution. In this research, one-way FSI is considered for the simulation of wind turbines.

3.2.3 Load Combinations

Linear combinations of seismic and operational loads with load factor of one is suggested by IEC (2005), or GL (2003) guidelines. However, a study by Asareh (2015) suggests 0.75 as the load factor for operational and seismic load interaction during extreme seismic and wind events.

The decoupling approach of analysis of responses is implemented in this study. For the finite element model developed in ANSYS Workbench 2022, maximum displacements and stresses of the wind turbine tower are investigated independently due to wind and seismic loads. Then, the response parameters due to aerodynamic and seismic interaction are computed by using the square root of square sum (SRSS) combination rule.

Upon the completion of the analyses, the output of the simulations is post-processed to determine the P-Δ (second order) effect of the tower of the wind turbines due to aerodynamics and seismic load interaction.

3.2.4 Operation Conditions

Wind turbines are not entirely static structures since the rotor of wind turbines is designed to rotate for generating power during operation. Therefore, operational dynamics will influence the structural response due to aerodynamic damping.

Different turbine operational scenarios such as (i) Parking/idling conditions with the presence of seismic loads, (ii) normal operational conditions with no earthquake, (iii) normal operational conditions with earthquake, and (iv) earthquake-induced emergency shutdown is simulated with various loading conditions to determine response behavior (top displacement and maximum stresses of the wind turbine tower) of wind turbine towers.

3.2.5 Stability Analysis of Wind Turbines

In order to prevent stability failure, which causes the structure to collapse before yielding (premature failure), proper care should be given to the verification of wind turbines during the design and analysis. Therefore, in addition to screening for buckling, the P-Δ (second order) effect of the tower should be taken into account to prevent stability failure.

In the second-order analysis, the structure's deformation as a result of applied loads is taken into account. P-Δ and p-δ effects are the two categories of second-order effects. P-δ is the result of loads acting on the displaced location of joints or nodes in a structure, whereas P-Δ is the result of loads acting on the deflected shape of a member between joints and nodes. Second-order effects are also called geometrical nonlinearities.

According to Eurocode 3, section 5.2.1 (4), if the deformation significantly increases the forces in the structure or if the deformations significantly alter structural behavior, the effects of the deformed geometry of the structure (second-order effects) must be taken into account. For elastic global analysis, clause 5.2.1 says that the second-order effects are significant if the parameter $\alpha_{cr} < 10$, where α_{cr} is determined by first-order analysis.

$$\alpha_{cr} = \left(\frac{H_{ED}}{V_{ED}}\right)\left(\frac{h}{\delta_{h,ED}}\right) \qquad (40)$$

Where: $\boldsymbol{\alpha_{cr}}$ is the factor by which the design loading would have to be increased to cause elastic instability in a global mode

$\boldsymbol{H_{ED}}$ is the design value of the horizontal reaction at the bottom of the storey to the horizontal loads and the equivalent horizontal forces

$\boldsymbol{V_{ED}}$ is the total design vertical force on the structure on the bottom of the storey

$\boldsymbol{\delta_{h,ED}}$ is the horizontal displacement at the top of the story, relative to the bottom of the story.

h is the story height.

These secondary effects increase the member's deformation and introduce new stresses to it. As a result, the structure gets weaker or could become unstable. Deierlein et al. (2010) assert that P-Δ may be a factor that results in dynamic instability, ratcheting of residual deformations, and loss of lateral resistance [73].

In this study, wind turbines can be represented as cantilever columns. The first order top transverse displacement (δ) of the cantilever column loaded by axial (N) and horizontal (F) forces, is given by:

$$\delta = \frac{Fh^3}{3EI} \qquad (41)$$

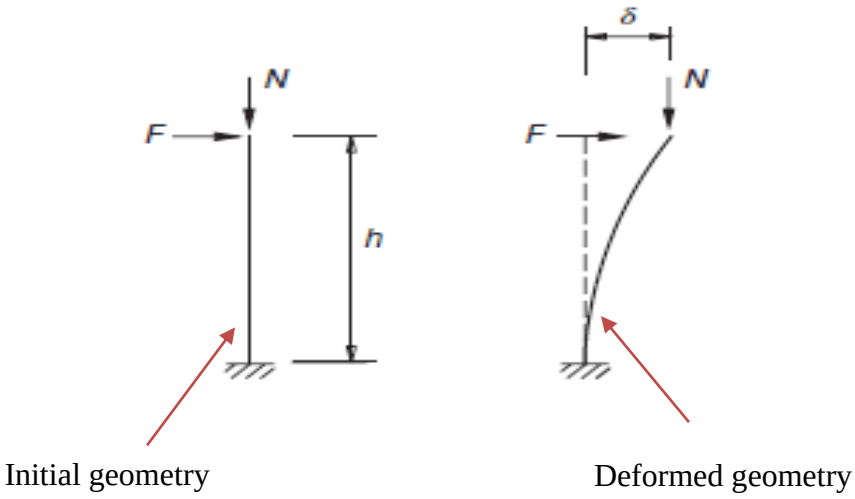

Figure 3.3: Cantilever Column in the initial and deformed configuration

CHAPTER FOUR: MODELING AND ANALYSIS

In order to develop finite element models that can be used to analyze the effect of wind and earthquake load interaction on the stability of land-based wind turbine towers, it is necessary to identify the material properties of the turbines, the geometry of the turbines and load combinations. Three turbine models are developed by using ANSYS Workbench 2022 for analysis under various load combinations. The development of these models is discussed in this chapter.

4.1 Material Properties for modeling

Wind turbines are often made of steel (66-79% of the overall turbine mass), fiberglass, resin, or plastic (11-16%), iron or cast iron (5-17%), copper (1%), and aluminum (0-2%), according to a report from the National Renewable Energy Laboratory (Table 30) [74].

Steel material with a modulus of elasticity of 200 GPa, a Poisson ratio of 0.3, a yield strength of 250 MPa, and a density of 7850 kg/m^3 is used to simulate the tower, hub, and nacelle. However, during computation, the structural paint, flanges, bolts, and welding point masses are not considered. The effective density is changed to ensure the structure's mass matches what is actually there. The nacelle, a hollow steel box containing a rotor, magnets, electrical cables, and other components for producing electricity, is also significantly lighter than a steel box of equivalent volume. Hence, an equivalent low density for the nacelle in the finite element model is considered.

Most blades are made with fiberglass-reinforced polyester or epoxy. Carbon fiber or aramid (Kevlar) is also used as reinforcement material. The material used for modeling of the blade is composite material.

Table 4.1 shows material properties of components of developed finite element models of wind turbines with appropriate approximations and modifications.

Table 4.1: Material properties of wind turbines of developed Finite Element Models

No.	*Parameter*	*Steel*	*Composite of 65kW wind turbine*	*Composite of 1.5MW wind turbine*	*Composite of 5MW wind turbine*
1	Modulus of Elasticity in the x direction (GPa)	200	35	7.78	7.78
	Modulus of Elasticity in the y and z directions (GPa)	200	9	7.78	7.78
2	Coefficient of Thermal Expansion in y and z (/^{o}c)	$1.2x10^{-5}$	$2.5\ x10^{-5}$	$3\ x10^{-5}$	$3\ x10^{-5}$
	Coefficient of Thermal Expansion in x (/^{o}c)	$1.2\ x10^{-5}$	$5.5\ x10^{-6}$	$4.5\ x10^{-7}$	$4.5\ x10^{-7}$
3	Poisson's Ratio in xy and xz plane	0.3	0.28	0.27	0.27
	Poisson's Ratio in yz plane	0.3	0.4	0.42	0.42
4	Shear Modulus of elasticity in xy and xz plane (GPa)	76.923	4.7	5	5
	Shear Modulus of elasticity in yz plane (GPa)	76.923	3.5	3.08	3.08
5	Tensile yield strength (MPa)	250	250	250	250
6	Tensile ultimate strength (MPa)	460	440	440	440

4.2 Geometric Properties for modeling

In order to make sure that the results of this research are reliable, it is important to develop the geometry of the models appropriately. Geometric data of wind turbines in this study is obtained from two sources for developing a finite element model for this research. The first source is from a full-scale Shake Table test conducted for a 65kW NORDTANK wind turbine at the University of California San Diego (UCSD) to explore the response of a parked turbine due to base excitation. The second source for 1.5MW and 5MW wind turbines is obtained from Wind Partnership for Advanced Component Technologies (WindPACT) wind turbine specifications provided by National Renewable Energy Laboratory (NREL).

The geometry of 1.5 MW and 5 MW wind turbine towers is modeled as a shell element with hollow circular cone with constant thickness. The geometry of the 65kW wind turbine tower, on the other hand, is made of three hollow cylindrical and two hollow conic transition sections and it is modeled accordingly with constant thickness.

The geometry of the nacelle is usually made of long sections with rounded or rectangular ends. The nacelle holds various mechanical components including the gear-box, generator, and shaft. Since this study does not evaluate any mechanical performance of the wind turbine, the nacelle is modeled as a solid element with a rectangular cross-section in all three models.

The geometry of the hub is modeled as a solid element with a circular cylindrical cross-section in all three models. Finally, the geometry of the blades is modeled as a shell element with cross-sections of blades developed appropriately with properties defined in Table 4.2.

Once all of the components of the wind turbine are developed, each configuration is assembled in ANSYS Workbench 2022. Each part contains its own material and section properties. After each part is properly defined and meshed, the whole turbine is assembled and given the appropriate constraints (boundary conditions) and loads.

Figure 4.1: Geometry of 65kW, 1.5MW and 5MW wind turbines respectively.

Table 4.2: Properties of NORDTANK wind turbine [75] and WindPACT Reference Wind Turbines (Jennifer Rinker and Katherine Dykes, 2018 [76])

No.	*Parameter*	*65kW NORDTANK wind turbine*	*1.5MW WindPACT Baseline Wind Turbine Model*	*5MW WindPACT Baseline Wind Turbine Model*
1	Rotor Orientation	Upwind	Upwind	Upwind
2	Configuration	Three blades	Three blades	Three blades
3	Rated wind speed	9.444 m/s	11 m/s	11.4 m/s
4	Rated Tip Wind Speed	53.6 m/s	75 m/s	75 m/s
5	Tower Mass	6400 kg	125,363 kg	775,094 kg
6	Nacelle Mass	2400 kg	52,839 kg	270,669 kg
7	Rotor Hub Mass	246.93 kg	19,186 kg	125,970 kg
8	Blade Mass	1653.07 kg	4,336 kg	27,854 kg
9	Hub Height	22.6 m	84 m	154 m
10	Blade Length/Radius	8 m	33.25 m	60.8 m
11	Blade Thickness	60 mm	400 mm	560 mm
12	Maximum Blade Chord	8% of radius	8% of radius	8% of radius
13	Hub Radius	5% of radius	5% of radius	5% of radius
14	Tower Height	21.95 m	82.39 m	151.07 m
15	Base Outer Diameter	2.02 m	5.66 m	10.17 m
16	Lower Section Length	6.06 m	-	-
17	Transition Length	1.9 m	-	-
18	Middle Outer Diameter	1.58 m	-	-
19	Middle Section Length	6.04 m	-	-
20	Top Outer Diameter	1.06 m	2.57 m	4.41 m
21	Top Section Length	6.05 m	-	-
22	Tower Thickness	5.3 mm	17.39 mm	35.70 mm

4.3 Finite Element Analysis of Wind Turbines for seismic loads

Each of the wind turbine's finite element models consists of a tall, thin tower, a nacelle, a hub, and a rotor. Shell components are used to mesh the tower and rotor blades, whereas solid elements are used to mesh the nacelle and hub. The tower's base is constrained in all directions. Structural steel was used for the tower, nacelle, and hub models. The nacelle weighs substantially less than a steel box with the same volume since it is a hollow steel box that houses a rotor, magnets, electrical cables, and other components for producing electricity. Hence, an equivalent low density for the nacelle in the FE model is

considered. However, carbon fiber composite material is used for modeling the rotor blades.

Table 4.3: Mass and density of turbine components of developed wind turbine models

No.	*Parameter*	*65kW NORDTANK wind turbine*	*1.5MW WindPACT Baseline Wind Turbine Model*	*5MW WindPACT Baseline Wind Turbine Model*
1	Tower Density (kg/m3)	11248.396	6966.868	6574.033
2	Tower Mass (kg)	6400.000	129060.000	812150.000
3	Nacelle Density (kg/m3)	226.223	356.115	323.287
4	Nacelle Mass (kg)	2400.000	73470.000	391880.000
5	Hub Density (kg/m3)	2284.908	3231.272	6320.939
6	Hub Mass (kg)	246.930	19186.000	125970.000
7	Blades Density (kg/m3)	1983.954	371.265	731.249
8	Blades Mass (kg)	1653.070	4336.000	27854.000

Table 4.4: Mesh statistics of developed finite element wind turbine models

No.	*Parameter*	*65kW NORDTANK wind turbine*	*1.5MW WindPACT Baseline Wind Turbine Model*	*5MW WindPACT Baseline Wind Turbine Model*
1	Number of nodes in Tower	9180	12716	14866
	Number of elements in Tower	3048	4228	4956
2	Number of nodes in Nacelle	8592	9207	10815
	Number of elements in Nacelle	1916	2176	2399
3	Number of nodes in Hub	270	1433	1795
	Number of elements in Hub	42	390	595
4	Number of nodes in Blades	1506	3000	3510
	Number of elements in Blades	411	861	1017

Figure 4.2: Mesh of 65kW, 1.5MW and 5MW wind turbines from left to right respectively.

4.4 Model verification for natural frequency of wind turbines

Natural frequency is the frequency at which a system tends to oscillate in the absence of any driving or excitation force, and the motion pattern of a system oscillating at its natural frequency is referred to as the natural mode. A modal analysis technique is used to analyze a structure's behavior and determine its inherent frequencies and mode shapes. Either experimental modal analysis or finite element analysis can be used for the numerical simulation of natural frequency and natural modes.

The first 42 modes were analyzed by using ANSYS modal analysis that included more than 88% of the effective mass. From the effective mass to total mass ratio obtained it is seen that the first two modes have fundamental effects on the wind turbine's dynamic behavior in the corresponding fore-aft (FA) and side-side (SS) directions as shown in Table 4.5, whereas the other modes have a much smaller effect.

Table 4.5: Modal participation factor of the first two modes of the wind turbine towers at parked condition from ANSYS modal analysis

No.	Modes	65kW Wind Turbine	1.5MW Wind Turbine	5MW Wind Turbine
1	1st Mode of Tower SS	51.869%	64.837%	62.369%
2	1st Mode of Tower FA	43.859%	62.367%	60.330%
3	2nd Mode of Tower FA	14.151%	14.330%	15.129%
4	2nd Mode of Tower SS	13.794%	9.803%	11.272%

Validating the natural frequencies of the wind turbines is necessary in order to create an adequate finite element model for the examination of the impact of seismic and aerodynamic load interactions on the structural stability of wind turbine towers. Making sure that developed finite element models have less than 10% inaccuracy from empirically observed values is crucial.

In order to validate the FEM established in this study, the modal analysis of the wind turbine is performed for the first two modes' natural frequencies since the first two modes are the most significant modes in the analysis of the wind turbine. Experimentally observed natural frequencies of 65kW, 1.5MW and 5MW wind turbines are compared with their respective natural frequencies of wind turbine towers obtained from developed finite element models as summarized in Table 4.6.

In order to verify the experimental/reference results, the natural frequencies of the first and second modes of wind turbines in the fore-aft (FA) and side-side (SS) directions are compared with those of obtained from finite element models analysis.

Table 4.6: Full-system natural frequencies of the first two modes of the wind turbine towers in Hertz (Hz) at parked condition

No.	***Item***	***Type of modal Analysis***	***65kW Wind Turbine***	***1.5MW Wind Turbine***	***5MW Wind Turbine***
1	Natural Frequency of 1st Mode of Tower SS	Experimental	1.7 Hz	0.394 Hz	0.219 Hz
		Finite Element Method (ANSYS)	1.5479 Hz	0.3924 Hz	0.22419 Hz
		Percentage error	-8.95%	-0.41%	+2.37%
2	Natural Frequency of 1st Mode of Tower FA	Experimental	1.7 Hz	0.394 Hz	0.219 Hz
		Finite Element Method (ANSYS)	1.8017 Hz	0.3996 Hz	0.22957 Hz
		Percentage error	+5.98%	+1.42%	+4.83%
3	Natural Frequency of 2nd Mode of Tower FA	Experimental	11.7-12.3 Hz	2.786 Hz	1.502 Hz
		Finite Element Method (ANSYS)	9.6537 Hz	2.6968 Hz	1.4872 Hz
		Percentage error	-17.49%	-3.2%	-0.985%
4	Natural Frequency of 2nd Mode of Tower SS	Experimental	11.7-12.3 Hz	2.974 Hz	1.613 Hz
		Finite Element Method (ANSYS)	11.794 Hz	3.0986 Hz	1.5446 Hz
		Percentage error	+0.8%	+4.2%	-4.24%

It can be seen that the frequencies of the first fore-aft (FA) and side-side (SS) modes of the wind predicted in this study are very close to the experimental results. A relatively larger deviation is observed in the 2nd fore-aft mode frequency. The reason is that the connection structures are not considered. However, the absolute errors between the FEM results and experimental results are lower than 10% for the first mode. Therefore, the comparison has confirmed that the FEM is well established.

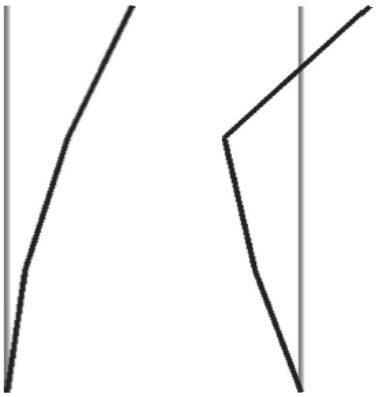

(a) 1.7 HZ (b) 11.7 – 12.3 HZ

Figure 4.3: Experimentally observed natural frequency in FA direction of (a) first mode (b) second mode (for 65kW)

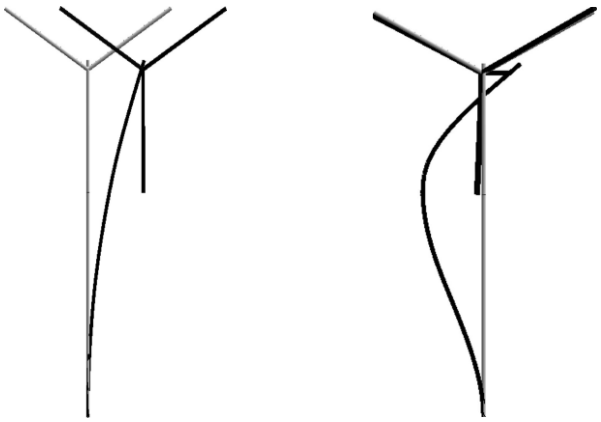

(a) 1.7 HZ (b) 11.7 – 12.3 HZ

Figure 4.4: Experimentally observed natural frequency in SS direction of a) first mode b) second mode (for 65kW)

The above experimentally obtained values are used for validation of results that are obtained from the finite element analysis (FEA) of the developed wind turbine models.

4.4.1 Natural frequencies of 65kW turbine from FEA

From developed finite element models, the following results are obtained from analysis by using ANSYS Workbench 2022 as shown in Figures 4.5 and 4.6.

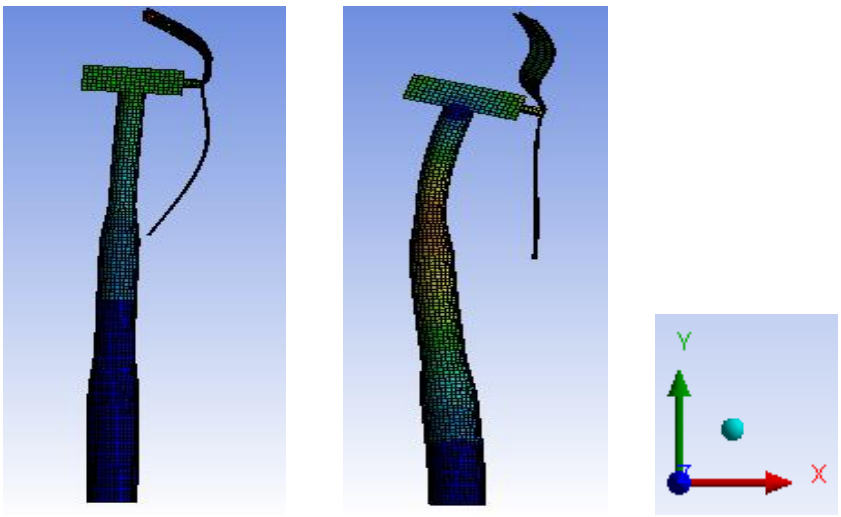

(a) 1.8017 Hz (b) 9.6537 Hz

Figure 4.5: Natural frequency in FA direction of (a) first mode (b) second mode (for 65kW)

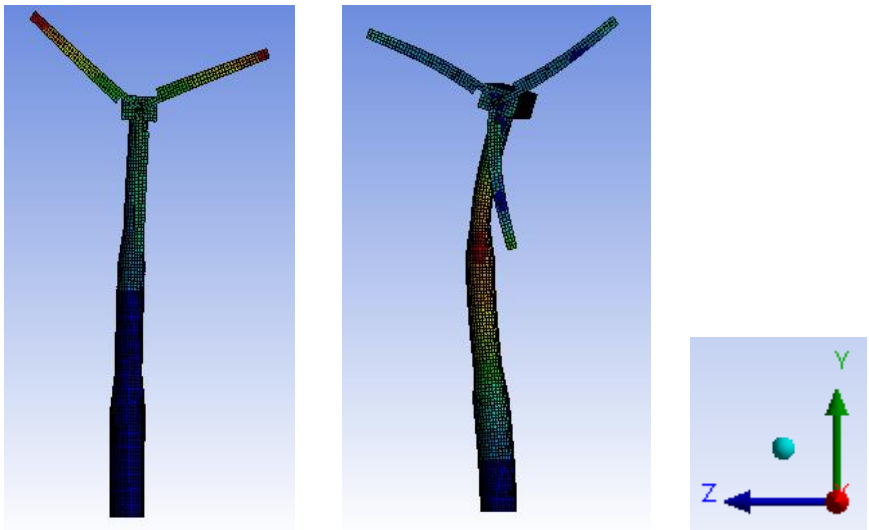

(a) 1.5479 Hz (b) 11.794 Hz

Figure 4.6: Natural frequency in SS direction of (a) first mode (b) second mode (for 65kW)

4.4.2 Natural frequencies and modes of 1.5MW turbine from FEA

From developed finite element models, the following results are obtained from analysis by using ANSYS Workbench 2022 as shown in Figures 4.7 and 4.8.

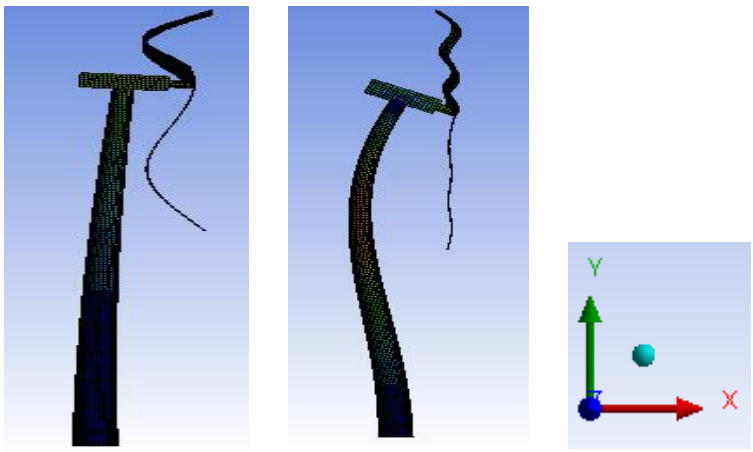

(a) 0.39961 Hz (b) 2.6968 Hz

Figure 4.7: Natural frequency in FA direction of (a) first mode (b) second mode (for 1.5MW)

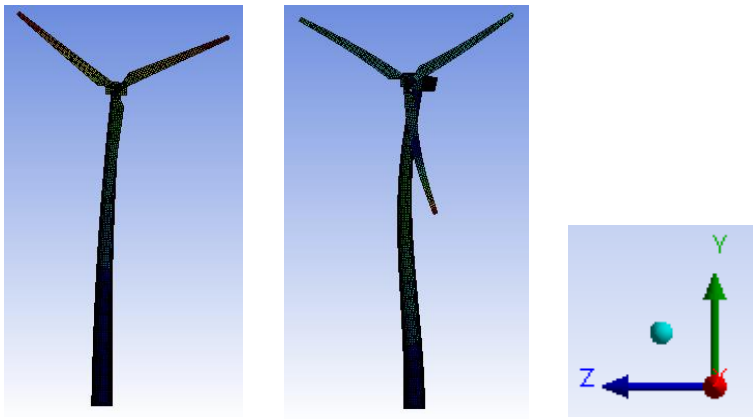

(a) 0.3924 Hz (b) 3.0986 Hz

Figure 4.8: Natural frequency in SS direction of (a) first mode (b) second mode (for 1.5MW)

4.4.3 Natural frequencies and modes of 5MW turbine from FEA

From developed finite element models, the following results are obtained from analysis by using ANSYS Workbench 2022 as shown in Figures 4.9 and 4.10.

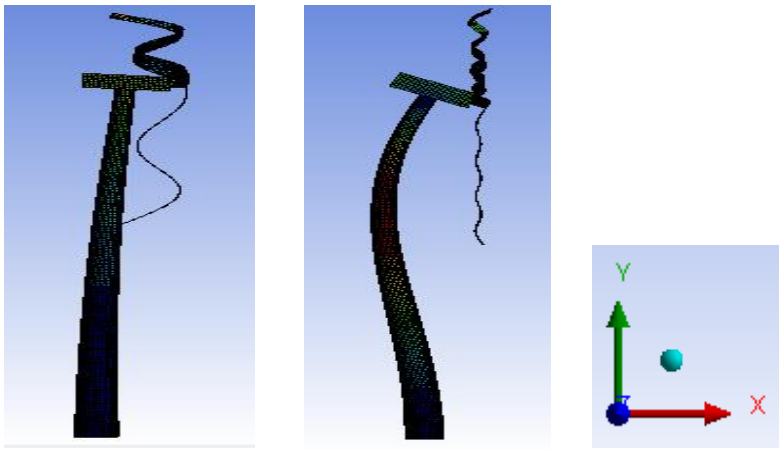

(a) 0.22957 Hz (b) 1.4872 Hz

Figure 4.9: Natural frequency in FA direction of (a) first mode (b) second mode (for 5MW)

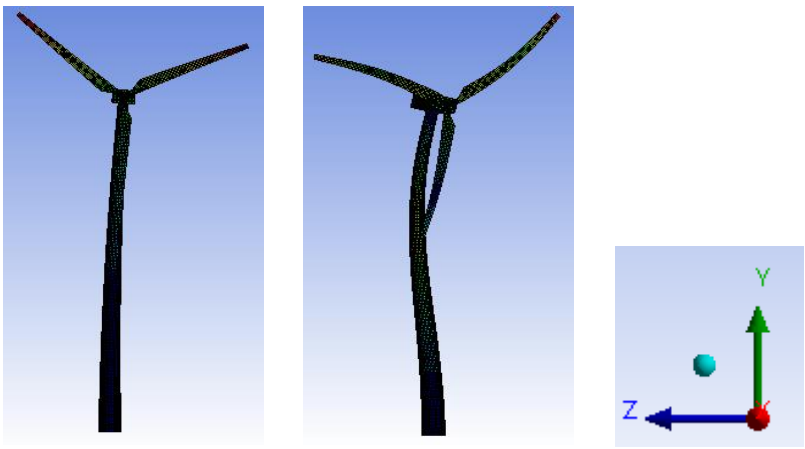

(a) 0.22419 Hz (b) 1.5446 Hz

Figure 4.10: Natural frequency in SS direction of (a) first mode (b) second mode (for 5MW)

4.5 Numerical Analysis of Wind Turbines for Aerodynamic loads

Analysis of the effect of wind load on wind turbines is best represented by using fluid dynamics. Thus, Computational Fluid Dynamics (CFD) is used for the aerodynamic analysis of wind turbines by using the finite volume method using ANSYS Fluid Flow CFX. The finite volume method is the most widely used discretization technique in CFD and it divides the main flow domain into control volumes such as a stationary and rotating domain for analysis of wind turbine models and then integrates the equations over each control volume.

4.5.1 Geometric wind farm models of wind turbines

The first step in aerodynamic analysis of wind turbine models is to select the shape of the general flow domain. A rectangular prism is selected to represent the shape of the flow domain as shown in Figure 4.11. After the general domain shape has been defined, the rotating domain and stationary domain of the wind turbine are defined and the wind turbine models are placed at the center of the general flow domain. The dimensions of all domains chosen for simulation in this study are shown in Table 4.7 and 3D geometric models are developed in ANSYS SpaceClaim for tower, nacelle, hub and blades.

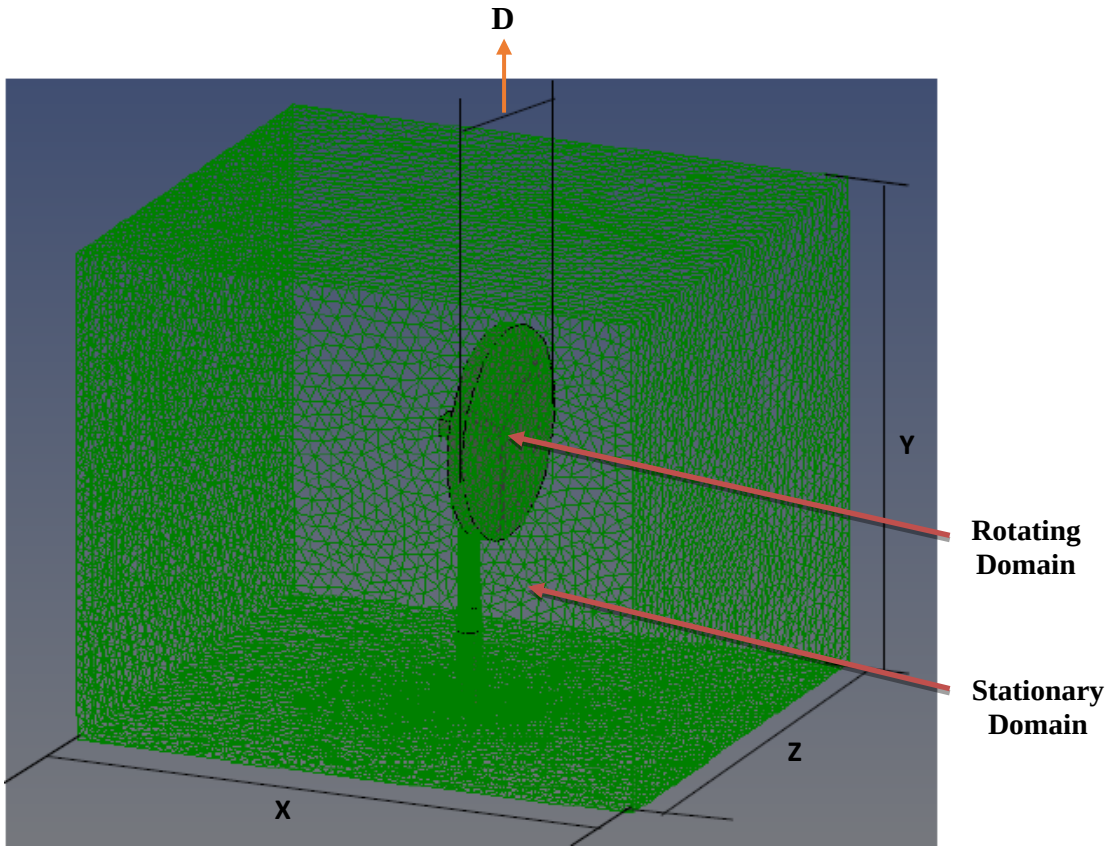

Figure 4.11: Flow domain of wind turbine

The dimension represented by the above figure is the flow domain which divides into rotating and stationary domains as shown in Figure 4.11. A summary of the dimensions of the flow domain for each wind turbine is shown in Table 4.7.

Table 4.7: Dimensions of flow domain and rotating domain for each wind turbine

Item	***65kW Wind Turbine***	***1.5MW Wind Turbine***	***5MW Wind Turbine***
X (m)	45	100	200
Y (m)	40	140	280
Z (m)	40	100	200
D (m)	17	68	125

4.5.2 Meshing of wind turbines using ANSYS CFX

The next step is the meshing of all domains. Meshing in computational fluid dynamics (CFD) needs to produce high-quality meshes in order to obtain accurate results. In this study, the tetrahedral mesh has been chosen with advanced size function in ANSYS due to the complexity of the model. This function can be effective for creating high-quality meshes around the solid walls. CFD problems require the creation of finer mesh with slow transition. Meshing statistics for each wind farm model developed are shown in Table 4.8.

Table 4.8: Meshing for each wind farm models

Mesh Statistics	***65 KW Wind Turbine***	***1.5MW Wind Turbine***	***5MW Wind Turbine***
Number of nodes	599418	681272	835361
Number of elements	423586	484303	595902

Meshing for the whole domain which includes both the flow domain and the solid domain (wind turbine) is created for wind farm models. Figure 4.12 through Figure 4.14 shows the final mesh that has been created in the ANSYS Fluid Flow CFX.

The model setup is another important step for the aerodynamic analysis of wind turbine models in ANSYS CFX. After appropriate and suitable meshes are created, it is necessary to define boundary conditions, types of analysis, interfaces, etc.

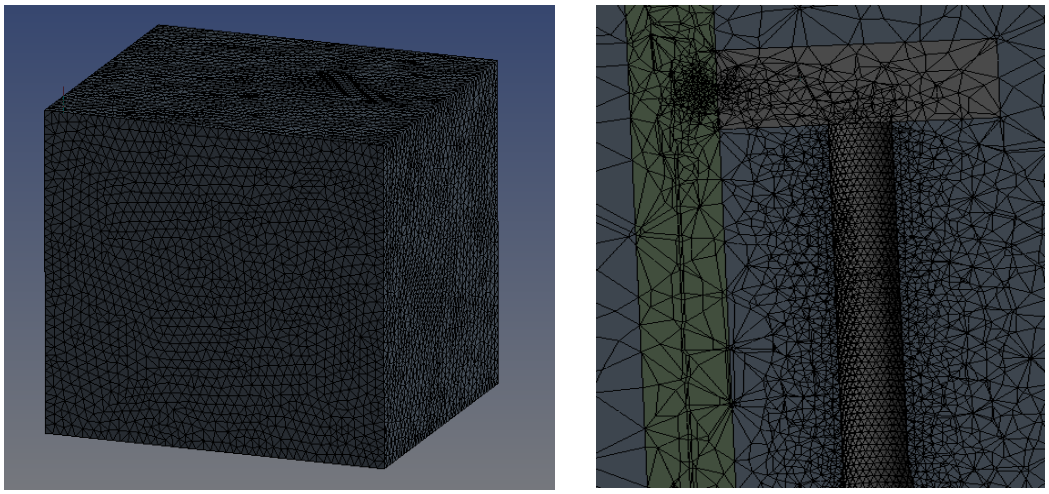

(a) (b)

Figure 4.12: ANSYS CFX final meshes for 65kW Wind Turbine (a) whole domain

(b) section view

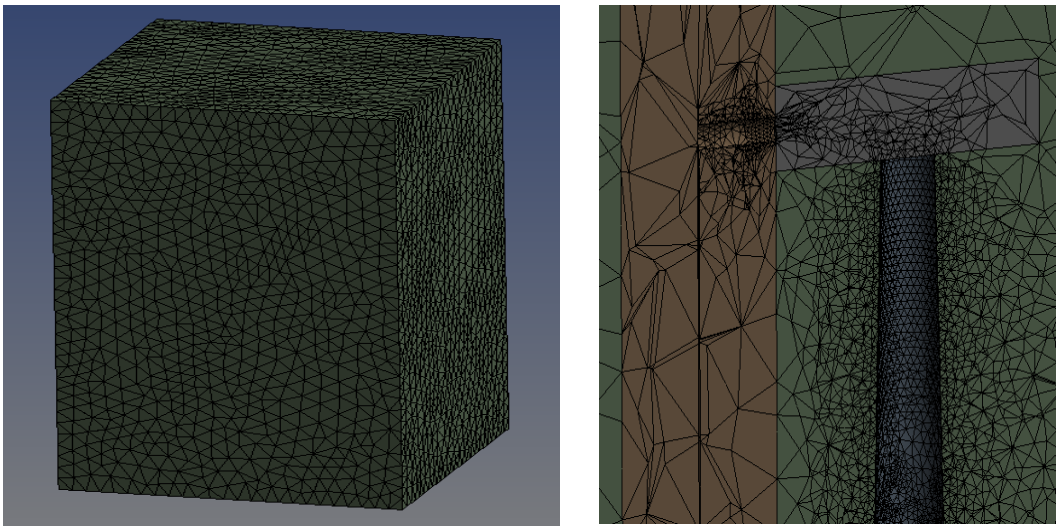

(a) (b)

Figure 4.13: ANSYS CFX final meshes for 1.5MW Wind Turbine (a) whole domain

(b) section view

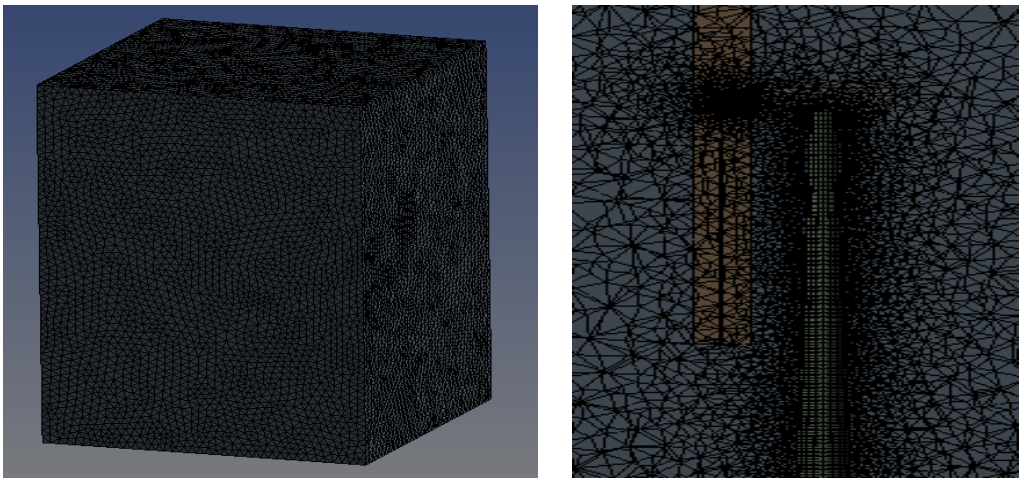

(a) (b)

Figure 4.14 ANSYS CFX final meshes for 5MW Wind Turbine (a) whole domain (b) section view

4.5.3 Fluid flow CFX Model set up for each wind turbines

After appropriate and suitable meshes are created, it is necessary to define domains, boundary conditions, types of analysis, interfaces, etc. In order to solve the problem, the flow domain is discretized into two types of domains which are stationary and rotating domains as shown in Figure 4.11.

In order to rotate the rotor in ANSYS, we should use transient analysis instead of steady-state analysis since we need to account for turbulence of the wind. Therefore, the total time and time step should be defined in the analysis section. Simulation of wind turbines for wind loads is conducted for a total time of 40 seconds with a time step of 0.1 seconds. Figure 4.11 represents the domains that have been used during the simulation.

4.5.3.1 Boundary Conditions of wind turbine models

The speed of wind varies with change in height of the wind turbine. In this study variation in temperature is not considered and the air is assumed to be at 25^0C with medium turbulence intensity of 5%. A set of 14 different velocity inlet is considered to study the effect of variation of wind speed magnitude on the stability of wind turbine towers. Velocities of 1, 3, 5, 7, 9, 11, 13, 15, 17, 19, 21, 23, 25 and 75m/s are used for simulation for all types of wind turbine models used in this study.

The type of outlet has been considered an opening class where fluid can be exited and entered through the boundary surfaces. The value of relative pressure is also supposed to

be zero due to the unbounded area around the wind turbine. Figure 4.15 shows the assumed boundary conditions in the simulation. No-slip sidewalls with smooth wall roughness are considered for analysis.

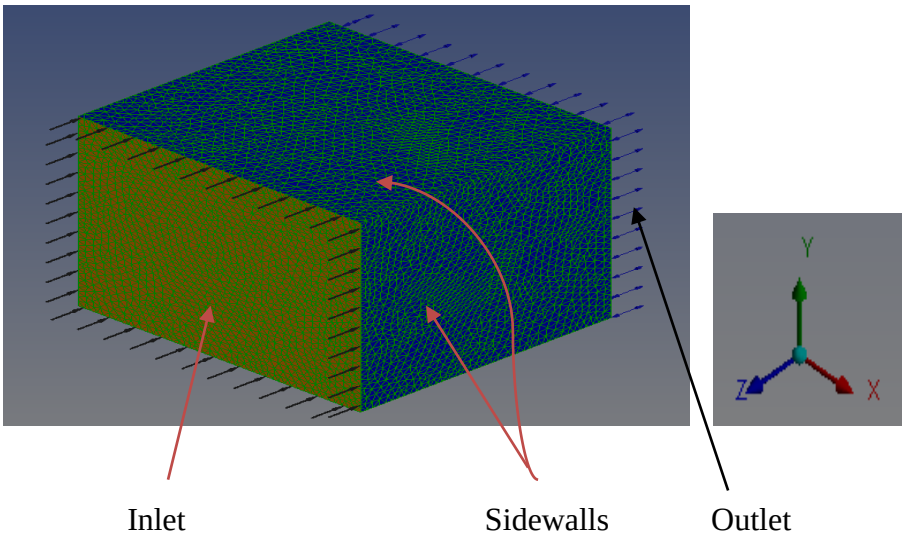

Figure 4.15: Boundary conditions in CFX for wind turbines

The Shear Stress Transport (SST) turbulence model is chosen for both the stationary domain and the rotating domain due to the advantage of this model compared to other models discussed in the next chapter.

The angular velocity of the rotating domain should be set at 20 rev/min, 15 rev/min and 12.1 rev/min for 65kW, 1.5MW and 5MW wind turbines respectively. Therefore, the rotor speed has been fixed at the constant value in the software. Boundary conditions and type of analysis are summarized in Table 4.9.

Table 4.9: Boundary conditions and type of analysis used for simulation of the turbines

Simulation Parameters	***Type/value***
Inflow	Air (at 25^0c)
Turbulence intensity at the inflow	5%
Outflow	Opening (0 Pa)
Sidewalls	No slip walls
Analysis type	Transient
Turbulence model	Shear Stress Transport (SST)
Time step	0.1s
Simulation time	40s

4.5.4 Structural Model Set Up

Finally, the pressure created due to wind load in CFD analysis should be mapped to static structural (mechanical) analysis to determine stresses and deflections in the tower of each wind turbine. The significant feature of the structural part is importing the effective forces from the CFX into the mechanical. Mapping of the forces on each node in CFX into the mechanical node depends on some factors such as the quality of the mesh, element size, etc. Thus, the percentage of mapping and the value of forces after importing the loads should be checked in order to be sure that all the forces are properly mapped. Figure 4.16 illustrates the imported loads on the rotor, nacelle and the tower from CFX into the Mechanical.

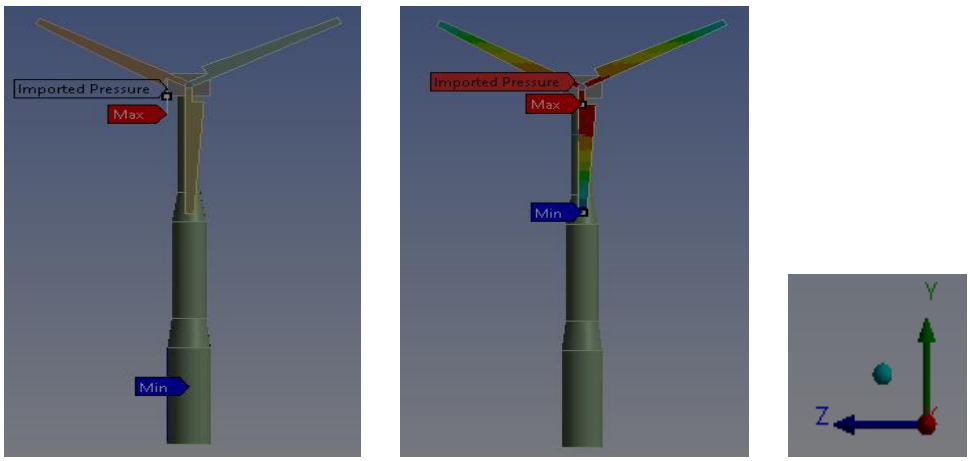

(a)

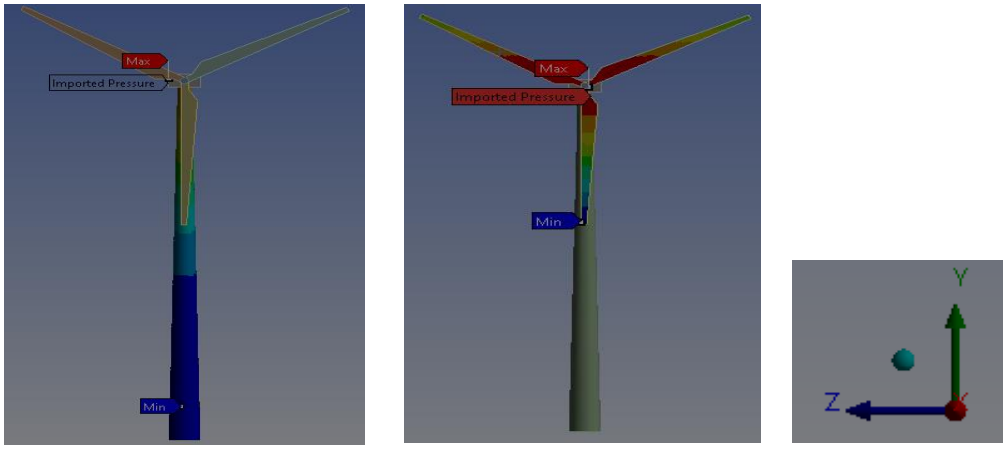

(b)

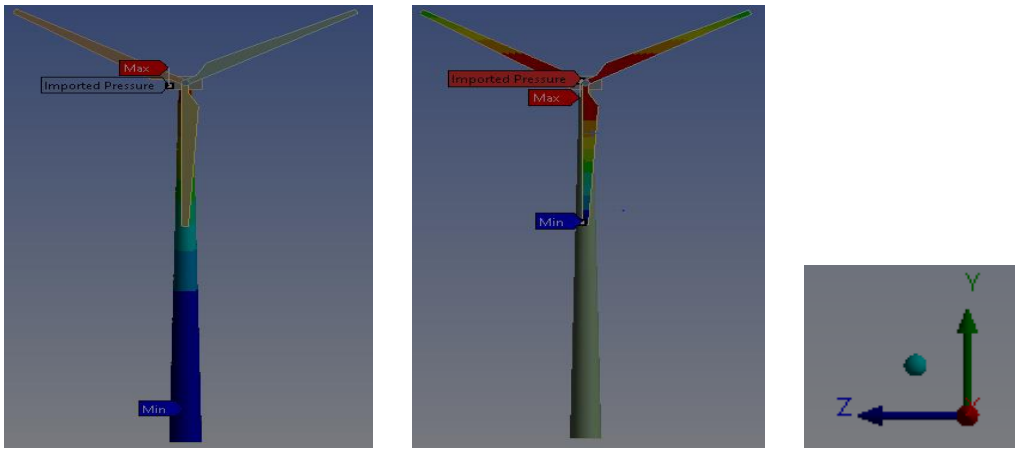

(c)

Figure 4.16: Imported loads on the rotor, nacelle and the tower for (a) 65kW wind turbine (b) 1.5MW wind turbine (c) 5MW wind turbine

CHAPTER FIVE: RESULTS AND DISCUSSION

5.1 Introduction

After completing analyses, results of response behavior such as top tower displacement, maximum Von Mises stress, second order (P-Δ) effect and Eigenvalue buckling of the wind turbine towers are obtained using ANSYS Workbench 2022. The results are partitioned based on the operation conditions of the wind turbines for ease of comparison between the loads and turbine models. Top tower displacements and second order (P-Δ) effect analysis are used to study the global stability of wind turbine towers. However, peak Von Mises stress and buckling of the wind turbine towers are used to study local stability. This chapter presents results obtained from all of the simulations that are conducted for analysis of the stability of 65kW, 1.5MW and 5MW wind turbine towers under seismic and aerodynamic load interaction, and provides a detailed discussion on comparison between the models and their operating conditions.

5.2 Results from Simulation of Wind Turbines

This study is highly significant to understand the characteristics of response behavior of different types of seismic loads, based on the magnitude and distance earthquake records are measured from source i.e., either near-field or far-field, when coupled with wind load on stability of 65kW, 1.5MW and 5MW wind turbine towers. Furthermore, it helps to study changes in responses to changes in the size of wind turbines and to study the impact of changes in operating condition of wind turbines under selected load interactions.

In this study, 12 earthquake excitations of which 6 are near field and 6 are far-field excitations coupled with 14 sets of wind speeds ranging from 1 to 75 m/s have been investigated using ANSYS Workbench 2022 for three different types of installed wind turbines. Installation of wind turbines in seismic regions is growing to meet renewable energy demand around the world and analyzing the stability of wind turbines in these regions is significant to minimize failure. Thus, it is important to study the response behavior of wind turbines with changes in seismic loads from weak to strong in magnitude as discussed in Chapter 3. Simulations are conducted for a total time of 40 seconds for different operation conditions such as parking, normal operation and seismic-induced emergency shutdown conditions. Generally, 168 simulations with

different earthquake loads and wind speeds are performed for the three operation scenarios for each wind turbine which brings total number of simulations to 2304.

5.2.1 Parking/Idling Condition with the Presence of Seismic Loads

Parking condition indicates that the rotor of wind turbines remains static due to cut-off wind speed of less than 3m/s. In this section, this scenario coupled with seismic excitations is studied for three different types of wind turbine towers. For non-operation conditions, the damping ratio used for simulation is 1% as dictated by ASCE 7-10 standard.

5.2.1.1 Top displacement of the wind turbine tower

The maximum displacement of the wind turbine towers due to selected ground motions and wind speed of 1m/s for non-operation conditions are shown in Figure 5.1.

The results show that for a 65kW wind turbine, the maximum tower displacement is 46.8mm from Loma Prieta far-field seismic record and the minimum tower displacement is 1.03mm from the Volcano far-field record. For a 1.5MW wind turbine, the maximum tower displacement is 579.61mm from Loma Prieta near-field seismic record and the minimum tower displacement is 2.23mm from the Volcano far-field record. For a 5MW wind turbine, the maximum tower displacement is 466.91mm from Loma Prieta near-field seismic record and the minimum tower displacement is 2.16mm from the Volcano far-field record.

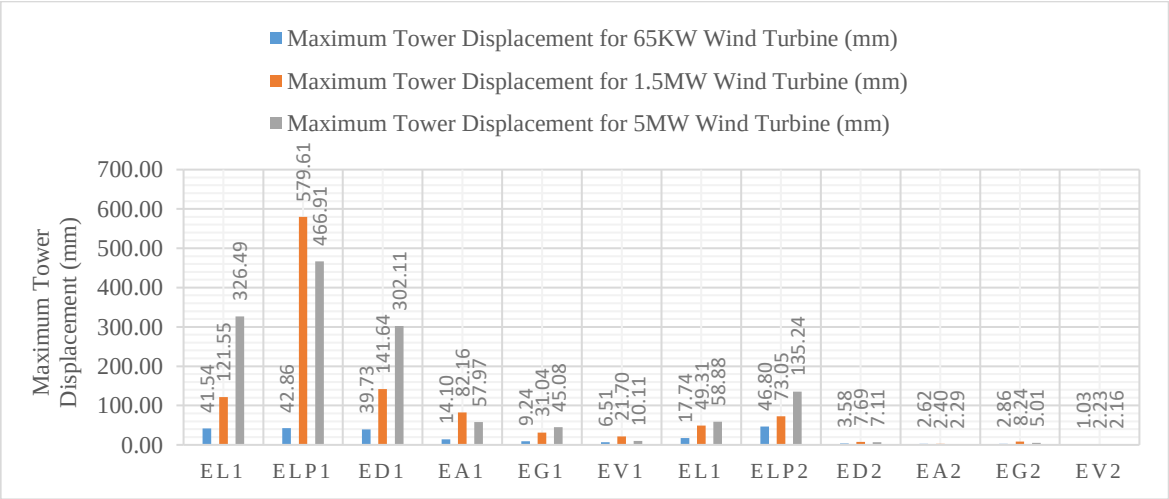

Figure 5.1: Top displacement of the tower when wind speed is 1m/s for 65kW, 1.5MW and 5MW wind turbines under seismic excitations

5.2.1.2 Maximum Von Mises stress of the wind turbine tower

The maximum Von Mises stresses of the wind turbine tower due to selected ground motions and non-operational wind load are shown in Figure 5.2.

The results show that for a 65kW wind turbine, the maximum Von Mises stress is 60.56MPa from Loma Prieta far-field seismic record and the minimum Von Mises stress is 1.38MPa from Volcano far-field record. For a 1.5MW wind turbine, the maximum Von Mises stress is 101.58MPa from Loma Prieta near-field seismic record and the minimum Von Mises stress is 1.37MPa from Volcano far-field record. For a 5MW wind turbine, the maximum Von Mises stress is 49.70MPa from Landers near-field seismic record and the minimum Von Mises stress is 0.57MPa from Volcano far-field record.

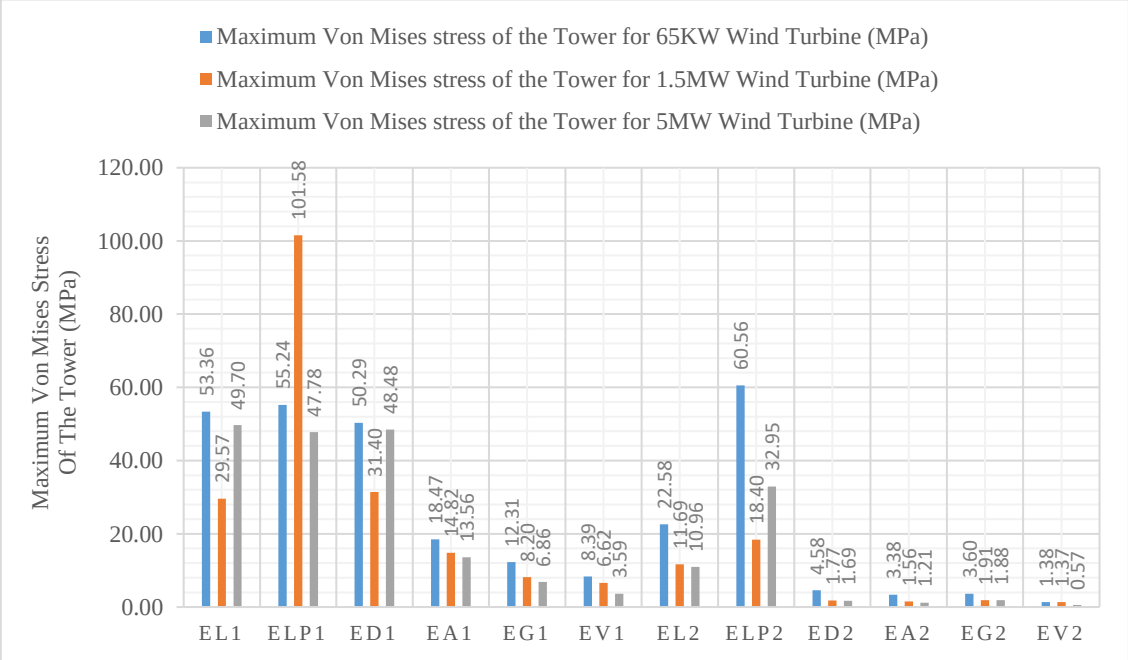

Figure 5.2: Maximum Von Mises stress of the tower when wind speed is 1m/s for 65kW, 1.5MW and 5MW wind turbines under seismic excitations

5.2.2 Normal Operation Condition with the Presence of Seismic Loads

For normal operational conditions, the damping ratio used for simulation is 5% as dictated by ASCE 7-10 standard. A wind speed of 3 m/s to 25 m/s is used to study the top displacement of the wind turbine tower under different seismic excitations.

5.2.2.1 Top displacement of the wind turbine tower

The maximum displacements of the wind turbine tower due to selected ground motions

and operational wind loads are shown in Figure 5.3 and the remaining results are shown in Appendix B.

The results from Figure 5.3 show that for a 65kW wind turbine, the maximum tower displacement is 28.22mm from Dillon near-field seismic record and the minimum tower displacement is 0.77mm from the Volcano far-field record. For a 1.5MW wind turbine, the maximum tower displacement is 348.15mm from Loma Prieta near-field seismic record and the minimum tower displacement is 1.76mm from the Volcano far-field record. For a 5MW wind turbine, the maximum tower displacement is 323.01mm from Loma Prieta near-field seismic record and the minimum tower displacement is 1.57mm from the Volcano far-field record.

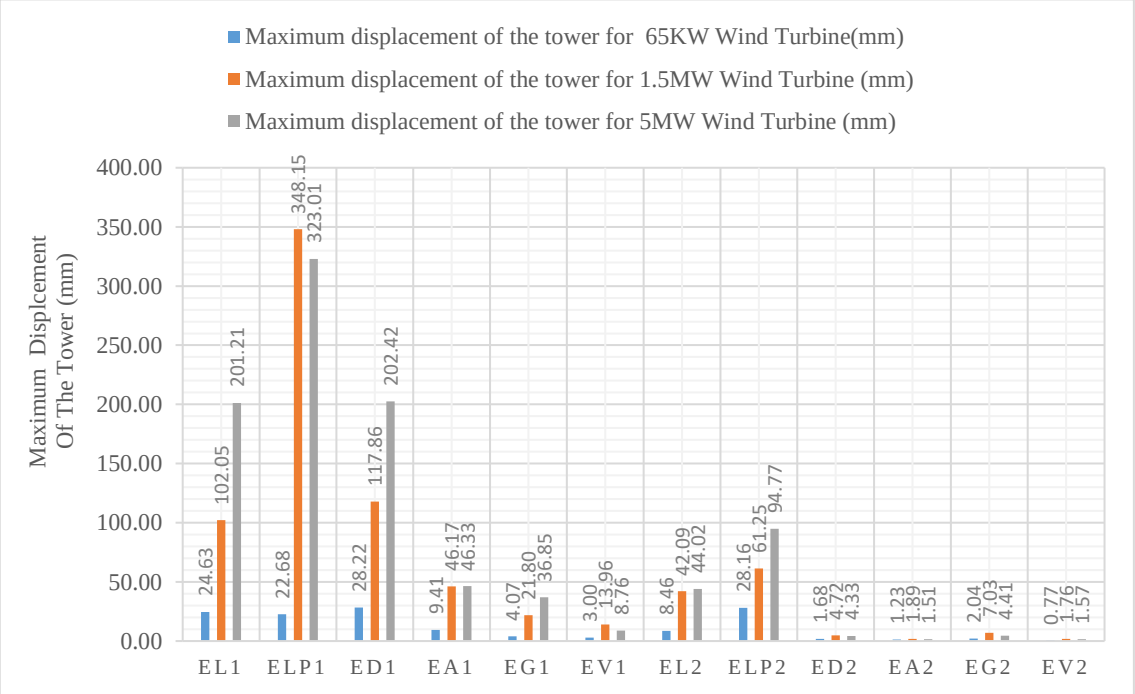

Figure 5.3: Top displacement of the tower when wind speed is 3m/s for 65kW, 1.5MW and 5MW wind turbines under seismic excitations

The maximum result is obtained when the wind speed is 25 m/s as shown in Appendix B. For a 65kW wind turbine, the maximum tower displacement is 28.22mm from Dillon near-field seismic record and the minimum tower displacement is 0.82mm from the Volcano far-field record. For a 1.5MW wind turbine, the maximum tower displacement is 348.20mm from Loma Prieta near-field seismic record and the minimum tower displacement is 6.25mm from the Volcano far-field record. For a 5MW wind turbine, the

maximum tower displacement is 323.07mm from Loma Prieta near-field seismic record and the minimum tower displacement is 6.17mm from the Volcano far-field record.

Generally, change in wind speed shows little effect on the maximum results which shows that earthquake loads are dominant loads as shown in Figure 5.3 and Appendix B.

5.2.2.2 Maximum Von Mises stress of the wind turbine tower

The maximum Von Mises stresses of the wind turbine tower due to selected ground motions and operational wind load are shown in Figure 5.4 and the remaining results are shown in Appendix B.

The maximum of results shows that for a 65kW wind turbine, the maximum Von Mises stress is 45.63MPa from Loma Prieta far-field seismic record and the minimum Von Mises stress is 1.34MPa from Volcano far-field record. For a 1.5MW wind turbine, the maximum Von Mises stress is 66.53MPa from Loma Prieta near-field seismic record and the minimum Von Mises stress is 1.13MPa from Volcano far-field record. For a 5MW wind turbine, the maximum Von Mises stress is 34.92MPa from Dillon near-field seismic record and the minimum Von Mises stress is 0.58MPa from Volcano far-field record.

Generally, change in wind speed shows little effect on the results which indicates that earthquake loads are dominant loads as shown in Figure 5.4 and Appendix B.

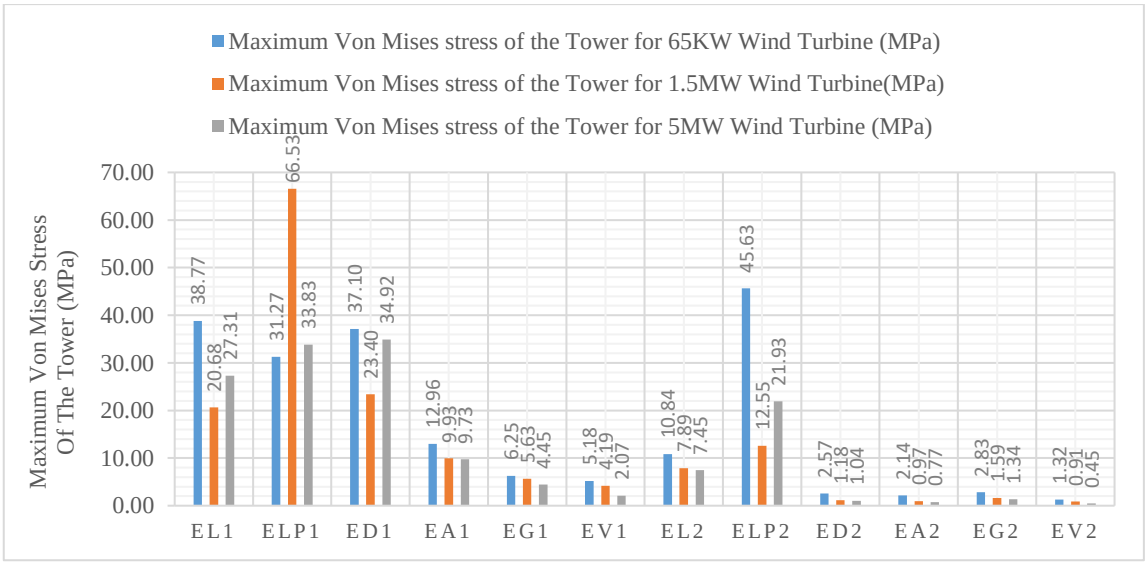

Figure 5.4: Maximum Von Mises stress of the tower when wind speed is 3 m/s for 65kW, 1.5MW and 5MW wind turbines under seismic excitations

5.2.3 Earthquake-Induced Emergency Shutdown Condition

For non-operational conditions due to earthquake-induced emergency shutdown, the damping ratio used for simulation is 1% as dictated by ASCE 7-10 standard.

5.2.3.1 Top displacement of the wind turbine tower

The maximum displacements of the wind turbine tower due to selected ground motions and wind loads are shown in Figure 5.5.

The results from Figure 5.5 show that for a 65kW wind turbine, the maximum tower displacement is 46.86mm from Loma Prieta far-field seismic record and the minimum tower displacement is 2.65mm from the Volcano far-field record. For a 1.5MW wind turbine, the maximum tower displacement is 582.11mm from Loma Prieta near-field seismic record and the minimum tower displacement is 53.90mm from the Volcano far-field record. For a 5MW wind turbine, the maximum tower displacement is 469.97mm from Loma Prieta near-field seismic record and the minimum tower displacement is 53.60mm from the Volcano far-field record.

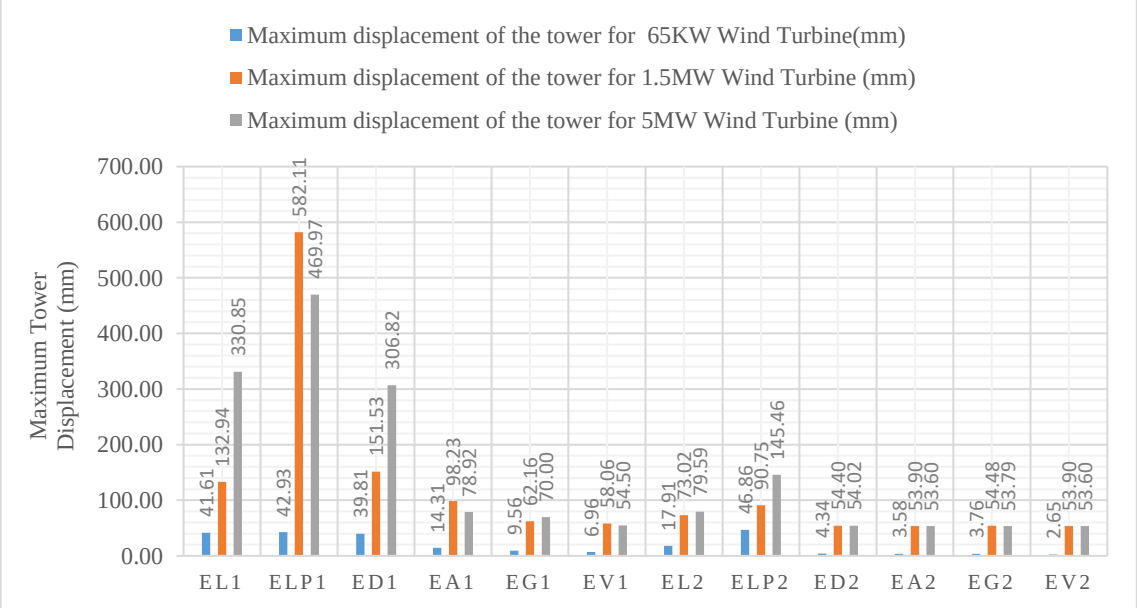

Figure 5.5: Top displacement of the tower when wind speed is 75 m/s for 65kW, 1.5MW and 5MW wind turbines under seismic excitations

5.2.3.2 Maximum Von Mises stress of the wind turbine tower

The maximum Von Mises stresses of the wind turbine tower due to selected ground motions and wind loads are shown in Figure 5.6.

The results show that for a 65kW wind turbine, the maximum Von Mises stress is 60.61MPa from Loma Prieta far-field seismic record and the minimum Von Mises stress is 2.73MPa from Volcano far-field record. For a 1.5MW wind turbine, the maximum Von Mises stress is 101.76MPa from Loma Prieta near-field seismic record and the minimum Von Mises stress is 6.19MPa from Volcano far-field record. For a 5MW wind turbine, the maximum Von Mises stress is 49.80MPa from Landers near-field seismic record and the minimum Von Mises stress is 3.23MPa from Volcano far-field record.

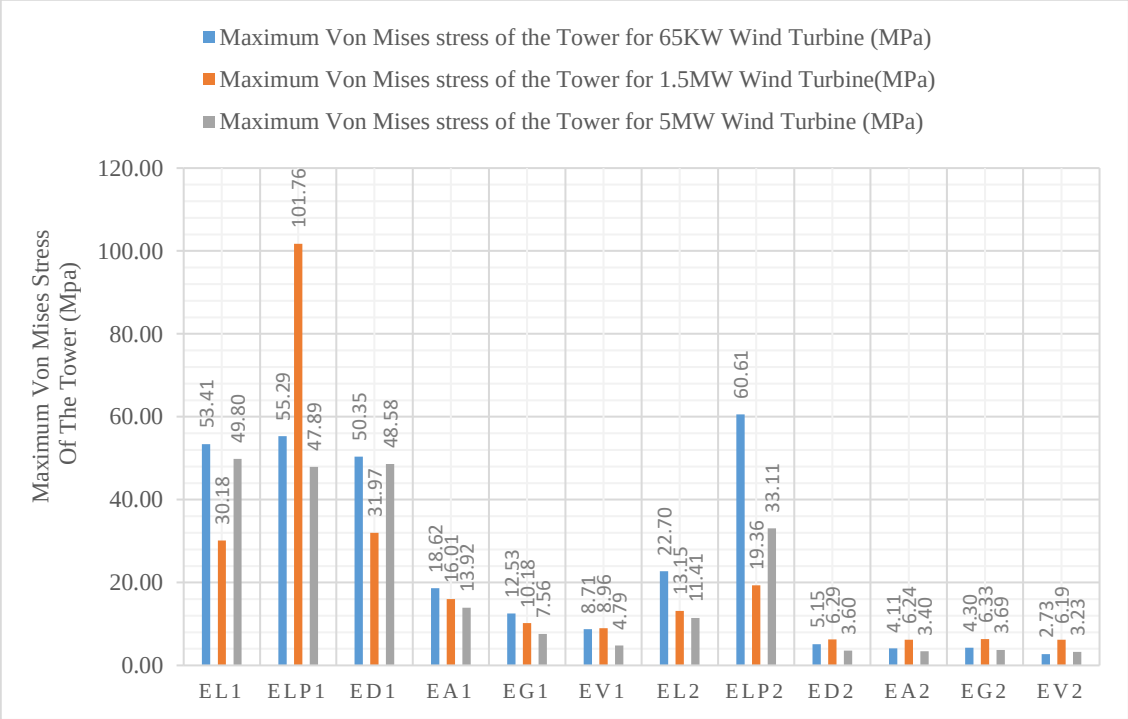

Figure 5.6: Maximum Von Mises stress of the tower when wind speed is 75 m/s for 65kW, 1.5MW and 5MW wind turbines under seismic excitations

The wind effect in this operation scenario is significant for wind turbine towers under study due to aerodynamic and seismic load interaction.

5.2.4 Stability Analysis of Wind Turbines

5.2.4.1 Second Order (P-Δ) Effect Analysis of Wind Turbine Tower

Second order effect contributes to structural instability in many engineering structures such as wind turbines. Table 5.1 shows the value of α_{cr} obtained from analysis which is a key parameter for determining the significance of second order effect as per Eurocode 3. α_{cr} is the factor by which the design loading would have to be increased to cause elastic instability.

Table 5.1 Value of α_{cr} for Parking condition with presence of seismic load

Item	α_{cr} from analysis
65kW Wind Turbine	35.695
1.5MW Wind Turbine	6.770
5MW Wind Turbine	3.750

The results show that 1.5MW and 5MW wind turbine towers are significantly affected by second order effect since the value of α_{cr} is less than 10. However, second order effect is negligible for 65kW wind turbine since the value of α_{cr} is greater than 10.

5.2.4.2 Eigenvalue Buckling Analysis of Wind Turbine Tower

Eigenvalue buckling is another factor that contributes to structural instability in many engineering structures and wind turbines are one of them. Results obtained from ANSYS Workbench 2022 Eigenvalue buckling analysis are shown in Table 5.2 below.

Table 5.2: Critical stress (δ_{cr}) from ANSYS Eigenvalue buckling analysis

Item	δ_{cr} from analysis (GPa)
65KW Wind Turbine	169.240
1.5MW Wind Turbine	305.450
5MW Wind Turbine	287.020

The results show that critical stress is higher than Von Mises stresses for all load combinations of wind turbine towers.

Thus, the structural stability of the wind turbine towers is safe against local buckling. The first buckling mode of wind turbine towers is shown in Figure 5.7.

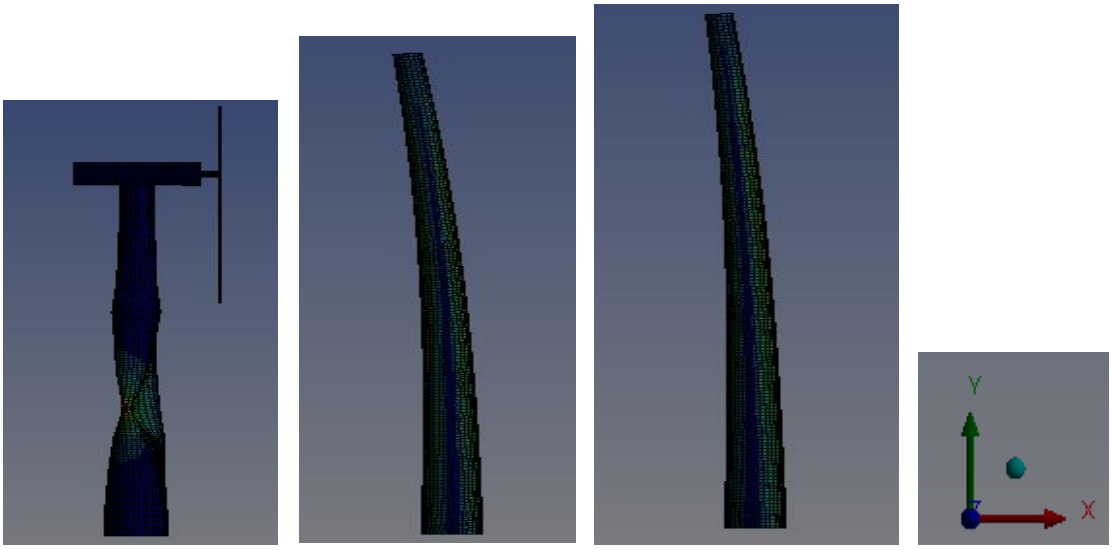

Figure 5.7: First Eigenvalue buckling mode of the tower for 65kW, 1.5MW and 5MW wind turbines respectively

5.3 Discussion of Results from Simulation of Wind Turbines

The results presented in this chapter provide valuable information for the response of each turbine model under different loading conditions. This section discusses various results obtained from the simulations through comparative analysis. Discussion on comparison of top tower displacement under different operation conditions of wind turbines.

5.3.1 Comparison of top tower displacements under different operation conditions of wind turbines

Comparisons between the three turbine models due to aerodynamic and seismic load interaction under three operating conditions are provided in Figure 5.8 through Figure 5.10.

Figure 5.8 shows that the maximum tower displacement for a 65kW wind turbine is 46.80mm, 28.22mm and 46.86mm for parking, operational and emergency shutdown conditions respectively. Thus, for 65kW wind turbine emergency shutdown condition shows the highest maximum tower displacement compared to other conditions. However; normal operation condition shows the lowest maximum tower displacement compared to other conditions due to a higher damping ratio. The effect of wind load is negligible between parking conditions and emergency shutdown conditions for moderate to strong seismic excitations but it is significant

for far-field records of weak seismic excitations like Gilroy and Volcano. In addition, the highest top tower displacement for cases under this study is not recorded from the highest magnitude earthquake load which shows that the configuration of acceleration vs time graph for earthquake records as shown in Appendix A has a significant effect rather than magnitude alone.

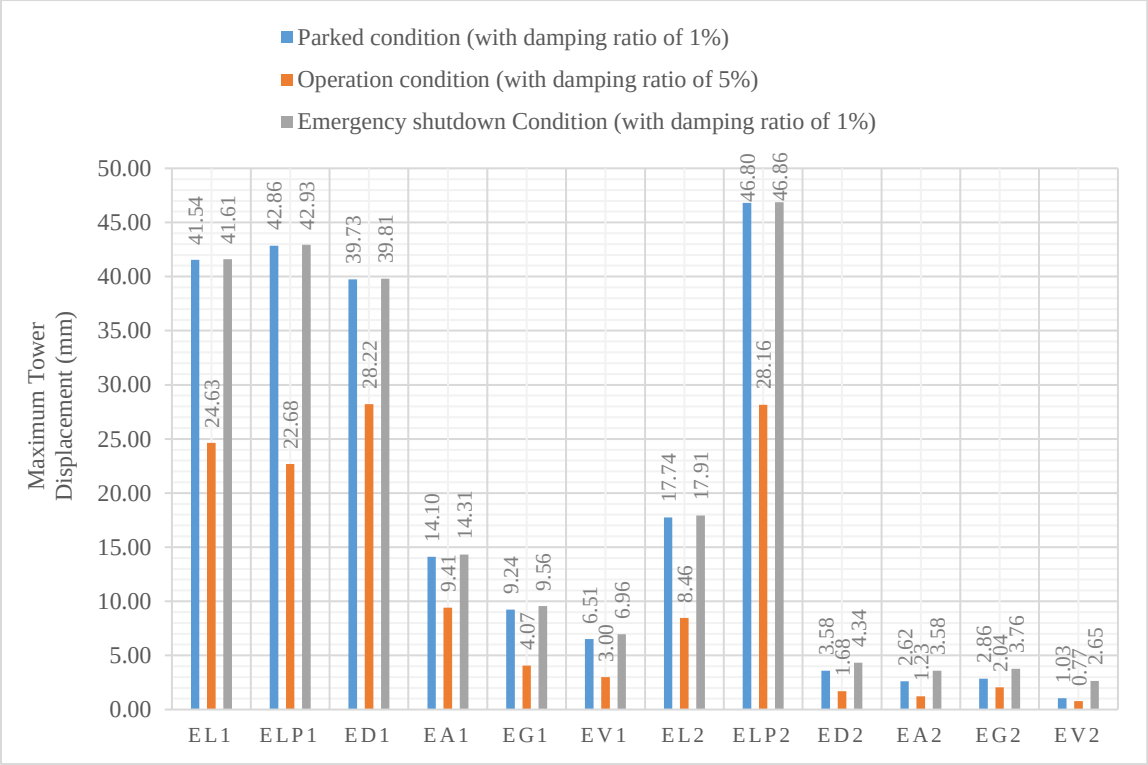

Figure 5.8: Top tower displacement for parking, operational and emergency shutdown conditions for 65kW wind turbine

Figure 5.9 shows that the maximum tower displacement for a 1.5MW wind turbine is 579.61mm, 348.15mm and 582.11mm for parking, operational and emergency shutdown conditions respectively. For 1.5MW wind turbine emergency shutdown condition shows the highest maximum tower displacement compared to other conditions. However; normal operation condition shows the lowest maximum tower displacement compared to other conditions due to a higher damping ratio. The effect of wind load is significantly high between parking conditions and emergency shutdown conditions under all seismic excitations which are due to the increase in the size of the wind turbine. Furthermore, the highest top tower displacement for cases under this study is not recorded from the highest magnitude earthquake load which indicates that the

configuration of acceleration vs time graph for earthquake records as shown in Appendix A has a significant effect over magnitude alone.

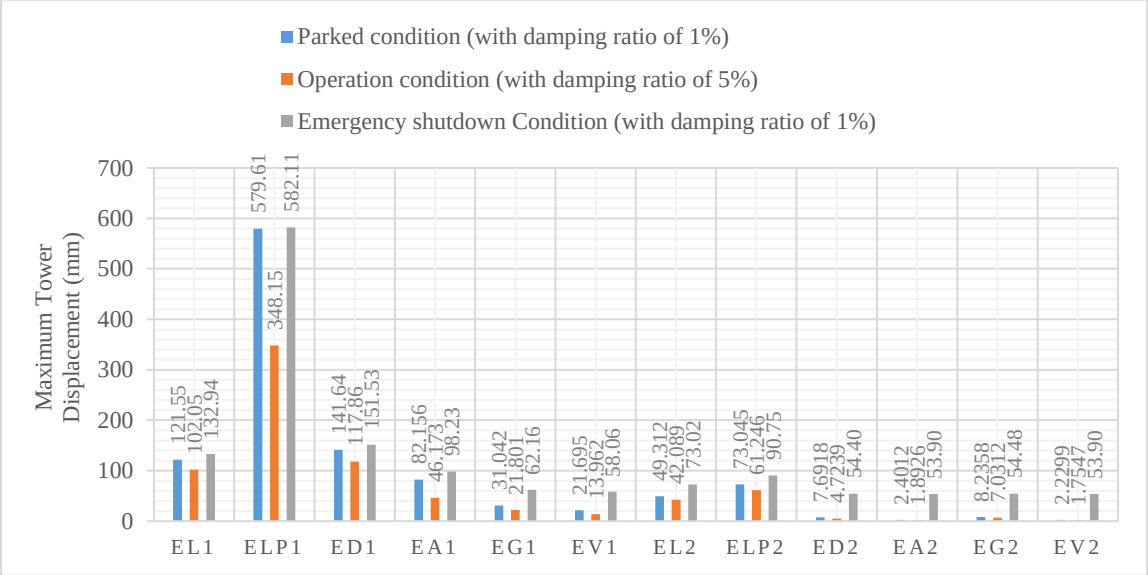

Figure 5.9: Top tower displacement for parking, operational and emergency shutdown conditions for 1.5MW wind turbine

Figure 5.10 shows that the maximum tower displacement for a 5MW wind turbine is 466.91mm, 323.07mm and 469.97mm for parking, operational and emergency shutdown conditions respectively. For 5MW wind turbine emergency shutdown condition shows the highest maximum tower displacement compared to other conditions. However; normal operation condition shows the lowest maximum tower displacement compared to other conditions due to a higher damping ratio. The effect of wind load is significantly high between parking conditions and emergency shutdown conditions under all seismic excitations which are due to the increase in the size of the wind turbine however its effect is smaller compared to a 1.5MW wind turbine. Furthermore, the highest top tower displacement for cases under this study is not recorded from the highest magnitude earthquake load which indicates that the configuration of acceleration vs time graph for earthquake records as shown in Appendix A has a significant effect over magnitude alone.

Overall, the configuration of acceleration vs time graph for earthquake records is found to have a significant effect rather than the magnitude and distance earthquake records are measured from the source alone. Further, the effect of wind load is higher for larger wind turbines compared to

smaller wind turbine. However, 1.5MW wind turbine have higher top tower displacements compared to 5MW wind turbine.

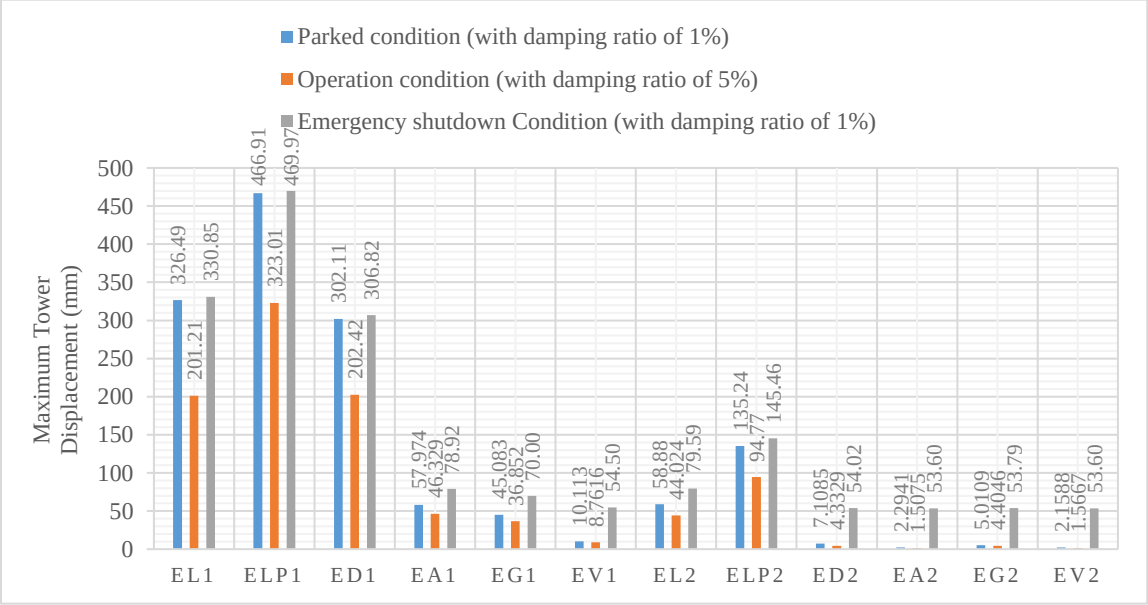

Figure 5.10. Top tower displacement for parking, operational and emergency shutdown conditions for 5MW wind turbine

5.3.2 Comparison of maximum Von Mises stress of the tower under different operation conditions of wind turbines

Comparisons between the three turbine models due to aerodynamic and seismic load interaction under three operation conditions are provided in Figure 5.11 through Figure 5.13.

Figure 5.11 shows that the maximum Von Mises stress of the tower for a 65kW wind turbine is 60.56MPa, 45.63MPa and 60.65MPa for parking, operational and emergency shutdown conditions respectively. Thus, for a 65kW wind turbine, emergency shutdown condition shows the highest maximum Von Mises stress of the tower compared to other conditions. However; normal operation condition shows the lowest maximum Von Mises stress of the tower compared to other conditions due to a higher damping ratio. Loma Prieta far-field record shows a higher effect on maximum Von Mises stress compared to Loma Prieta near-field record for 65kW wind turbine however for other 5 seismic records near-field records deliver higher stress compared to far-field records. Thus, maximum stresses formed in the wind turbine tower are not only dependent on the magnitude of ground motions and distance of earthquakes measured from the

source alone which implies that the configuration of acceleration vs time graph of earthquake records is also a significant factor.

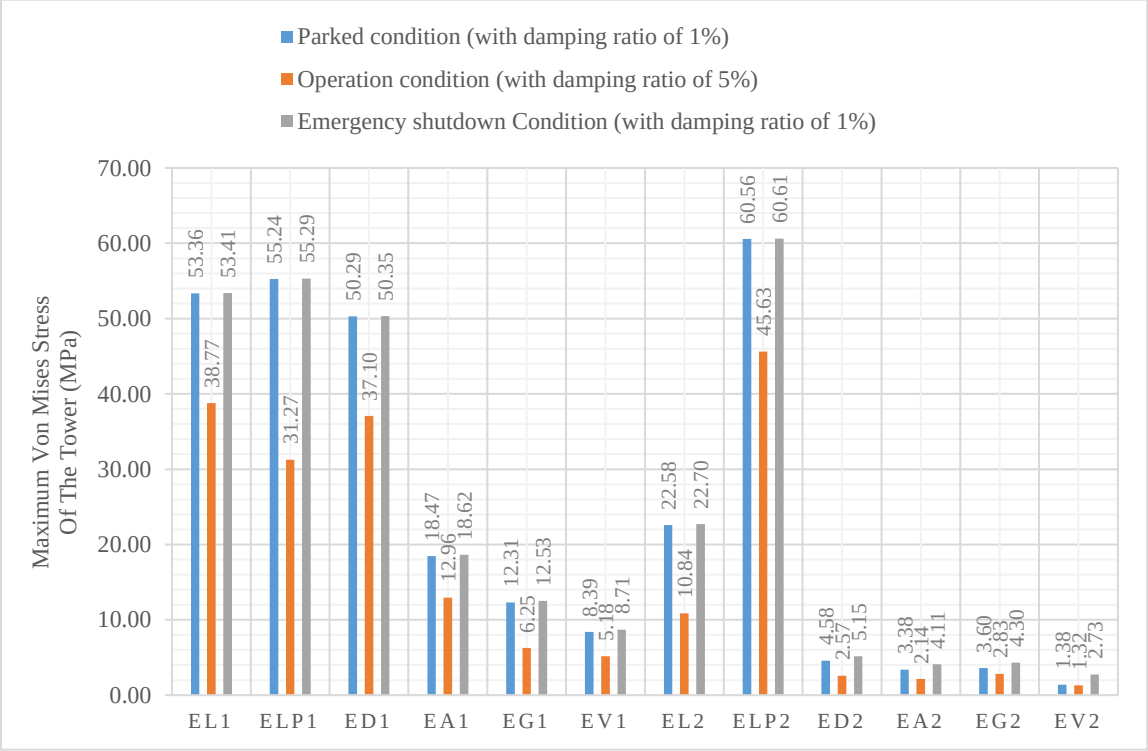

Figure 5.11: Maximum Von Mises stress of the tower for parking, operational and emergency shutdown conditions of 65kW wind turbine

Figure 5.12 shows that the maximum Von Mises stress of the tower for a 1.5MW wind turbine is 101.58MPa, 66.53MPa and 101.76MPa for parking, operational and emergency shutdown conditions respectively. Thus, for a 1.5MW wind turbine, emergency shutdown condition shows the highest maximum Von Mises stress of the tower compared to other conditions. However; normal operation condition shows the lowest maximum Von Mises stress of the tower compared to other conditions due to a higher damping ratio. The effect of wind load is significantly high between parking conditions and emergency shutdown conditions under moderate and weak seismic excitations. All near-field seismic records used for the study show higher Von Mises stress compared to their respective far-field records for 1.5MW wind turbines. However, the highest maximum Von Mises stress of the tower for cases under this study is not recorded from the highest magnitude earthquake load which implies that the configuration of acceleration vs time graph of earthquake records is also a significant factor.

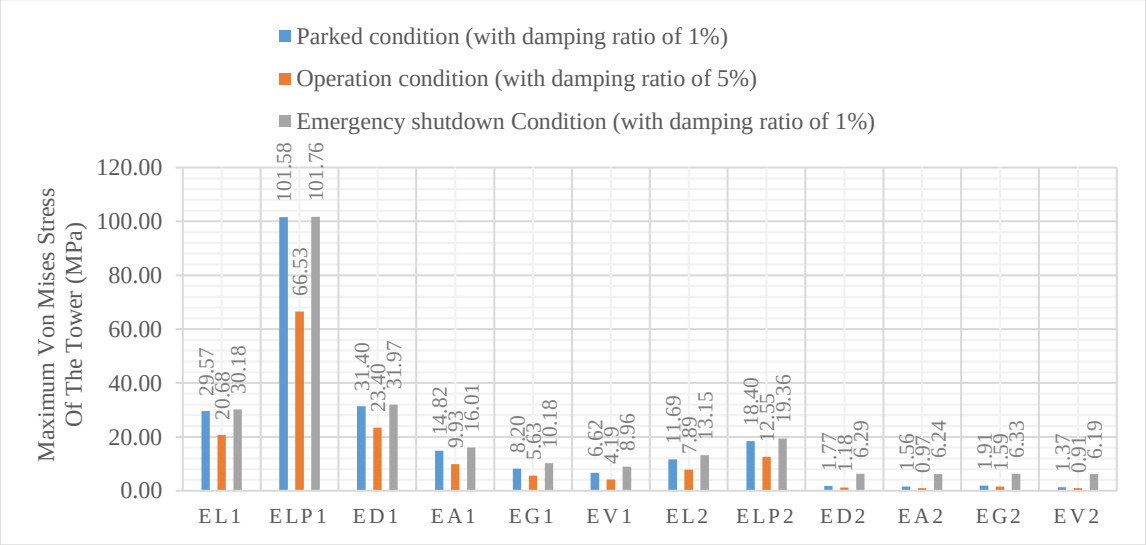

Figure 5.12: Maximum Von Mises stress of the tower for parking, operational and emergency shutdown conditions of 1.5MW wind turbine

Figure 5.13 shows that the maximum Von Mises stress of the tower for a 5MW wind turbine is 49.70MPa, 34.92MPa and 49.80MPa for parking, operational and emergency shutdown conditions respectively. Thus, for a 5MW wind turbine emergency shutdown condition shows the highest maximum tower displacement compared to other conditions. However; normal operation condition shows the lowest maximum tower displacement compared to other conditions due to a higher damping ratio. The effect of wind load is significantly high between parking conditions and emergency shutdown conditions under moderate and weak seismic excitations which is due to the increase in the size of the wind turbine however its effect is smaller compared to a 1.5MW wind turbine. All near-field seismic records used for the study show higher Von Mises stress compared to their respective far-field records for 5MW wind turbines. However, the maximum Von Mises stress of the tower created from cases under this study is not proportional to the magnitude of recorded earthquake loads which implies that the configuration of acceleration vs time graph of earthquake records is also a significant factor.

Overall, the configuration of acceleration vs time graph for earthquake records is found to have a significant effect rather than the magnitude of earthquake records and distance of earthquakes measured from source only. Further, the effect of wind load is higher for larger wind turbines for moderate and weak seismic excitations compared to smaller wind turbine. However, 1.5MW wind turbine have higher maximum Von Mises stress compared to 5MW wind turbine.

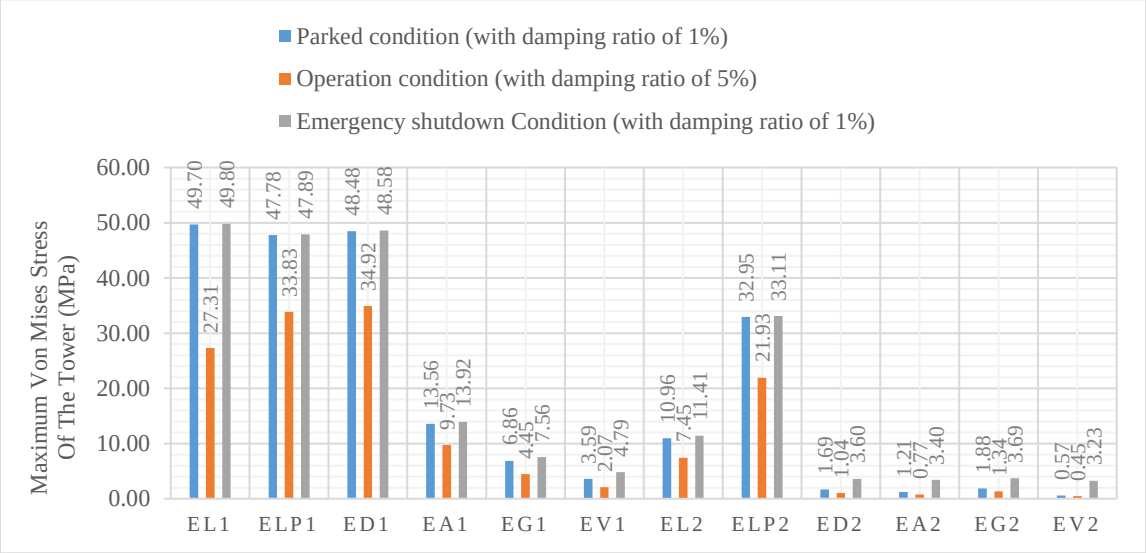

Figure 5.13: Maximum Von Mises stress of the tower for parking, operational and emergency shutdown conditions of 5MW wind turbine

Finally, the highest observed Von Mises stress in all wind turbine towers from the analysis is well below the yield stress of 250MPa which indicates local stability of wind turbine towers is ok.

5.3.3 Discussion on results from Stability analysis of wind turbines

5.3.3.1 Second order effect (P-Δ) analysis of wind turbine tower

Global deformation is significant for 1.5MW and 5MW wind turbines as per the analysis of Eurocode 3 which indicates the possibility of structural stability failure in the mentioned wind turbines. However, a 65KW wind turbine is safe against structural stability failure because second order effect from the analysis is negligible.

5.3.3.2 Eigenvalue Buckling analysis of wind turbine tower

Results from the Eigenvalue buckling analysis of ANSYS Workbench 2022, indicate that there will be no failure due to buckling for the wind turbine towers since the critical stress of the towers is greater than the Von Mises stresses of the towers. The yield stress of the wind turbine towers for all turbines is 250MPa and all maximum Von Mises stresses obtained due to aerodynamic and seismic load interaction are also below 250MPa.

CHAPTER SIX: CONCLUSIONS AND RECCOMENDATIONS

6.1 Conclusions

In this study, an analysis of the structural stability of wind turbine towers is performed due to aerodynamic and seismic load interaction under different operation conditions. The methodology implemented to conduct this study is a decoupling approach to analyze the effect of wind load and seismic load independently and combine results obtained by using the squire root of squire sum (SRSS) load combination method by using ANSYS Workbench 2022 finite element analyses. Then, global responses such as top tower displacement and second order (P-Δ) effect, and local responses such as maximum Von Mises stress and eigenvalue buckling analysis of wind turbine towers were conducted. Finally, critical operation condition, stability of wind turbine towers and the need for improvement of wind turbine models were checked.

This study is highly significant to understand the characteristics of response behavior of different types of seismic loads, based on the magnitude and distance earthquake records are measured from source i.e., either near-field or far-field, when coupled with wind load on stability of 65kW, 1.5MW and 5MW wind turbine towers. Furthermore, it helps to study changes in responses to changes in the size of wind turbines and to study the impact of changes in operating conditions of wind turbines under selected load interactions.

12 seismic excitations of which 6 are near field and 6 are far-field excitations are coupled with 14 sets of wind speeds ranging from 1 to 75m/s during analysis. Simulations are conducted for a total time of 40 seconds. In addition, different operating conditions of the wind turbines are also considered such as parking, normal operation and emergency shutdown conditions. 168 simulations with different seismic loads and wind speeds are performed for the three operation scenarios for each wind turbine model which bring the total number of simulations to 2304. Peak tower displacement is recorded at the top of the tower for wind turbines under this study. Maximum Von Mises stress is observed near the base of the tower for wind turbines under this study.

The following conclusions are drawn from the analysis of the stability of wind turbines:

1. Reliable finite element models are developed to represent the physical properties of installed wind turbines under this study for conducting the required analysis.

2. Earthquake loads are dominant loads compared to wind loads for all wind turbines. In addition, seismic load application in both horizontal directions showed a higher effect compared to the unidirectional seismic effect.
3. Earthquake-induced emergency shutdown condition is the most critical operation condition for all wind turbines.
4. A 1.5MW wind turbine has higher top tower displacement and maximum Von Mises stress than a 5MW wind turbine due to the effect of the shell property of the tower and the weight of wind turbines.
5. The second-order (P-Δ) effect from analysis of wind turbine towers shows that 1.5MW and 5MW wind turbine towers are significantly affected, but the P-Δ effect is negligible for 65kW wind turbine.
6. The characteristics of the acceleration vs. time records are also found to have a significant effect on the response behavior of the turbines rather than the magnitude and distance earthquake records are measured from the source alone.
7. Results obtained from eigenvalue buckling analysis by using ANSYS Workbench 2022, indicate that there will be no failure due to local buckling for the wind turbine towers since the critical stresses of the towers are greater than the Von Mises stresses of the wind turbine towers.

Overall, the shell property of the tower, the weight of wind turbines, and the pattern or characteristics of acceleration vs. time records play important roles for variable size wind turbines which are subjected to similar seismic and aerodynamic load combinations. In addition, regardless of the size variation of wind turbine models, earthquake-induced emergency shutdown operation conditions of the turbines deliver higher response compared to parking and normal operating conditions. Therefore, earthquake-induced emergency shutdown operation condition is critical operation condition for all wind turbine. Furthermore, the results indicate that earthquake loads are dominant loads compared to wind loads which shows that the effect of seismic loads should be considered for the design of wind turbines to be installed in seismic areas. Finally, the second-order (P-Δ) effect for 1.5MW and 5MW wind turbines was found to be significant. Thus, proper emphasis should be given to considering this impact during design to avoid structural stability failure in the mentioned wind turbine models.

6.2 Recommendations

In general, the results obtained from the finite element analysis presented in this study indicates the potential damage to wind turbines caused by earthquake loads in combination with wind loads under different operation conditions. The following recommendations are suggested on the scope and limitations of this study for further future research.

- Wind turbine models developed for this study are approximate to the geometry and material properties of wind turbines. Thus, the accuracy of results from this study can be improved by developing turbine models which are closer to the real geometry and material properties of turbine models.
- In this study, the effect of soil structure interaction has not been considered. Hence, this study can be further developed by considering different soil properties of the wind farm location.
- The fatigue analyses, which study the development of cracks near the base of the wind turbine due to the seismic loading on the system, could also be conducted for further checking of the local stability of wind turbine models in future works.

REFERENCES

1. *Suinyal Magar, Pradin (2017), "Response of Wind Turbines Subjected to Different Earthquakes"), Theses and Dissertations, 2146, https://commons. und.edu/theses/2146*
2. *Peter Jamieson 2018, "Innovation in Wind Turbine Design", Second Edition, John Wiley & Sons Ltd, USA.*
3. *Martin O. L. Hansen 2008, "Aerodynamics of Wind Turbines", Second Edition, Earthscan Publisher, UK and USA.*
4. IRENA 2019, "Transforming the energy system and holding the line on the rise of global temperatures", International Renewable Energy Agency, Abu Dhabi, *https://www.irena.org//media/Files/IRENA/Agency/Publication/2019/Sep/IRENATransforming_the_energy_ system_2019*
5. *Joyce Lee and Feng Zhao 2021, "Global wind report 2021", Global Wind Energy Council, Brussels, Belgium.*
6. *Weibull W. 1951, "A statistical distribution function of wide applicability", ASME Journal of Applied Mechanics, 18(3), pp. 239–297*
7. *Barbu, C. & Vyas, P. 2009, "System and method for loads reduction in a horizontal- axis wind turbine using upwind information", US patent application, 20,090,047,116.*
8. *McCaffrey, B. (2005), "Wind Turbine Technology. Albany: Global Energy Concepts".*
9. *Colin Anderson 2020, "Wind Turbines Theory and Practice", Cambridge University Press, UK*
10. *Wei Tong 2010, "Wind Power Generation and Wind Turbine Design", WIT Press, UK, pp. 23*
11. *A.R. Jha 2011, "Wind Turbine Technology", Taylor and Francis Group, USA, pp. 2-9*
12. *Ethiopian electric power 2015, "The Ethiopian energy sector–investment opportunities", UK-Ethiopia trade & investment forum, London, UK*
13. *Inclusive Green Growth in Ethiopia: Selected case studies, United Nations Economic Commission for Africa, 2015.*
14. *Guidelines for design of wind turbines DNV/Risø 2002, 2nd Edition, Copenhagen, pp. 2-3*

15. *Wei Tong 2010, "Wind Power Generation and Wind Turbine Design", WIT Press, UK, pp. 19*
16. *Wei Tong 2010, "Wind Power Generation and Wind Turbine Design", WIT Press, UK, pp. 19-20*
17. *Molina M. G. & Mercado P. E. (2011), "Modelling and Control Design of Pitch-Controlled Variable Speed Wind Turbines", Argentina*
18. *Gwon, T.g. (2011), "Structural Analyses of Wind Turbine Tower for 3 KW Horizontal-Axis Wind Turbines", San Luis Obispo: California Polytechnic State University.*
19. *I. Prowell, A. Elgamal, C. Uang and J. Jonkman 2010, "Estimation of seismic load demand for a wind turbine in the time domain," in European Wind Energy Conference: Warsaw, Poland*
20. *D. Witcher 2005, "Seismic analysis of wind turbines in the time domain," Wind Energy, 8(1): pp. 81–91*
21. *I. Prowell 2011, "An experimental and numerical study of wind turbine seismic behavior," Thesis Dissertation: University of California, San Diego, USA*
22. *E. Nuta 2010, "Seismic analysis of steel wind turbine towers in the Canadian environment," Thesis Dissertation: University of Toronto, Canada*
23. *N. Bazeos, G.D. Hatzigeorgiou, I.D. Hondros, H. Karamaneas, D.L. Karabalis and D.E. Beskos 2002, "Static, seismic and stability analyses of a prototype wind turbine steel tower", Engineering Structures, 24(8): pp. 1015–1025*
24. *I. Lavassas, G. Nikolaidis, P. Zervas, E. Efthimiou, I.N. Doudoumis and C.C. Baniotopoulos 2003, "Analysis and design of the prototype of a steel 1-MW wind turbine tower," Engineering Structures, 25(8): pp. 1097–1106*
25. Wind turbine accidents 2022, *https://www.google.com.sa/search?q=wind+turbine+accidents&safe=active&dcr=0&tbm=isch&tbo=u&source=univ&sa=X&ved=0ahUKEwid56Tbio_aAhWBERQKHar1AfcQsAQISA&biw=1920&bih=965#imgrc=1ZV-ywTuf_XRRM*
26. United states geological survey (USGS) 2022, "What materials are used to make wind turbines?", https://www.usgs.gov/faqs/what-materials-are-used-make-windtAccording%20to %20a%20report%20from,aluminum%20(0%2D2%25).

27. *RisØ 2001, "Guidelines for Design of Wind Turbines", second edition, Wind Energy Department, Risø National Laboratory, Copenhagen, Denmark.*
28. *Germanischer Lloyd's Guidelines for the Certification of Wind Turbines (GL, 2010)*
29. *EN 1998-1:2004: Eurocode 8: Design of structures for earthquake resistance – Part 1: General rules, seismic actions and rules for buildings.*
30. *IEC 61400-1 Ed 3: Wind Turbines – Part 1: Design Requirements (IEC, 2005)*
31. *N.A. Agbayani, "A Technical Overview of ASCE/AWEA RP2011: Recommended Practice for Compliance of Large Land-based Wind Turbine Support Structures," in Structures Congress 2014: ASCE, pp. 1759-1770, 2014.*
32. *ASCE-7-10, "Minimum design loads for buildings and other structures," in American Society of Civil Engineers, Reston, Virginia, 2010.*
33. *T. Bartlett Quimby 2008, "A Beginner's Guide to The Steel Construction Manual", 13th edition, https://www.bgstructuralengineering.com/BGSCM13 /BGSCM006/index.htm*
34. *European Norm (EN) 1993-1-1: Eurocode 3: Design of steel structures*
35. *Shafiqur Rehman, Md. Mahbub Alam and Luai M. Alhems 2018, "A review of wind-turbine structural stability, failure and alleviation", Advances in Civil, Environmental, & Materials Research (ACEM18), Korea*
36. *He Guangling, Tian Jingkui and Chang Desheng 2013, "Conceptual design of anti-typhoon for offshore wind turbines", Electric Power Construction, China, vol. 34, pp. 11-17*
37. *Kim S E 2002, "Thin-walled structures", Vol.40, pp.329-353*
38. *Congxin Yang, Yixiong and Bin Wang 2012, "Buckling analysis on large wind turbine tower", Advanced Materials Research Vols 512-515, pp. 604-607*
39. *Jui-Sheng Chou and Wan-Ting Tu 2011, "Failure analysis and risk management of a collapsed large wind turbine tower", Engineering Failure Analysis, Volume 18, Issue 1, pp. 295-313*
40. *Chou, J.S., Chiu, C.K., Huang, I.K., and Chi, K.N. (2013), "Failure analysis of wind turbine blade under critical wind loads", Engineering Failure Analysis 27, pp. 99-118.*

41. *Song Xi, Wu Yin-guang, Li Heng-Zhou and Dai Jian-xin 2013, "Stability Analysis and Numerical Simulation of the Conical Tower of the Wind Turbine", Applied Mechanics and Materials Vols. 249-250, pp. 759-764*
42. *Asareh, Mohammad-Amin (2015), "Dynamic behavior of operational wind turbines considering aerodynamic and seismic load interaction", Doctoral Dissertations, Paper 2375.*
43. *Yangtian Yan, Chun Li, Zhihao Li, "Buckling analysis of a 10 MW offshore wind turbine subjected to wind-wave-earthquake loadings", Elsevier, 2021.*
44. *Bazeos N, Hatzigeorgiou GD, Hondros ID, Karamaneas H, Karabalis DL, Beskos DE 2002, "Static, seismic and stability analyses of a prototype wind turbine steel tower", Engineering Structures, 24 pp. 1015–1025.*
45. *Lavassas I, Nikolaidis G, Zervas P, Efthimiou E, Doudoumis IN, Baniotopoulos CC 2003, "Analysis and design of the prototype of a steel 1-MW wind turbine tower", Engineering Structures, 25 pp. 1097–1106.*
46. *Witcher D 2005, "Seismic analysis of wind turbines in the time domain", Wind Energy, Vol. 8, pp. 81–91*
47. *Bossanyi EA 2000, "Bladed for Windows User Manual, in, Bristol, UK: Garrad Hassan and Partners".*
48. *Prowell I. 2011, "An experimental and numerical study of wind turbine seismic behavior", in: University of California, San Diego.*
49. *Ishihara T, Sawar MW. 2008, "Numerical and theoretical study on seismic response of wind turbines", in: European Wind Energy Conference and Exhibition, Brussels, Belgium: European Wind Energy Association.*
50. *Haenler M, Ritschel U. 2006, "Warnke I, Systematic modelling of wind turbine dynamics and earthquake loads on wind turbines", in: European Wind Energy Conference & Exhibition, Athens, Greece.*
51. *Nuta, E., Christopoulos, C., and Packer, J.A., (2011), "Methodology for seismic risk assessment for tubular steel wind turbine towers: application to Canadian seismic environment", Canadian Journal of Civil Engineering, 38, pp. 293–304*
52. *Kim DH, Lee SG 2014, "Lee IK, Seismic fragility analysis of 5 MW offshore wind turbine", Renewable Energy, Vol.65, pp. 250-256.*

53. *Hua Wei, Yanjun Cheng, Zhiyuan Peng and Haijun Wang 2011, "Finite Element Analysis for the Wind Resistance of the Tower of Wind Turbine", Advanced Materials Research Vols 189-193, pp. 1718-1721*
54. *Wei Chen, Shiyue Wang, Liang Cao, Huiming Wang and Ji Yao 2014, "The Finite Element Analysis of the Large Horizontal Axis Wind Turbine Generator Tower", Applied Mechanics and Materials Vols 444-445, pp. 836-840*
55. *Chun-you Zhang and Xiaoqiang Wu 2014, "Finite element analysis for the tower of 1.5 MW wind turbine", Applied Mechanics and Materials Vols. 644-650, pp. 3931-3935*
56. *Atul Sudhakar Patil 2015, "Response of a Wind Turbine Structure to Strong Ground Motions and High Velocity Winds", Theses, Treatises and Dissertations, Florida State University, USA*
57. *Asareh, Mohammad-Amin 2015, "Dynamic behavior of operational wind turbines considering aerodynamic and seismic load interaction", Doctoral Dissertations, Paper 2375.*
58. *Sadowski, A.J., Camara, A., Málaga-Chuquitaype, C., and Dai, K., (2017), "Seismic analysis of a tall metal wind turbine support tower with realistic geometric imperfections", Earthquake Engineering & Structural Dynamics, 46(2), pp. 201-219*
59. *Alberto Maria Avossa, Cristoforo Demartino, Pasquale Contestabile, Francesco Ricciardelli and Diego Vicinanza 2017, "Some Results on the Vulnerability Assessment of HAWTs Subjected to Wind and Seismic Actions".*
60. *Suinyal Magar, Pradin 2017, "Response of Wind Turbines Subjected to Different Earthquakes", Theses and Dissertations, 2146*
61. *Muhsen Awad Sassi 2017, "Nonlinear Dynamic Analysis of Wind Turbine Towers Subject to Design Wind and Seismic Loads", thesis*
62. *Fan J, Li Q, Zhang Y. 2018, "Collapse analysis of wind turbine tower under the coupled effects of wind and near-field earthquake", Wind Energy, pp. 1–13*
63. *Risø-DNV 2001, "Guidelines for Design of Wind Turbines," Wind Energy Department of Risø National Laboratory and Det Norske Veritas: Copenhagen, Denmark.*
64. *IEC 2005, "IEC 61400-1 Ed. 3: Wind Turbines - Part 1: Design Requirements," International Electrotechnical Commission: Geneva, Switzerland.*

65. *Zienkiewicz O. C. & Taylor R. L. (1977), "The Finite Element Method (Vol 3)", London: McGraw-hill.*
66. *Hughes, T. J. (1987), "The finite element method. Linear static and dynamic finite element analysis" Englewood Cliffs, N.J.: Prentice-Hall, Inc.*
67. *Hilber, H. M., Hughes, T. J., & Taylor, R. L. (1977), "Improved numerical dissipation for time integration algorithms in structural dynamics", Earthquake Engineering and Structural Dynamics, pp. 283-292.*
68. *Prowell, I., Veletzos, M., & Elgamal, A. (2008), "Full Scale Testing for Investigation of Wind Turbine Seismic Response".*
69. *Jonathan P Stewart, Shyh-Jeng Chiou, Jonathan D Bray, et al, 2002, "Ground motion evaluation procedures for performance-based design", Soil Dynamics and Earthquake Engineering, 22, 765–772*
70. *COSMOS Virtual Data Center; https://www.strongmotioncenter.org/vdc/scripts/earthquakes*
71. *United States Geological Survey (USGS) 1989, "The Severity of an Earthquake", https://pubs.usgs.gov/gip/earthq4/severitygip.html*
72. *Abtin Namiranian (2011), "3D Simulation of a 5MW Wind Turbine", MSc Thesis, Blekinge Institute of Technology, Karlskrona, Sweden*
73. *Deierlein, G. G., Reinhorn, A. M., and Willford, M. R. (2010), "Nonlinear Structural Analysis for Seismic Design", NEHRP Seismic Design Technical Brief No. 4., NIST GCR 10-917-5. Gaithersburg, MD: National Institute of Standards and Technology.*
74. *Christopher Mone et al 2017, "2015 Cost of Wind Energy Review", NREL report, USA*
75. *Prowell, Ian, Veletzos, Marc, Elgamal, Ahmed and Restrepo, José (2009), "Experimental and Numerical Seismic Response of a 65 kW Wind Turbine", Journal of Earthquake Engineering, 13: 8, pp. 1173-1175.*
76. *Rinker, Jennifer and Dykes, Katherine 2018, "WindPACT Reference Wind Turbines", Golden, CO: National Renewable Energy Laboratory. NREL/TP-5000-67667.*

APPENDIX A

1. Landers Earthquake Measured from Near-field station

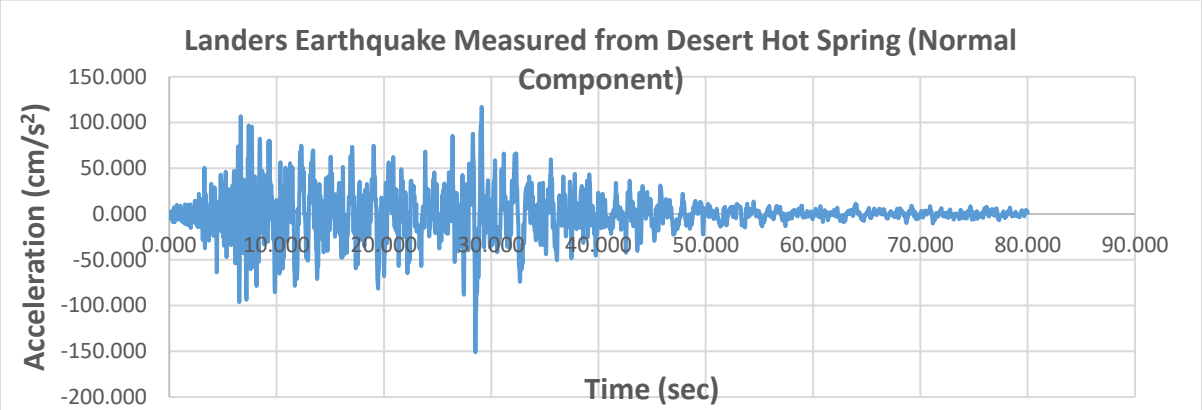

Figure 1: Horizontal acceleration Vs. Time graph for Landers Earthquake

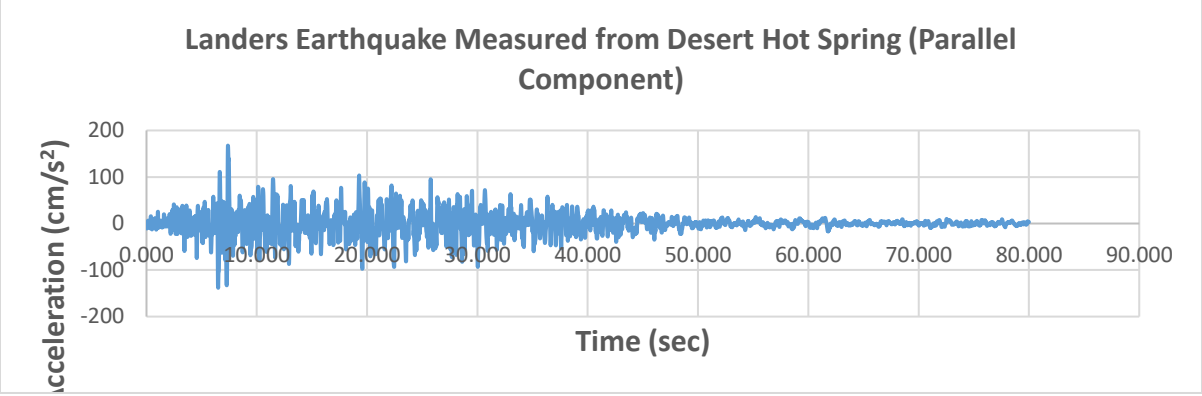

Figure 2: Horizontal acceleration Vs. Time graph for Landers Earthquake

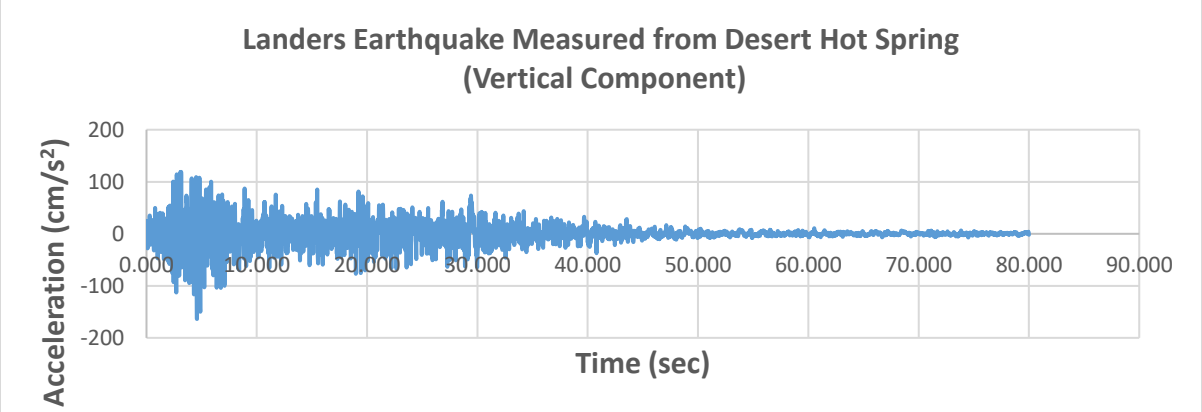

Figure 3: Vertical acceleration Vs. Time graph for Landers Earthquake

2. Landers Earthquake Measured from Far-field station

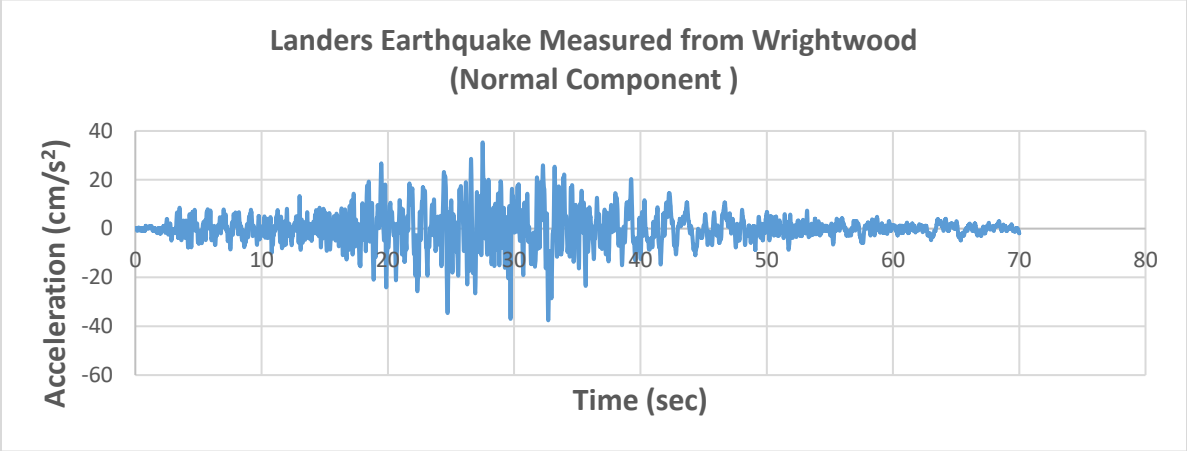

Figure 4: Horizontal acceleration Vs. Time graph for Landers Earthquake

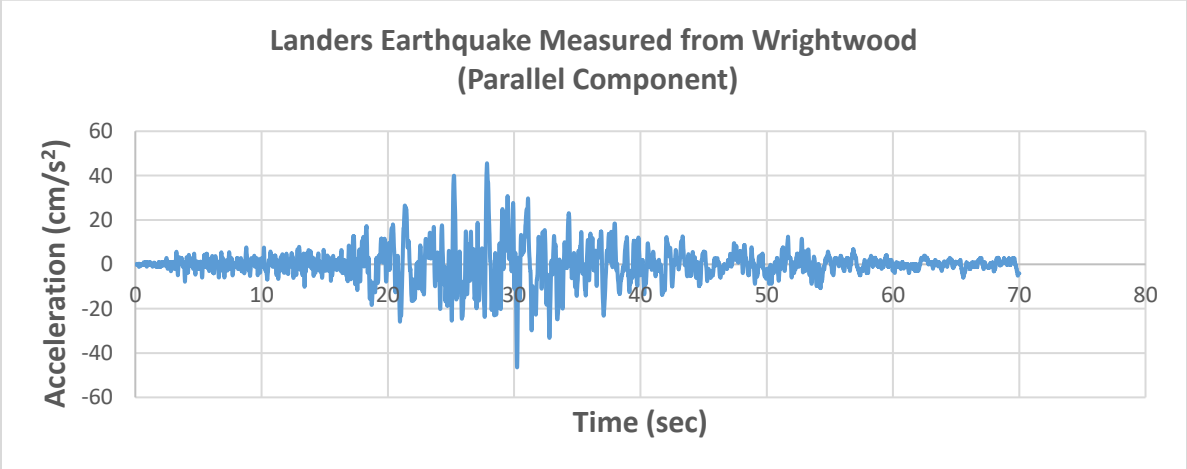

Figure 5: Horizontal acceleration Vs. Time graph for Landers Earthquake

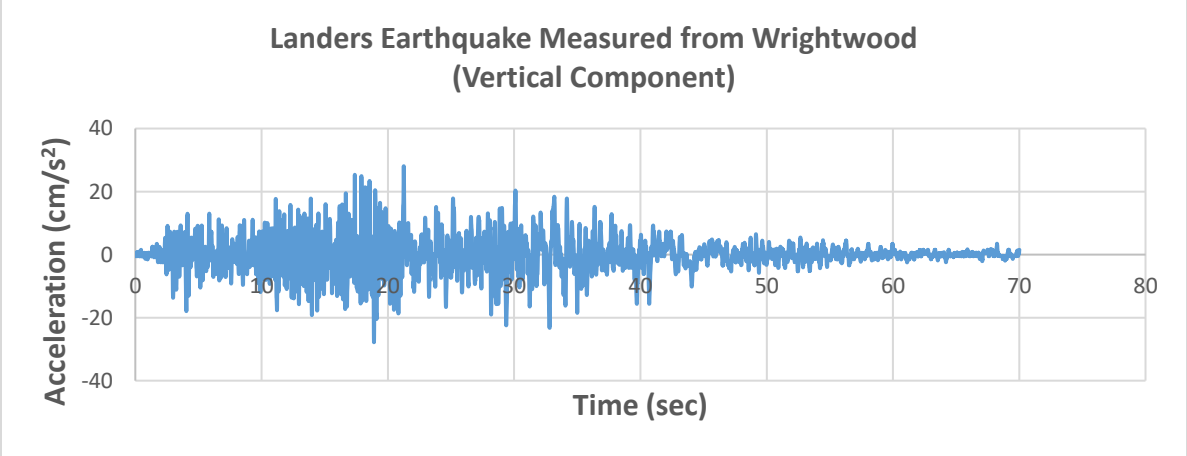

Figure 6: Vertical acceleration Vs. Time graph for Landers Earthquake

3. Loma Prieta Earthquake Measured from Near-field station

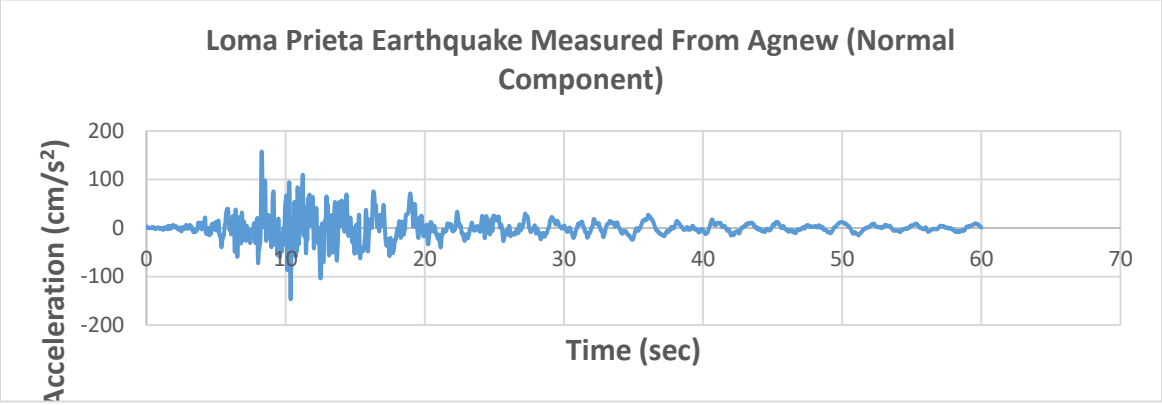

Figure 7: Horizontal acceleration Vs. Time graph for Loma Prieta Earthquake

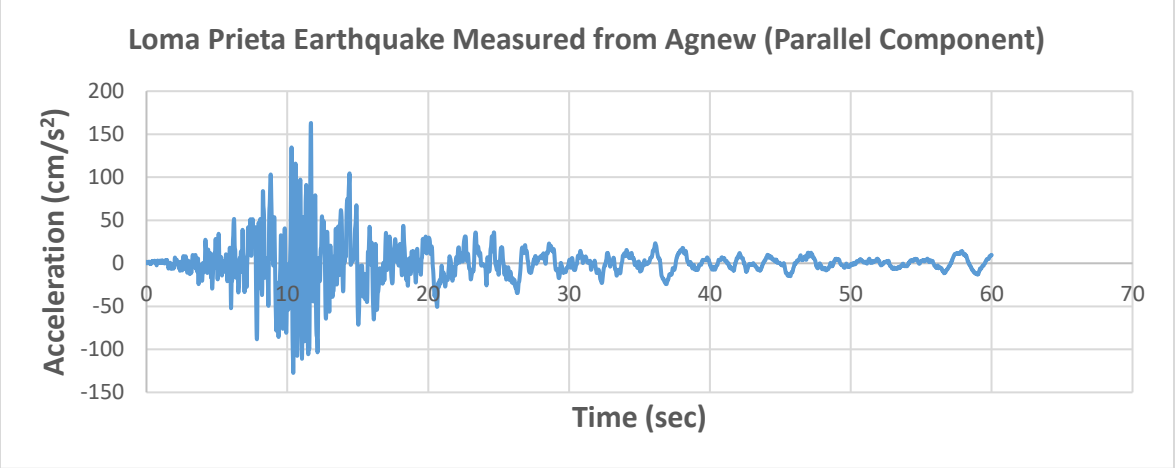

Figure 8: Horizontal acceleration Vs. Time graph for Loma Prieta Earthquake

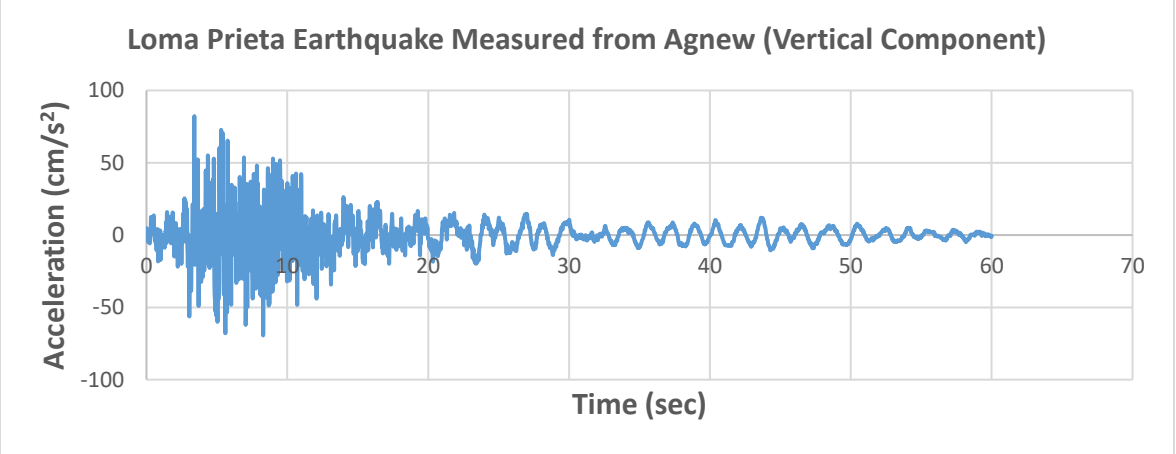

Figure 9: Vertical acceleration Vs. Time graph for Loma Prieta Earthquake

4. Loma Prieta Earthquake Measured from Far-field station

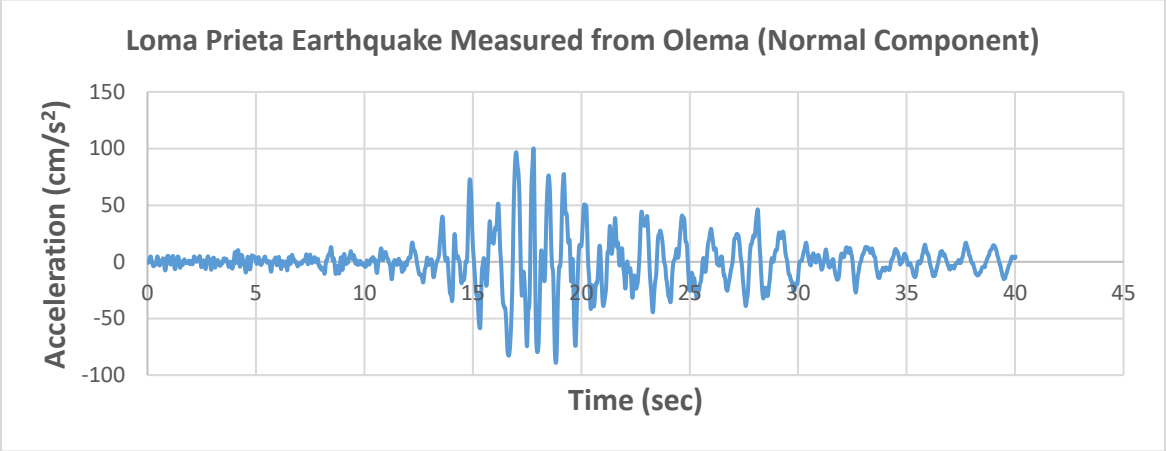

Figure 10: Horizontal acceleration Vs. Time graph for Loma Prieta Earthquake

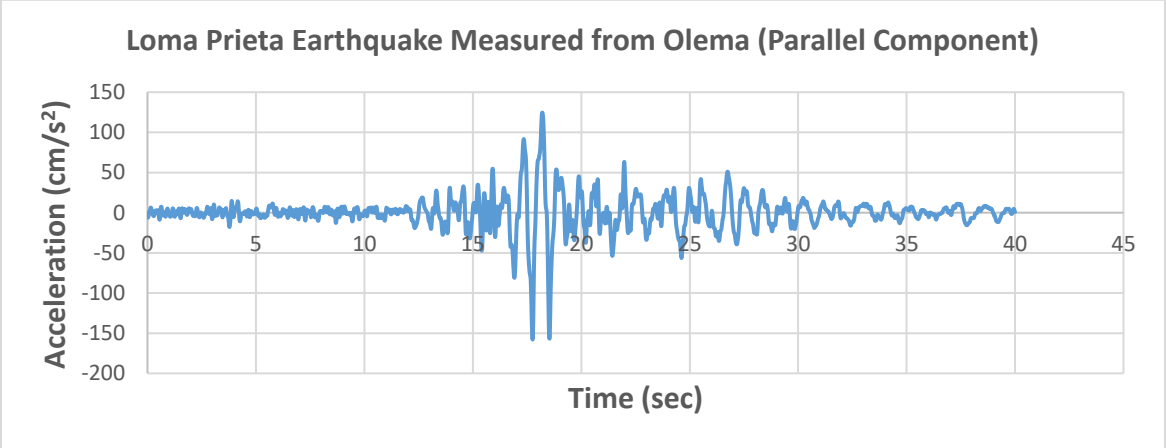

Figure 11: Horizontal acceleration Vs. Time graph for Loma Prieta Earthquake

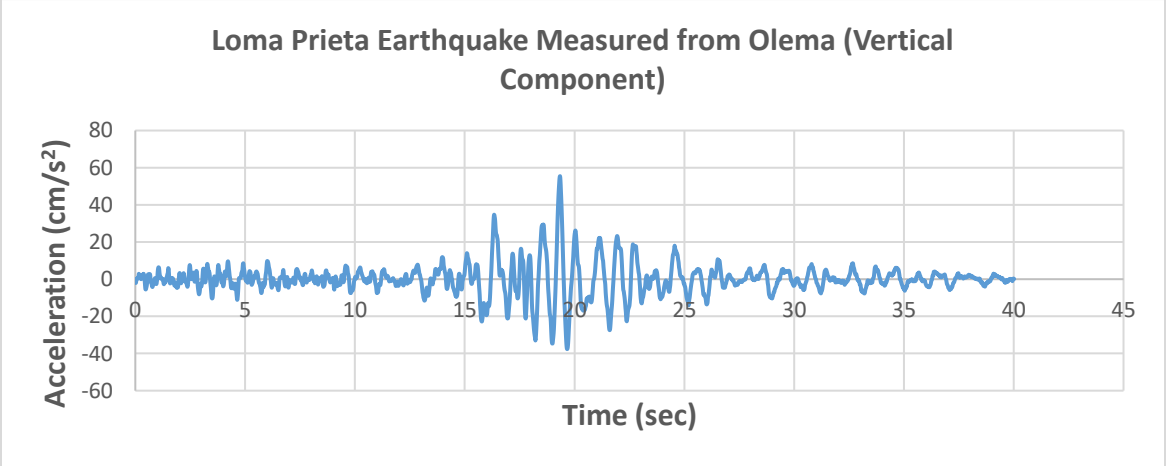

Figure 12: Vertical acceleration Vs. Time graph for Loma Prieta Earthquake

5. Dillon Earthquake Measured from Near-field station

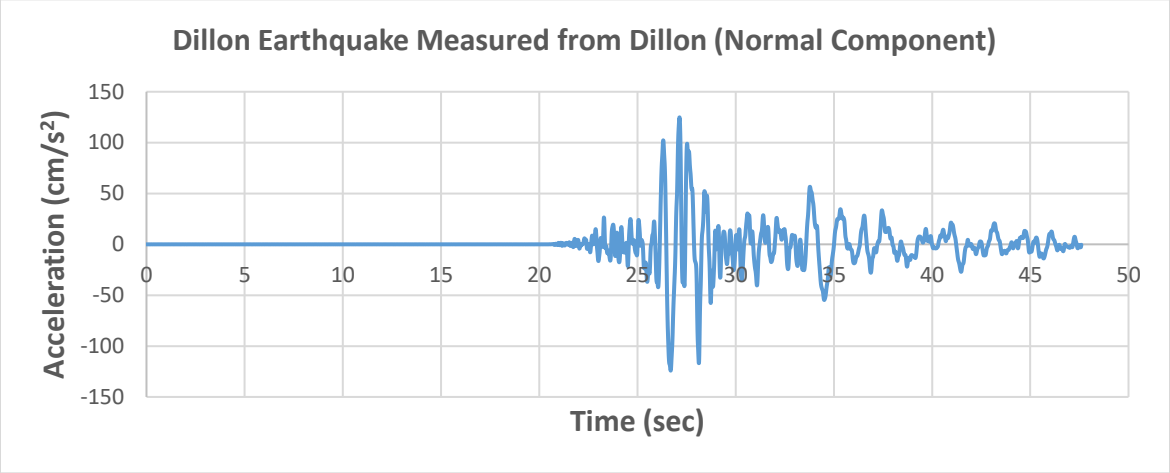

Figure 13: Horizontal acceleration Vs. Time graph for Dillon Earthquake

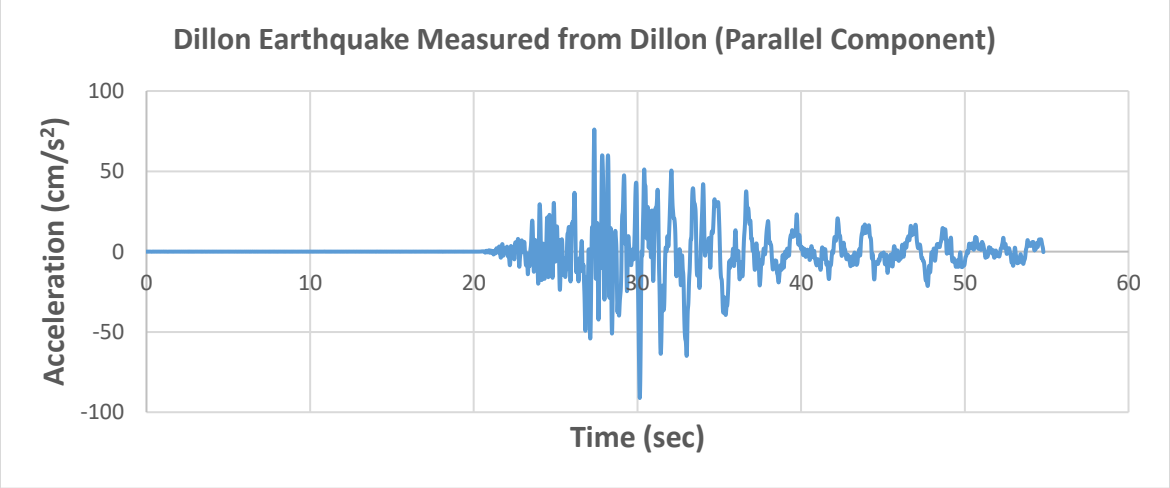

Figure 14: Horizontal acceleration Vs. Time graph for Dillon Earthquake

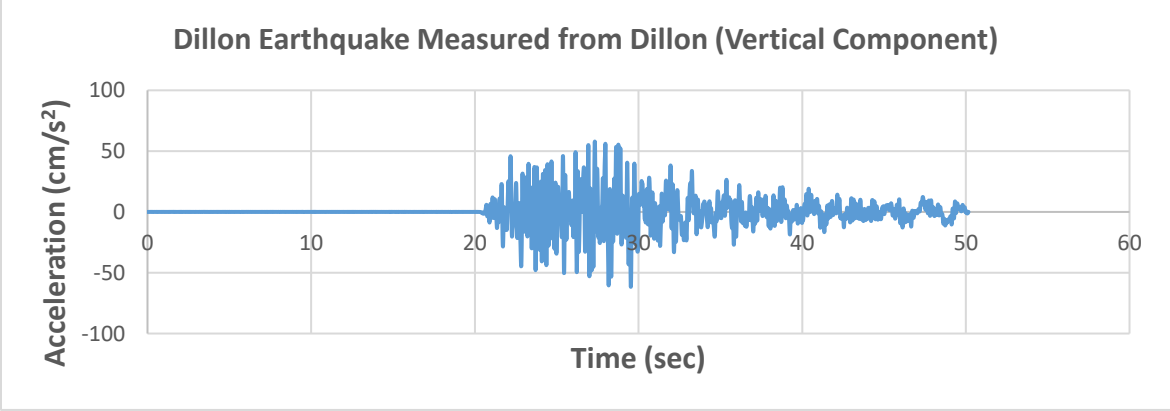

Figure 15: Vertical acceleration Vs. Time graph for Dillon Earthquake

6. Dillon Earthquake Measured from Far-field station

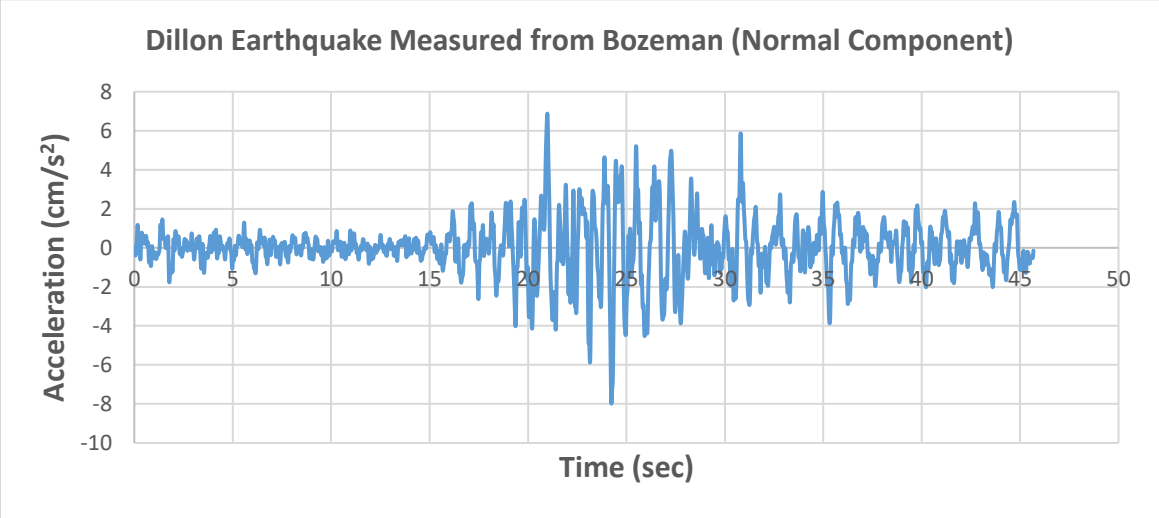

Figure 16: Horizontal acceleration Vs. Time graph for Dillon Earthquake

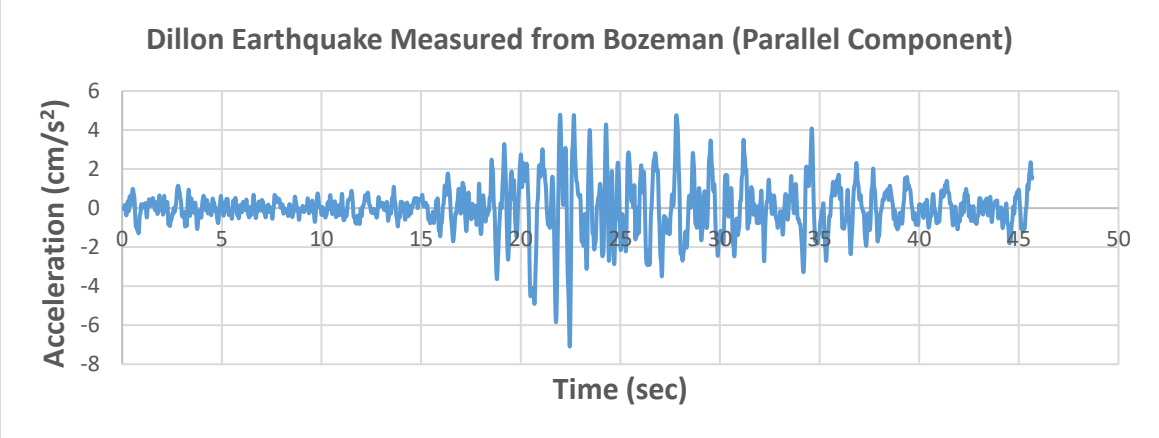

Figure 17: Horizontal acceleration Vs. Time graph for Dillon Earthquake

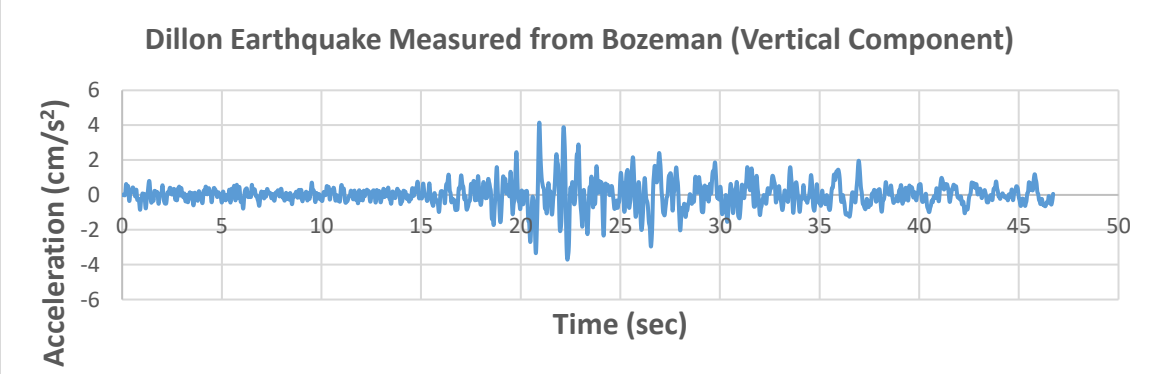

Figure 18: Vertical acceleration Vs. Time graph for Dillon Earthquake

7. Anza Earthquake Measured from Near-field station

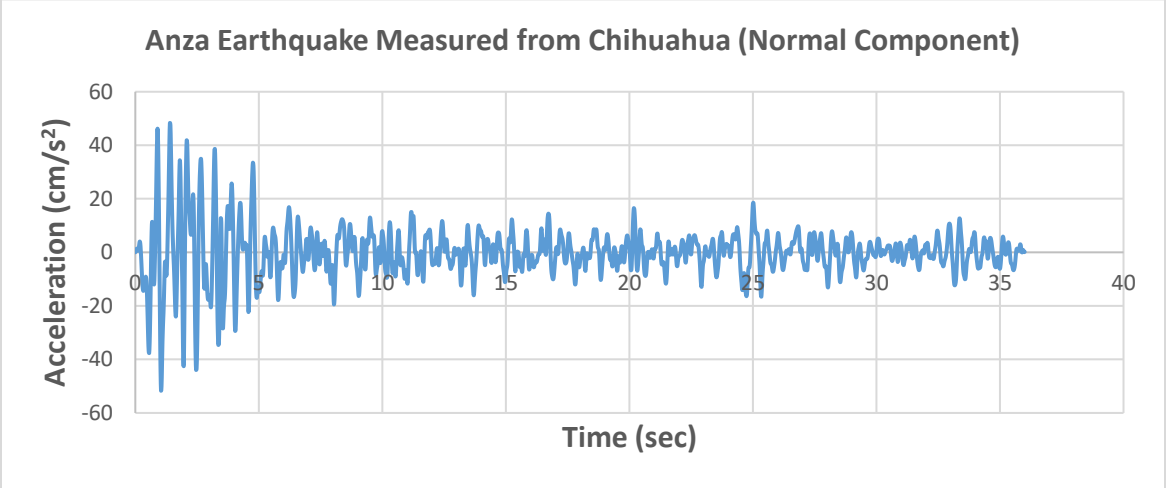

Figure 19: Horizontal acceleration Vs. Time graph for Anza Earthquake

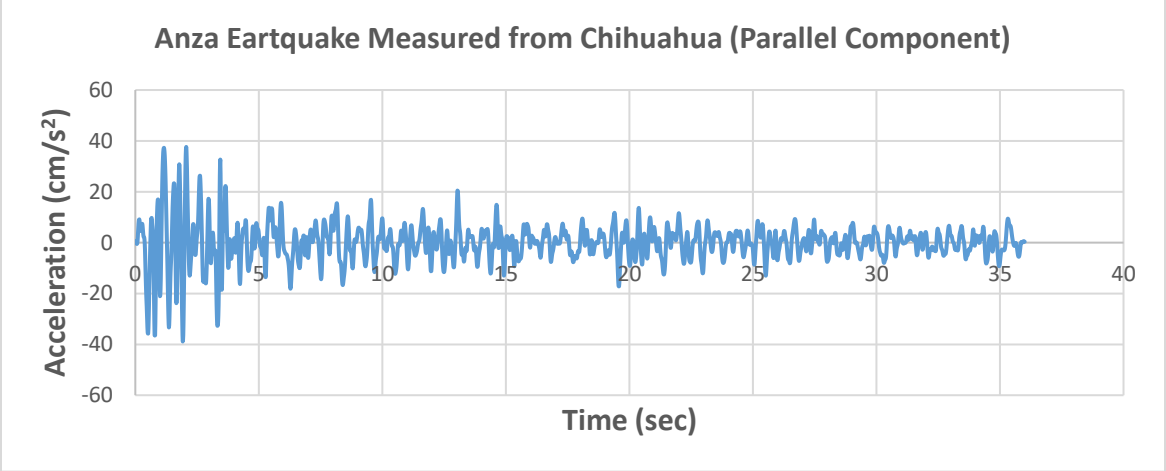

Figure 20: Horizontal acceleration Vs. Time graph for Anza Earthquake

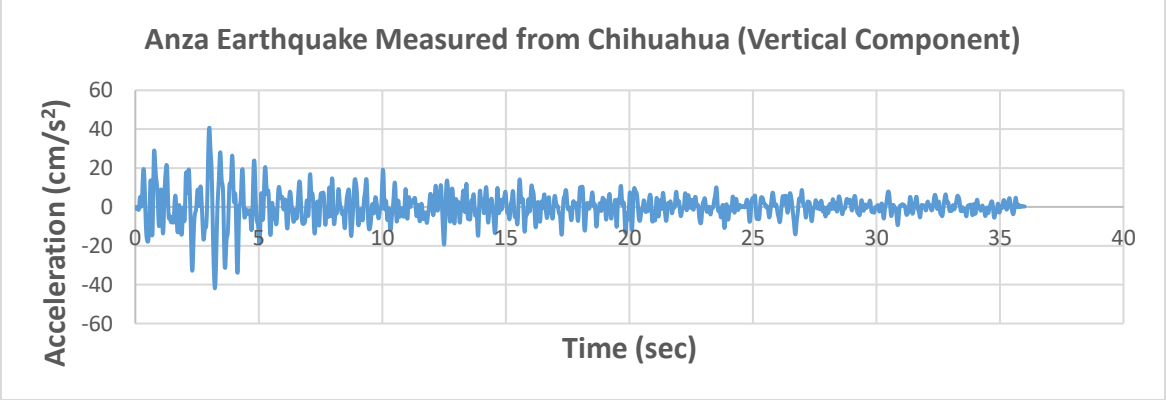

Figure 21: Vertical acceleration Vs. Time graph for Anza Earthquake

8. Anza Earthquake Measured from Far-field station

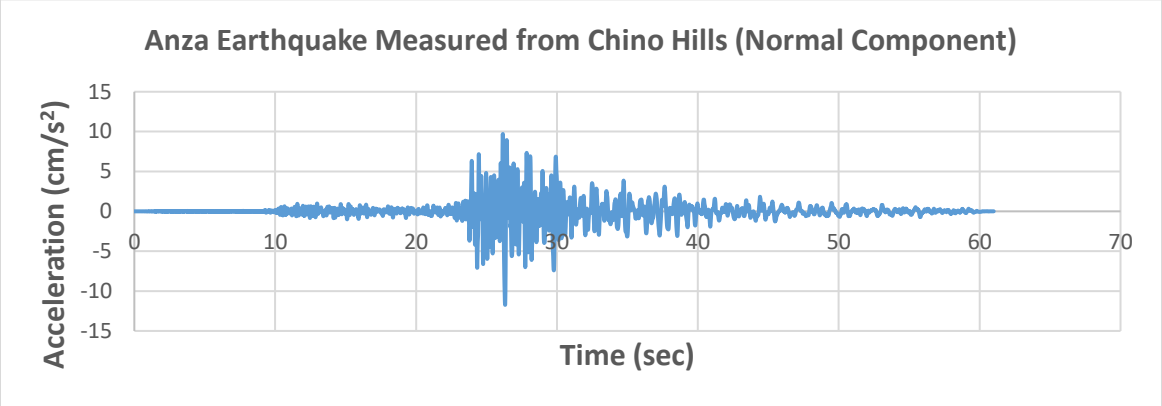

Figure 22: Horizontal acceleration Vs. Time graph for Anza Earthquake

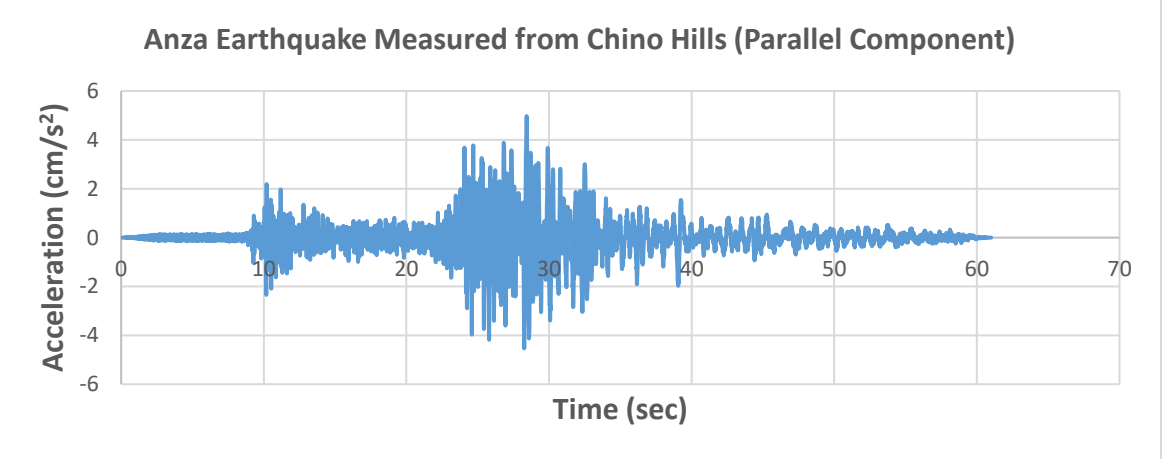

Figure 23: Horizontal acceleration Vs. Time graph for Anza Earthquake

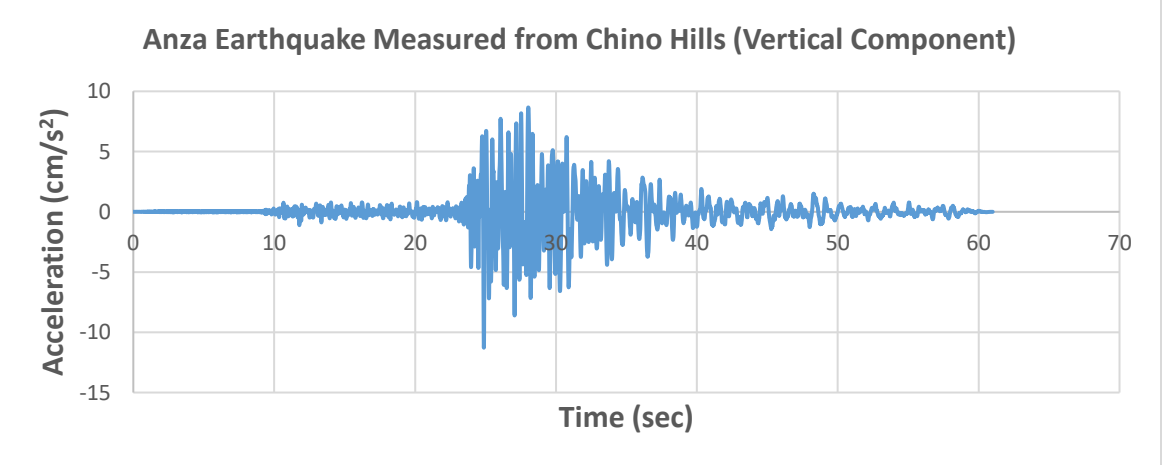

Figure 24: Vertical acceleration Vs. Time graph for Anza Earthquake

9. Gilroy Earthquake Measured from Near-field station

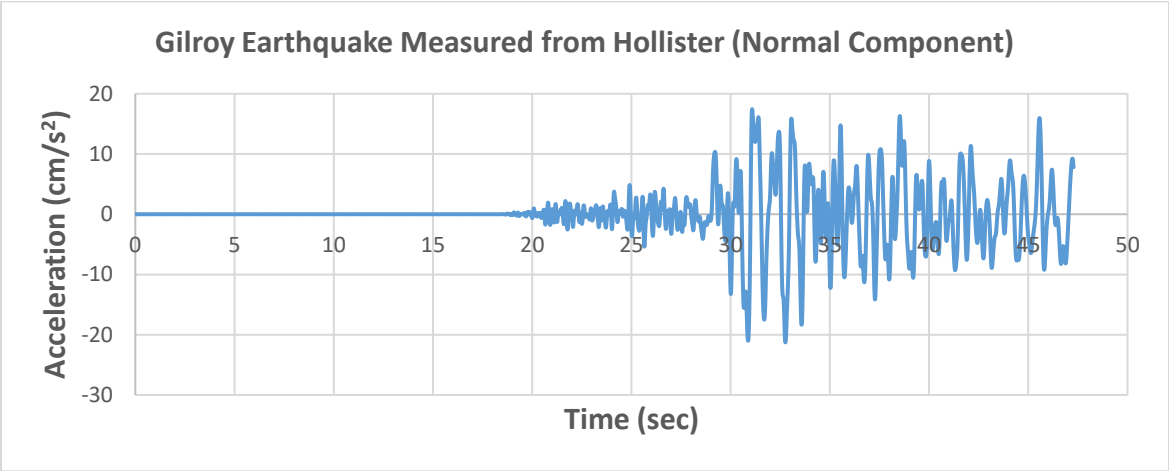

Figure 25: Horizontal acceleration Vs. Time graph for Gilroy Earthquake

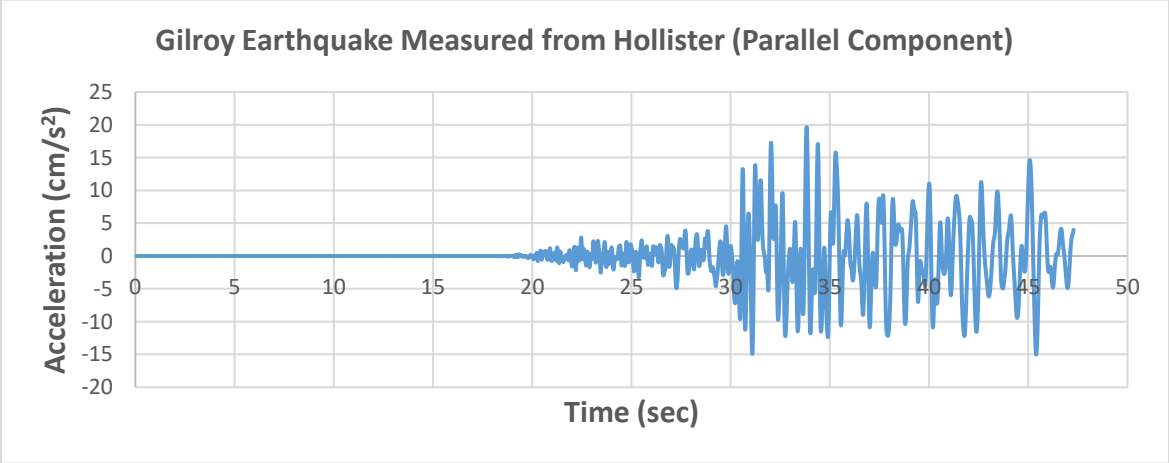

Figure 26: Horizontal acceleration Vs. Time graph for Gilroy Earthquake

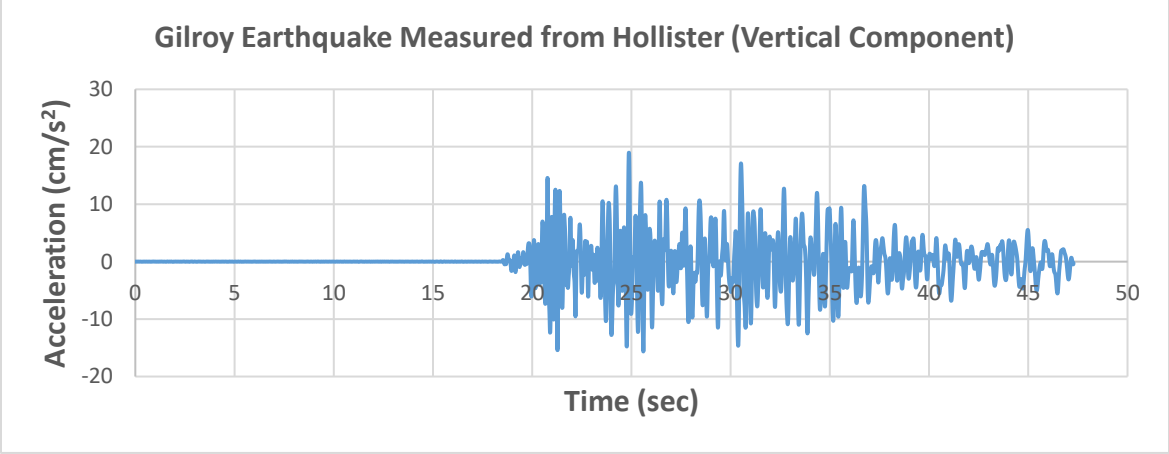

Figure 27: Vertical acceleration Vs. Time graph for Gilroy Earthquake

10. Gilroy Earthquake Measured from Far-field station

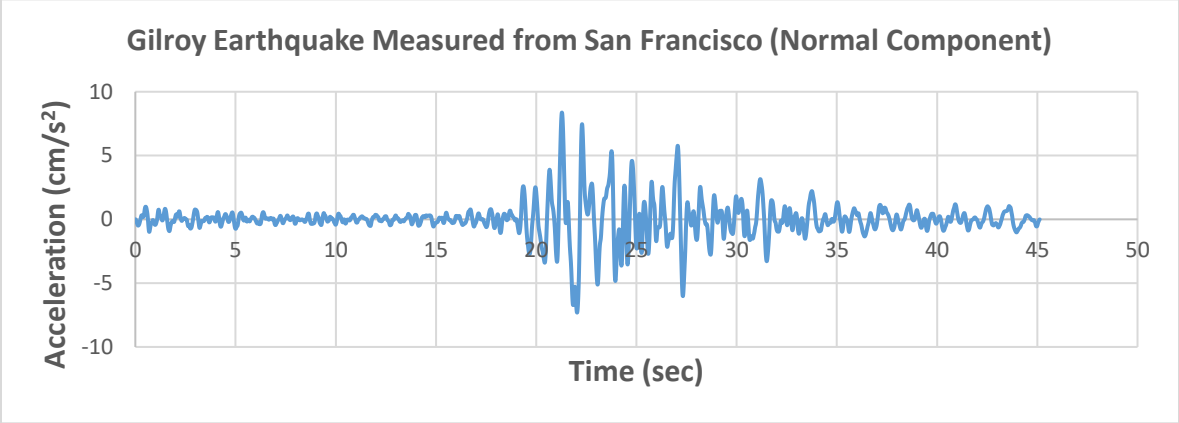

Figure 28: Horizontal acceleration Vs. Time graph for Gilroy Earthquake

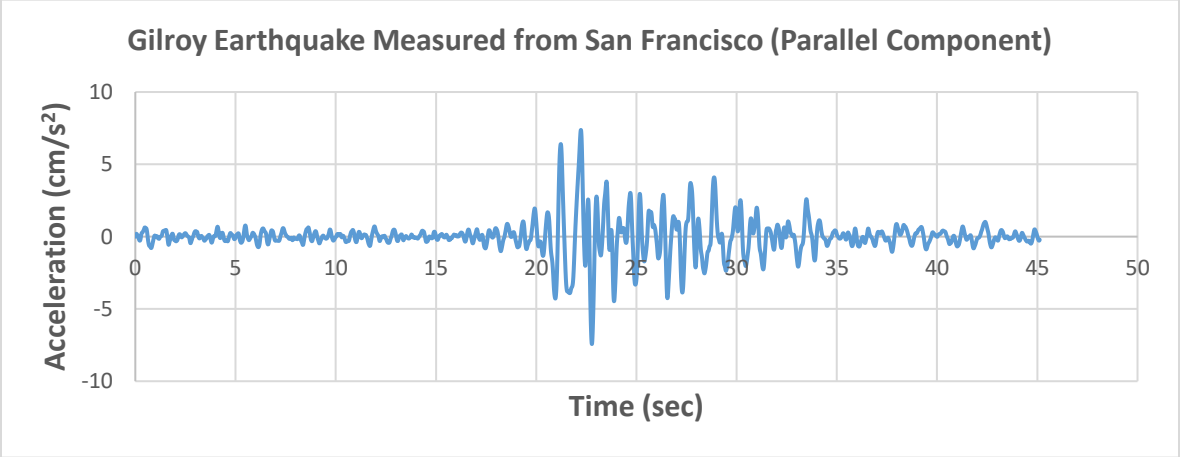

Figure 29: Horizontal acceleration Vs. Time graph for Gilroy Earthquake

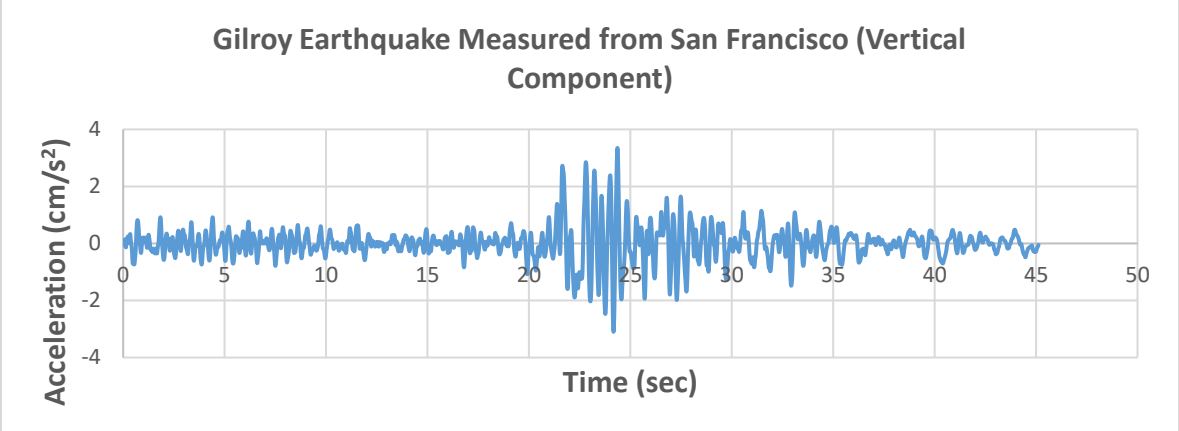

Figure 30: Vertical acceleration Vs. Time graph for Gilroy Earthquake

11. Volcano Earthquake Measured from Near-field station

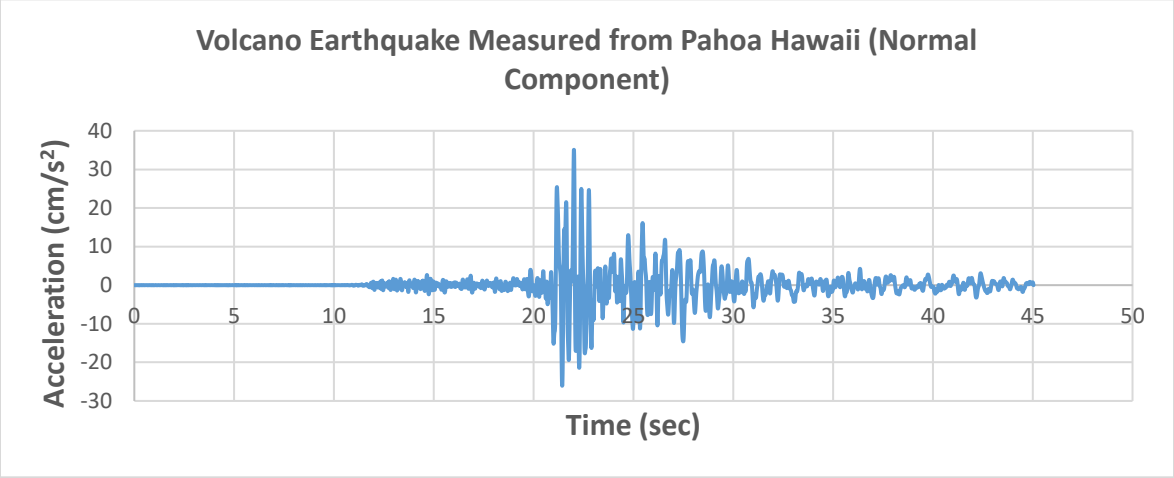

Figure 31: Horizontal acceleration Vs. Time graph for Volcano Earthquake

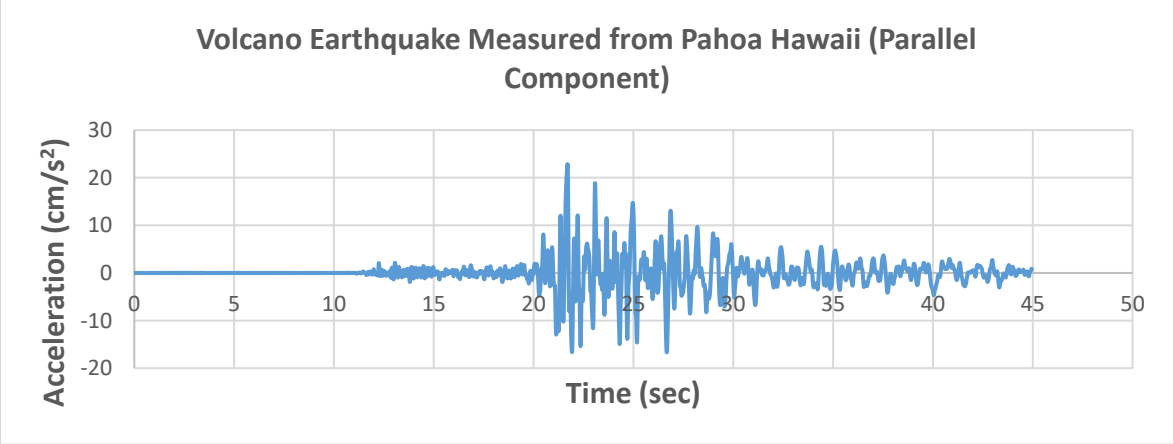

Figure 32: Horizontal acceleration Vs. Time graph for Volcano Earthquake

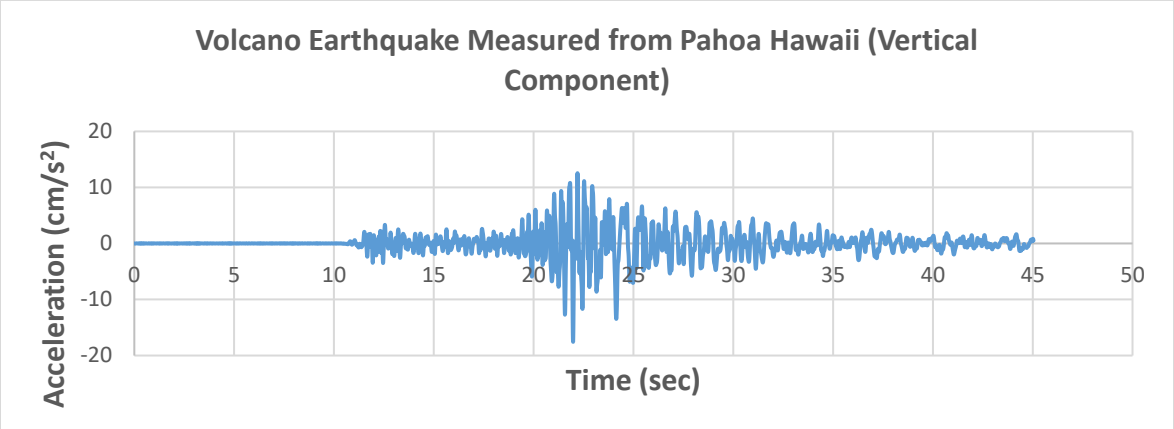

Figure 33: Vertical acceleration Vs. Time graph for Volcano Earthquake

12. Volcano Earthquake Measured from Far-field station

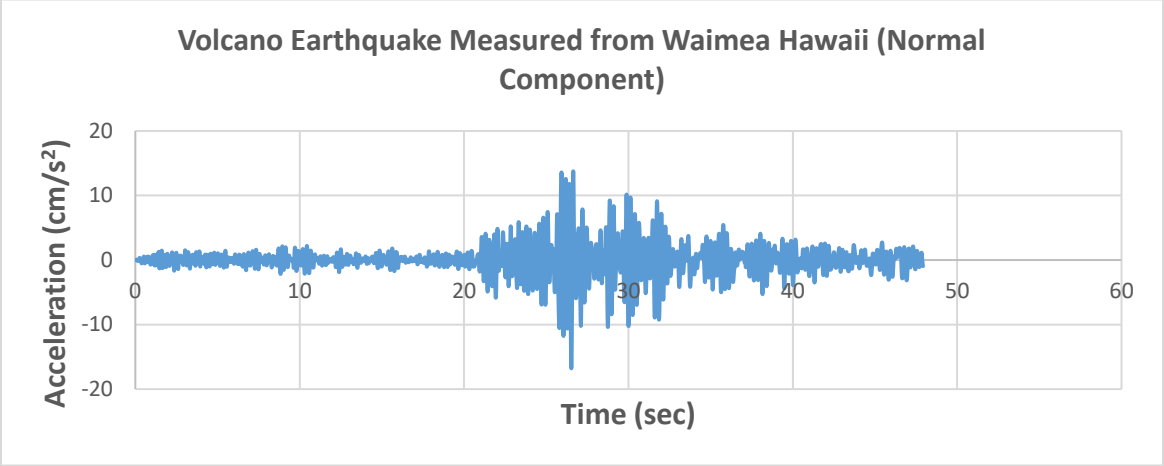

Figure 34: Horizontal acceleration Vs. Time graph for Volcano Earthquake

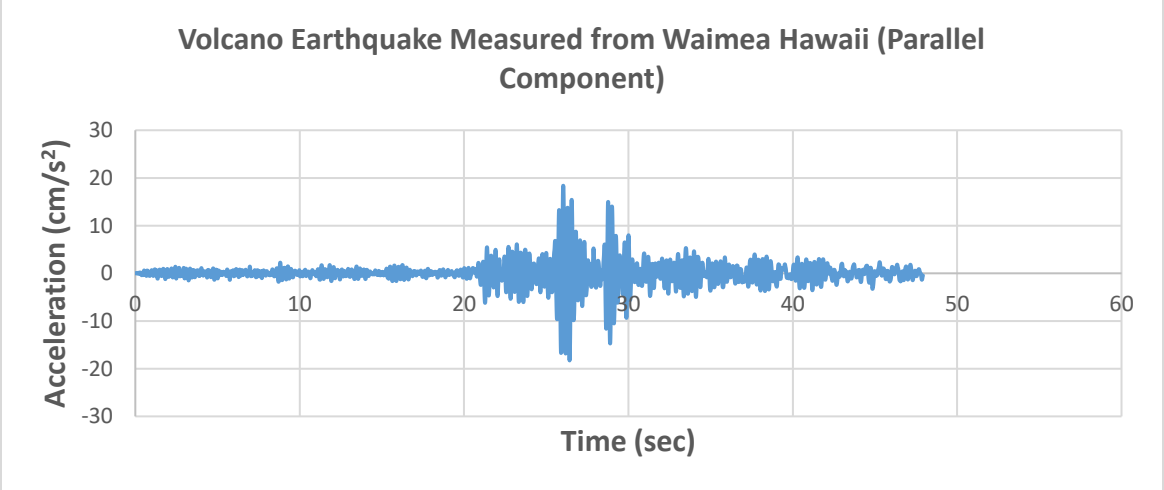

Figure 35: Horizontal acceleration Vs. Time graph for Volcano Earthquake

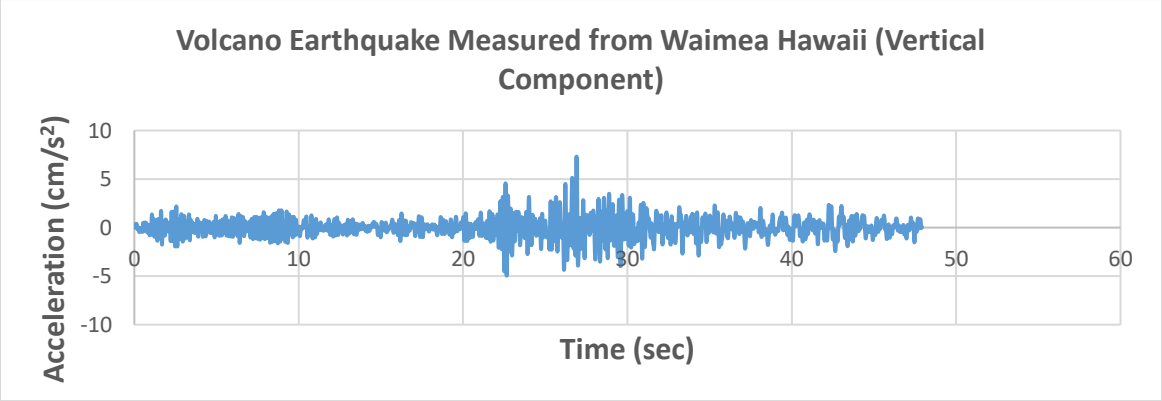

Figure 36: Vertical acceleration Vs. Time graph for Volcano Earthquake

APPENDIX B

1. Maximum Tower Displacement for Normal Operation Condition

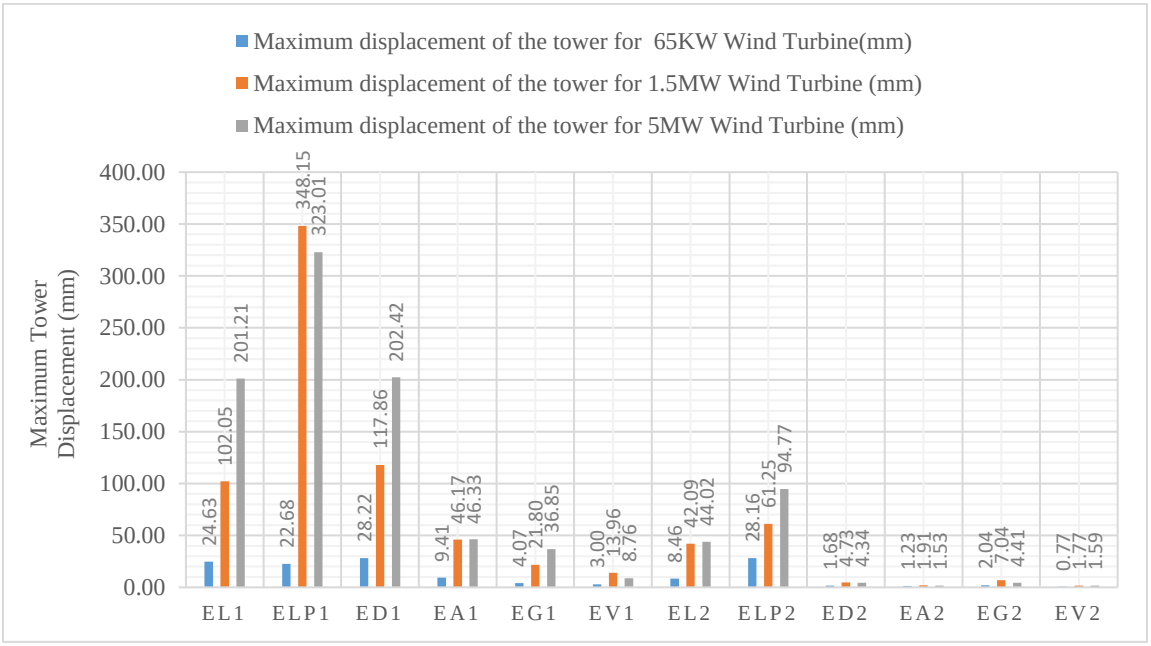

Figure 1: Top displacement of the tower when wind speed is 5m/s for 65kW, 1.5MW and 5MW wind turbines under seismic excitations

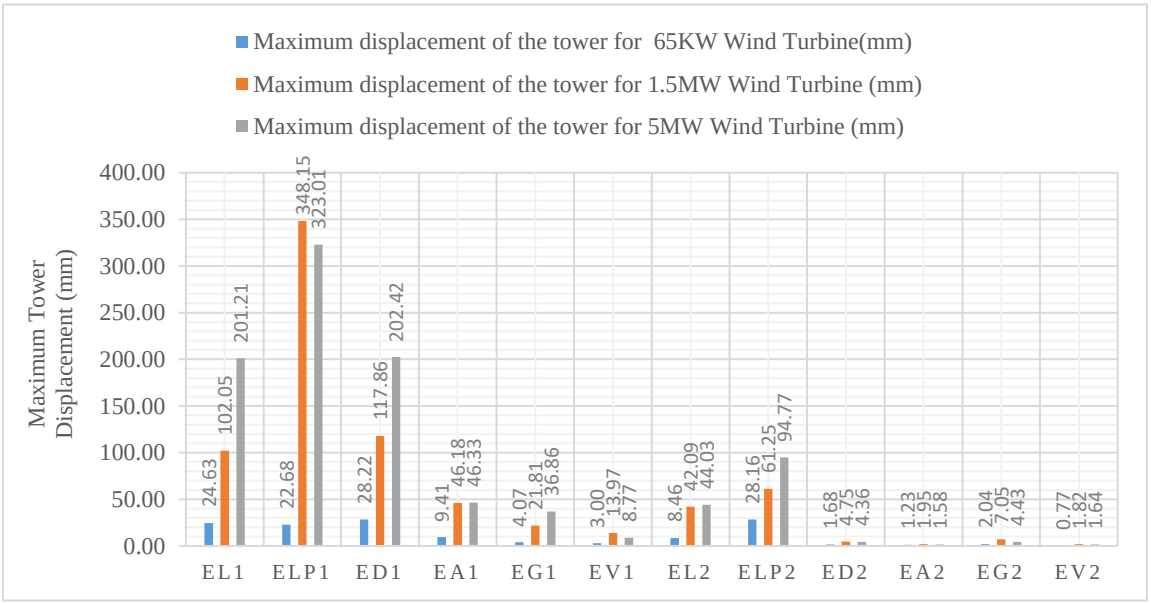

Figure 2: Top displacement of the tower when wind speed is 7m/s for 65kW, 1.5MW and 5MW wind turbines under seismic excitations

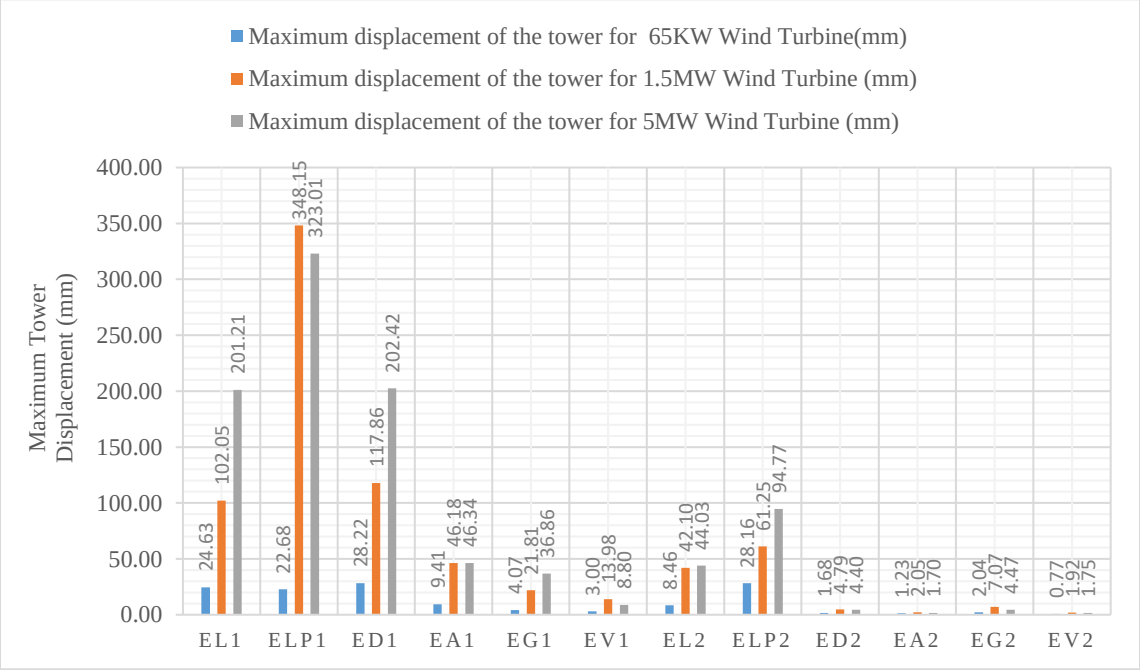

Figure 3: Top displacement of the tower when wind speed is 9 m/s for 65kW, 1.5MW and 5MW wind turbines under seismic excitations

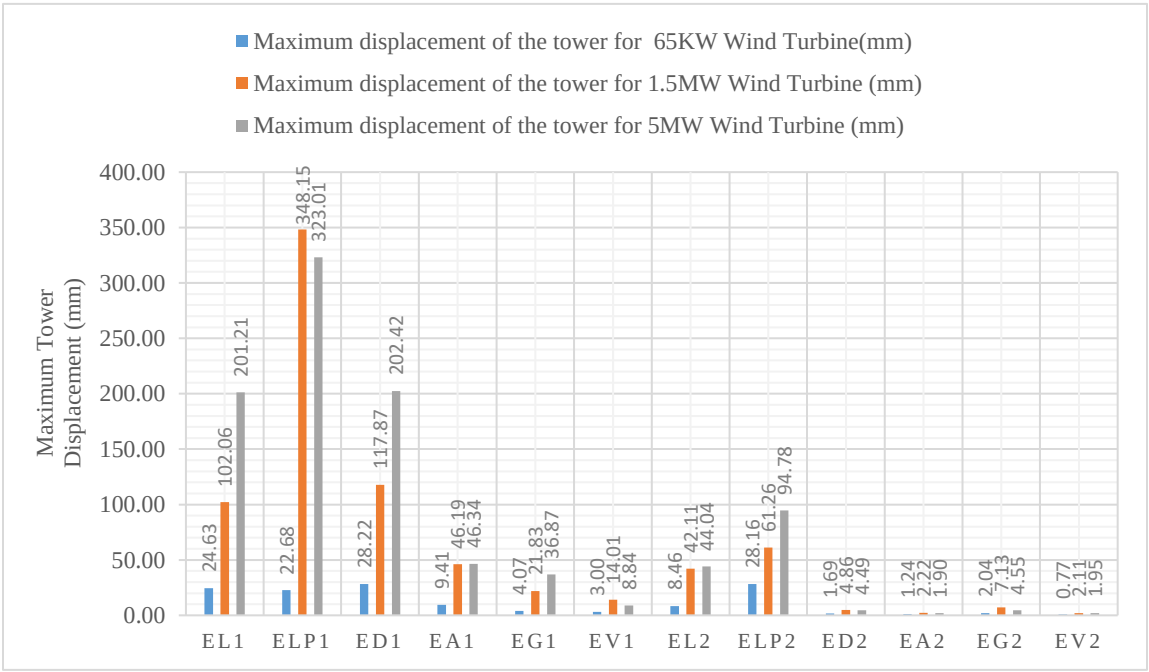

Figure 4: Top displacement of the tower when wind speed is 11 m/s for 65kW, 1.5MW and 5MW wind turbines under seismic excitations

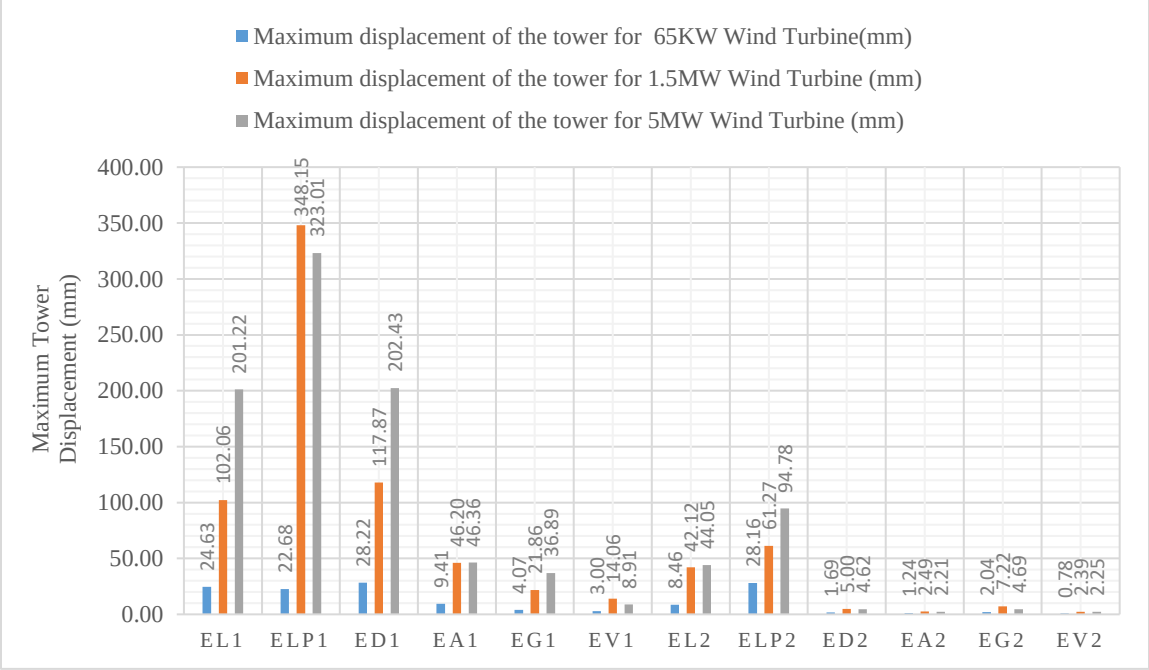

Figure 5: Top displacement of the tower when wind speed is 13 m/s for 65kW, 1.5MW and 5MW wind turbines under seismic excitations

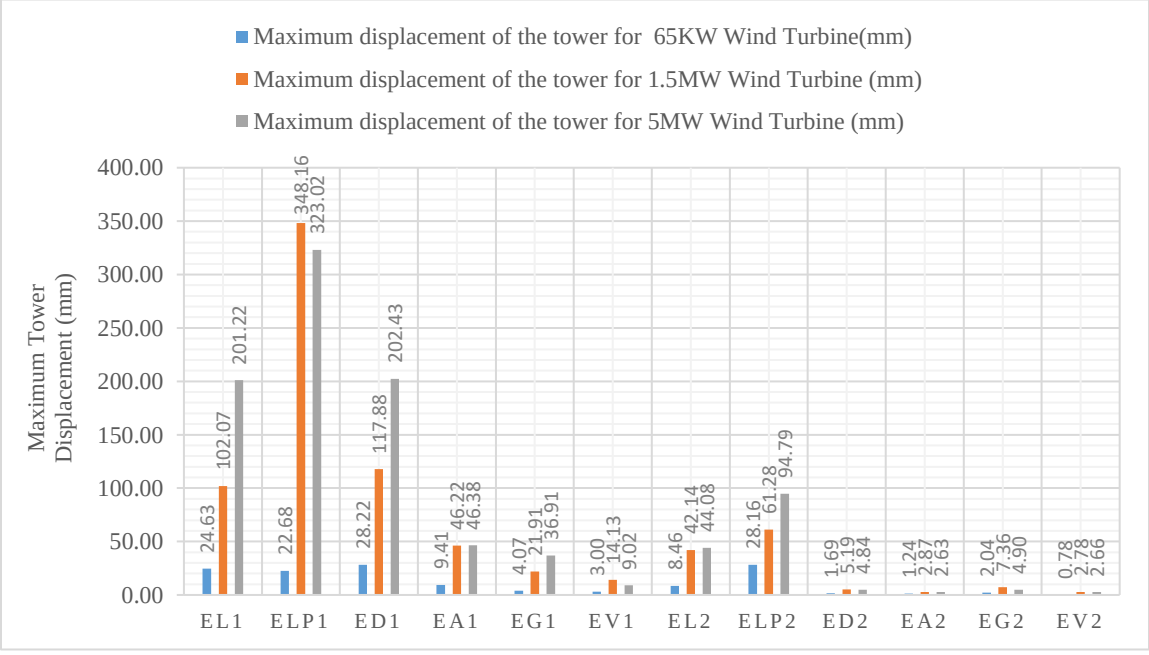

Figure 6: Top displacement of the tower when wind speed is 15 m/s for 65kW, 1.5MW and 5MW wind turbines under seismic excitations

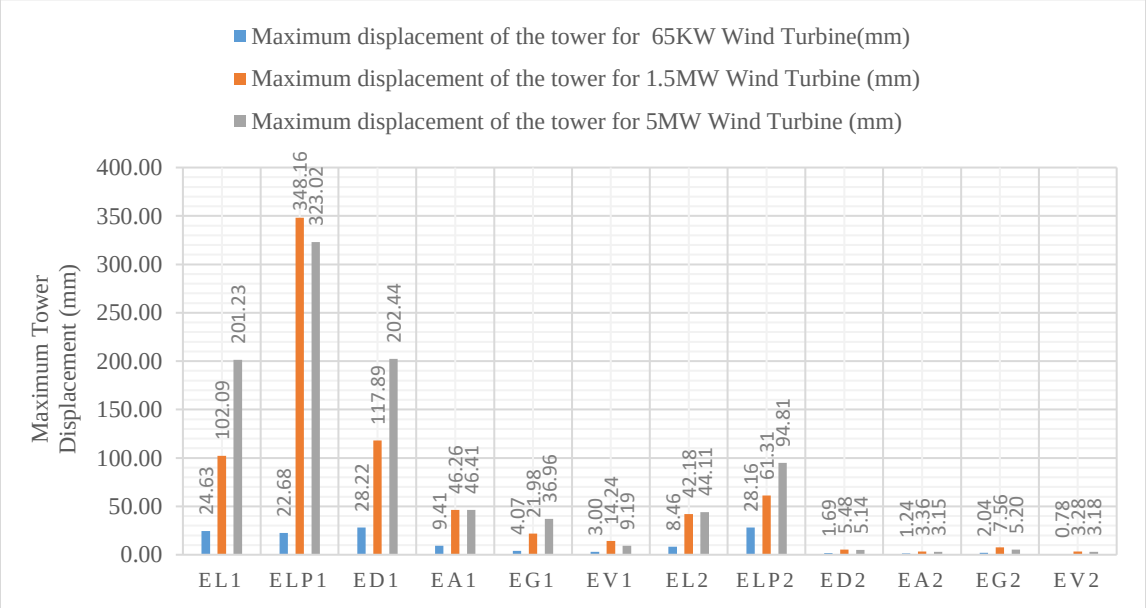

Figure 7: Top displacement of the tower when wind speed is 17 m/s for 65kW, 1.5MW and 5MW wind turbines under seismic excitations

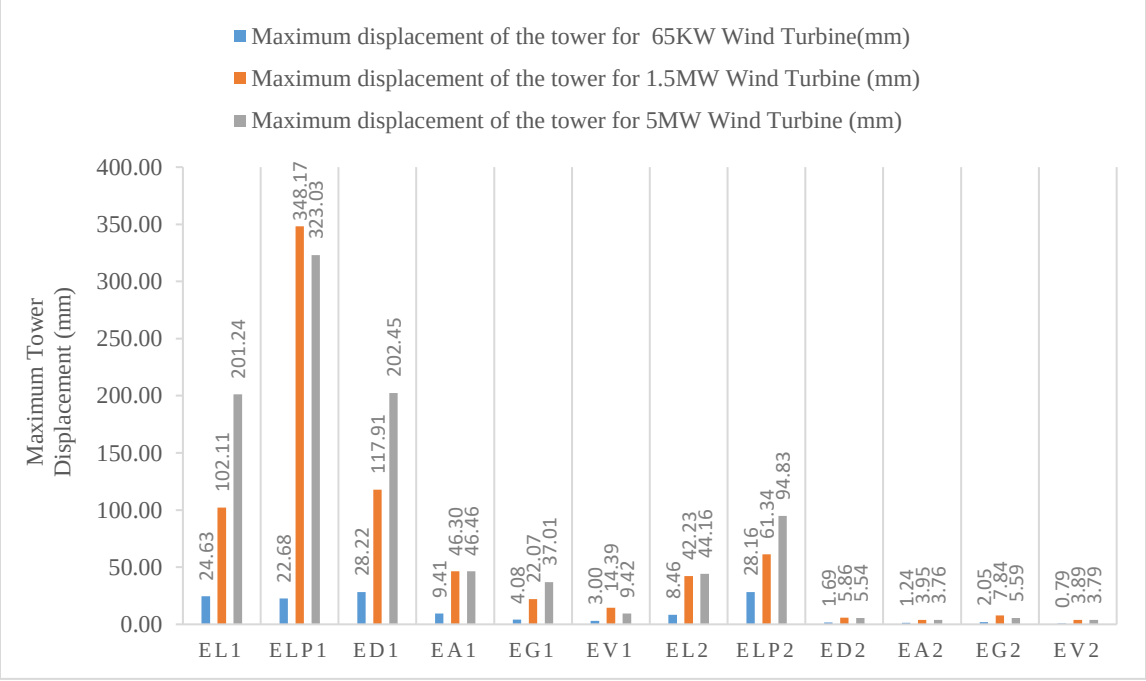

Figure 8: Top displacement of the tower when wind speed is 19 m/s for 65kW, 1.5MW and 5MW wind turbines under seismic excitations

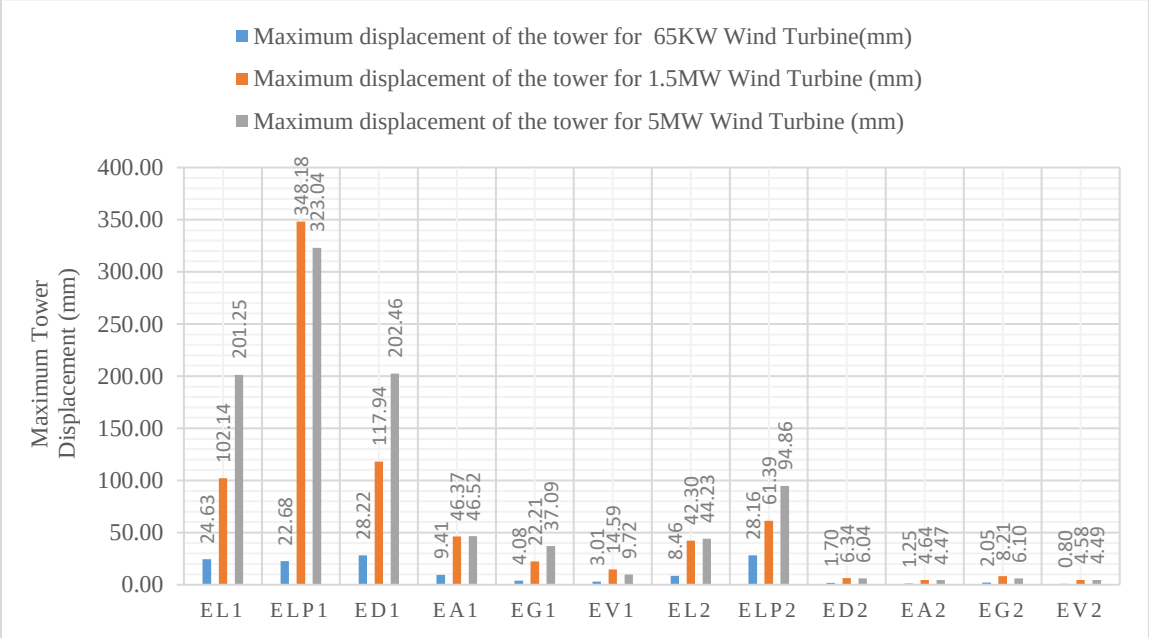

Figure 9: Top displacement of the tower when wind speed is 21 m/s for 65kW, 1.5MW and 5MW wind turbines under seismic excitations

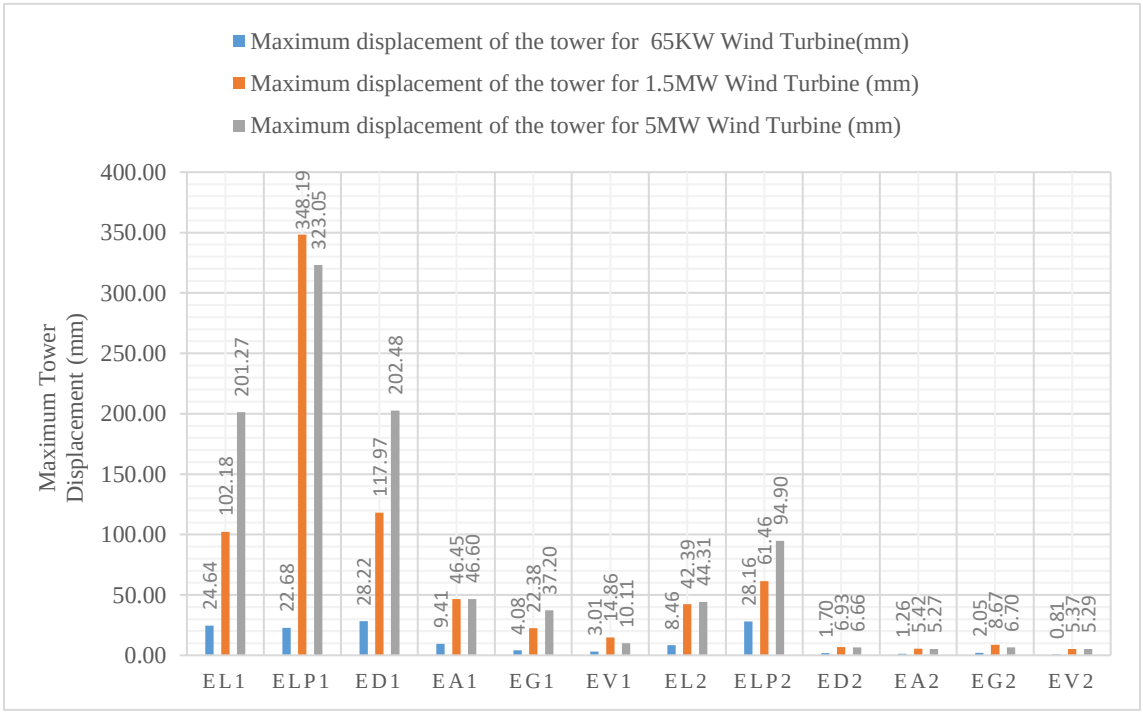

Figure 10: Top displacement of the tower when wind speed is 23 m/s for 65kW, 1.5MW and 5MW wind turbines under seismic excitations

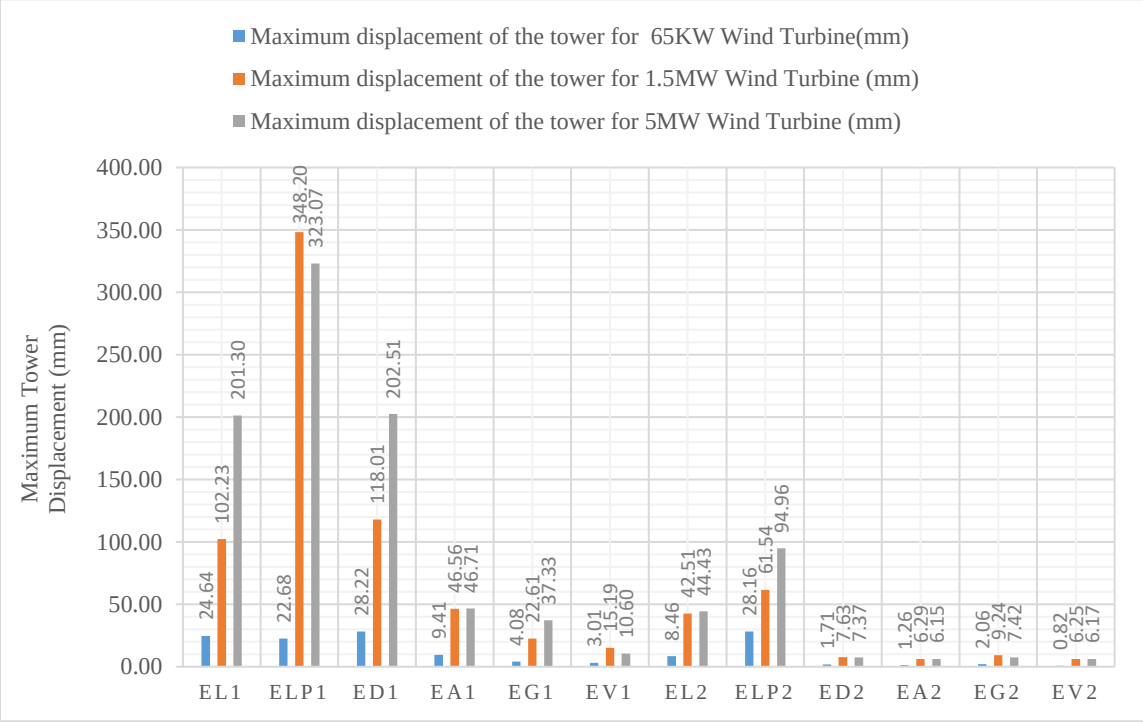

Figure 11: Top displacement of the tower when wind speed is 25 m/s for 65kW, 1.5MW and 5MW wind turbines under seismic excitations

2. Maximum Von Mises stress of the Tower for normal operation

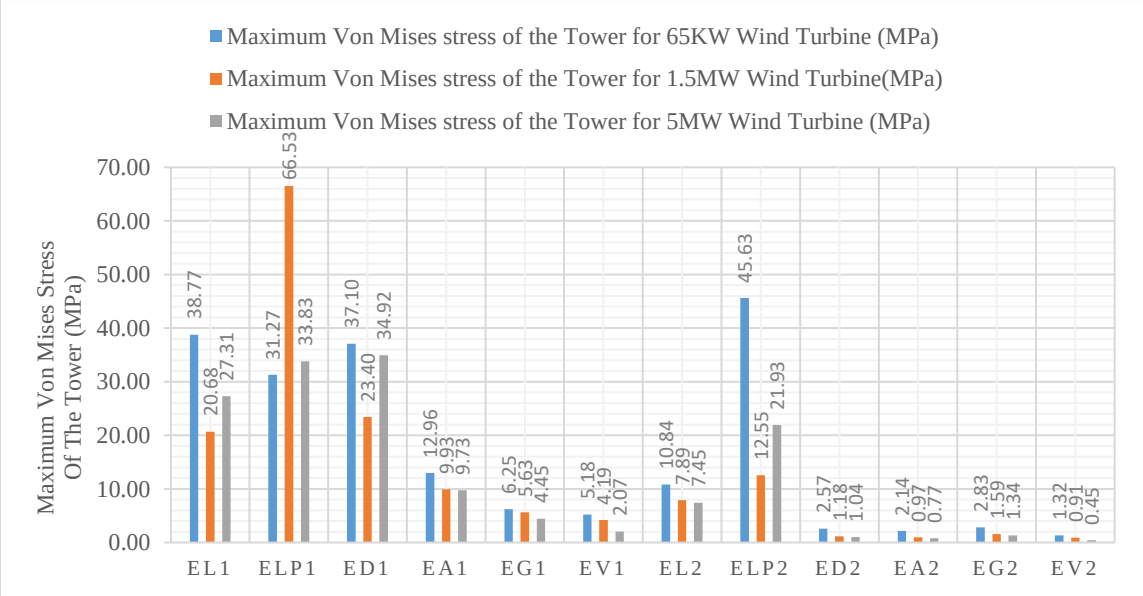

Figure 12: Maximum Von Mises stress of the tower when wind speed is 5 m/s for 65kW, 1.5MW and 5MW wind turbines under seismic excitations

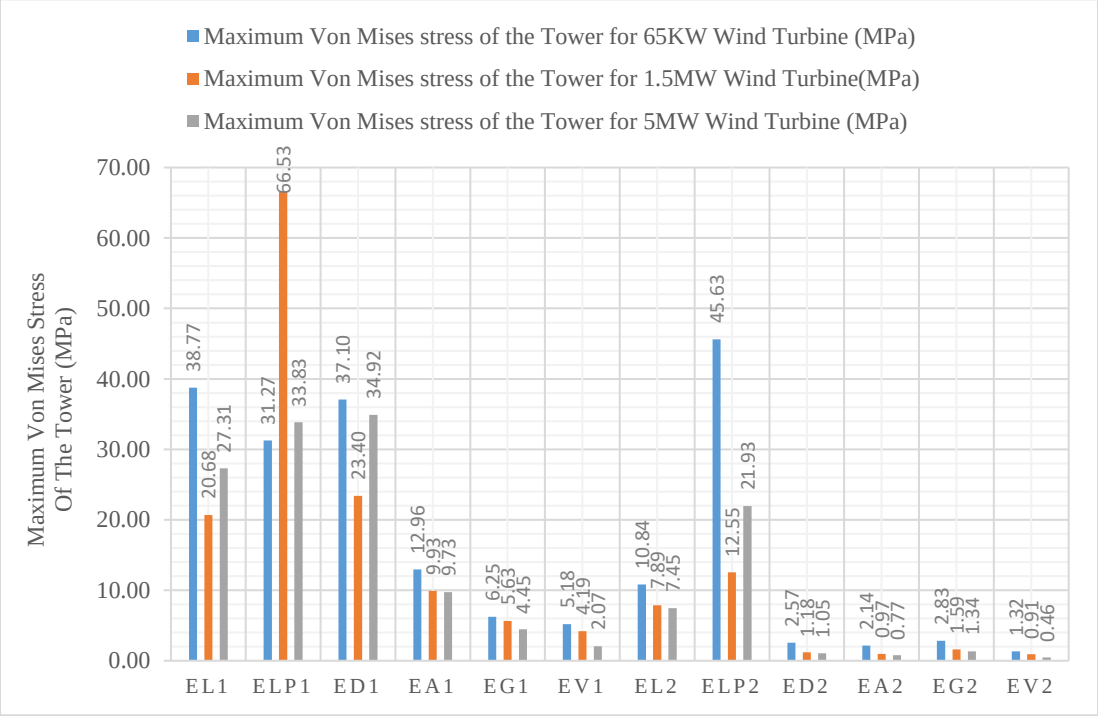

Figure 13: Maximum Von Mises stress of the tower when wind speed is 7 m/s for 65kW, 1.5MW and 5MW wind turbines under seismic excitations

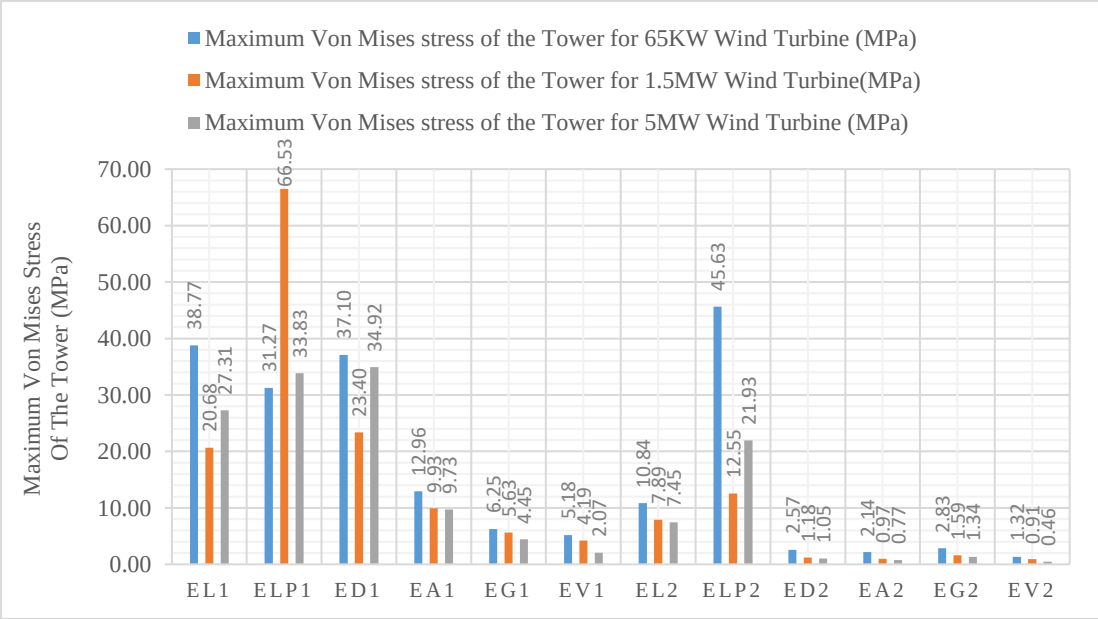

Figure 14: Maximum Von Mises stress of the tower when wind speed is 9 m/s for 65kW, 1.5MW and 5MW wind turbines under seismic excitations

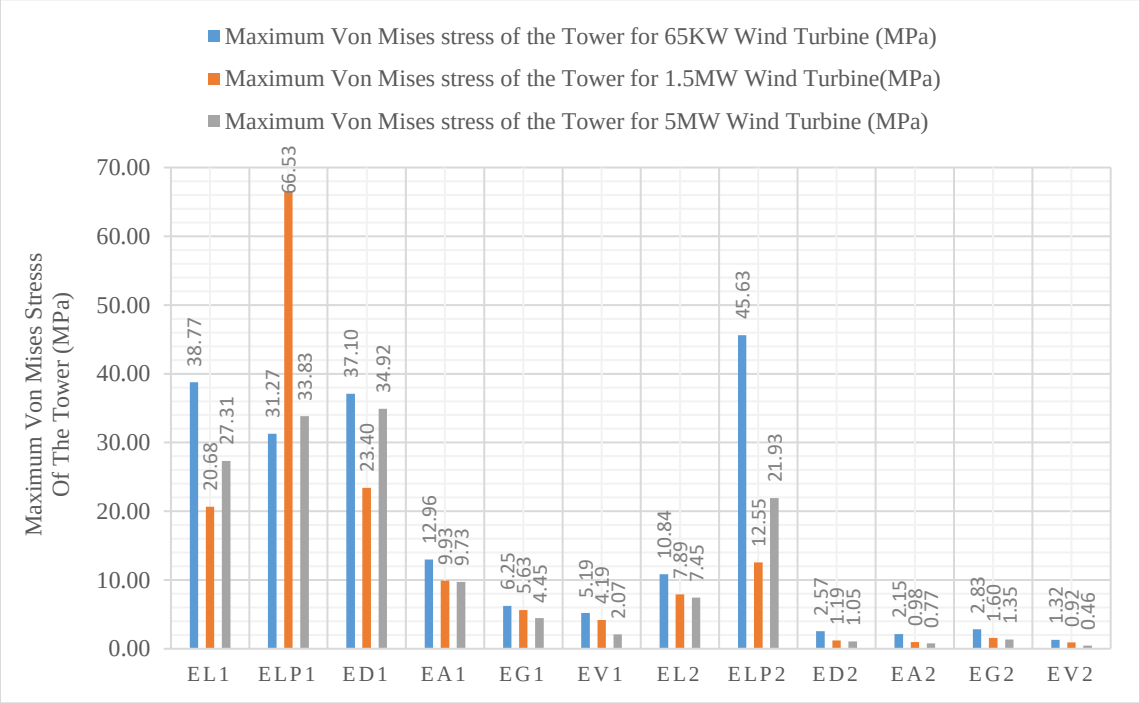

Figure 15: Maximum Von Mises stress of the tower when wind speed is 11 m/s for 65kW, 1.5MW and 5MW wind turbines under seismic excitations

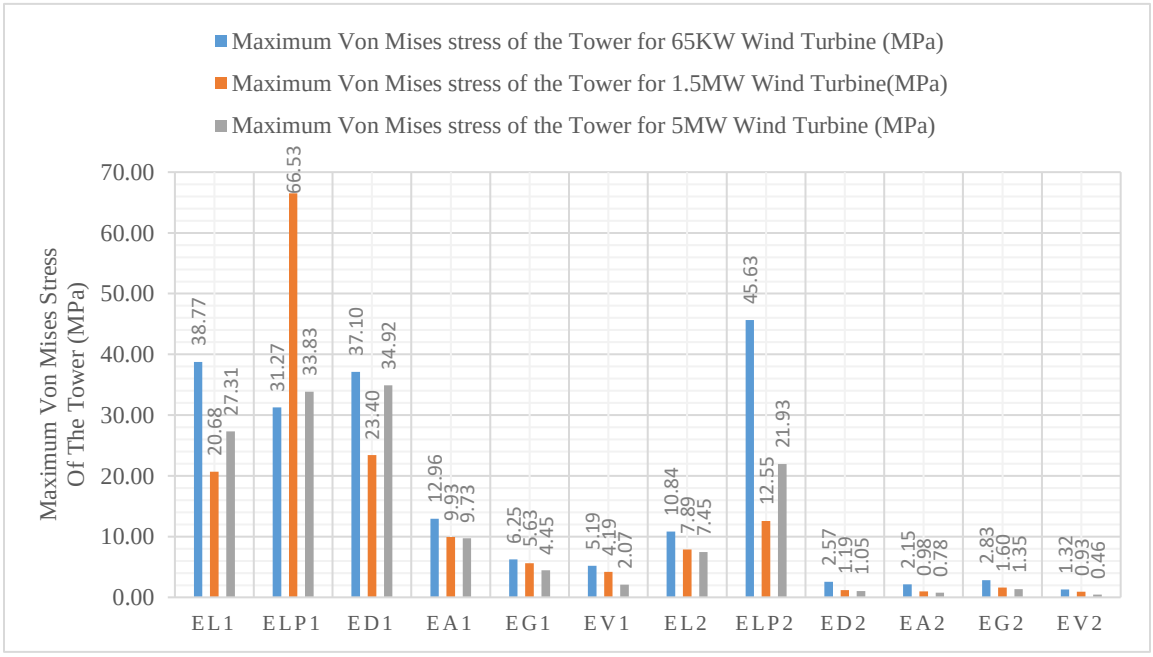

Figure 16: Maximum Von Mises stress of the tower when wind speed is 13 m/s for 65kW, 1.5MW and 5MW wind turbines under seismic excitations

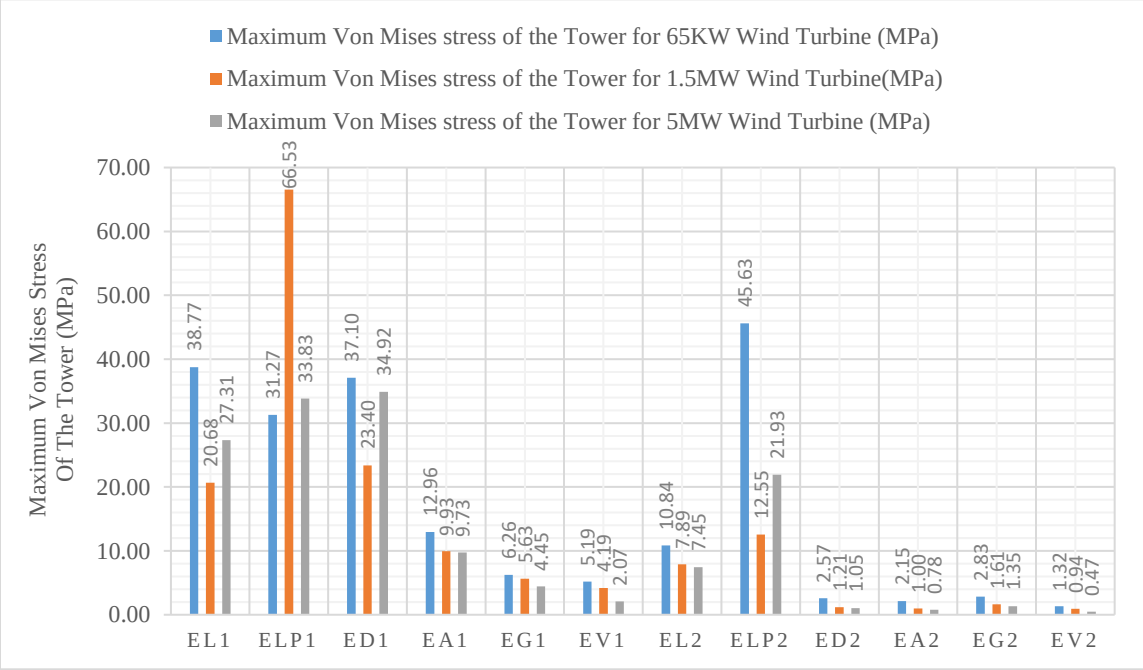

Figure 17: Maximum Von Mises stress of the tower when wind speed is 15 m/s for 65kW, 1.5MW and 5MW wind turbines under seismic excitations

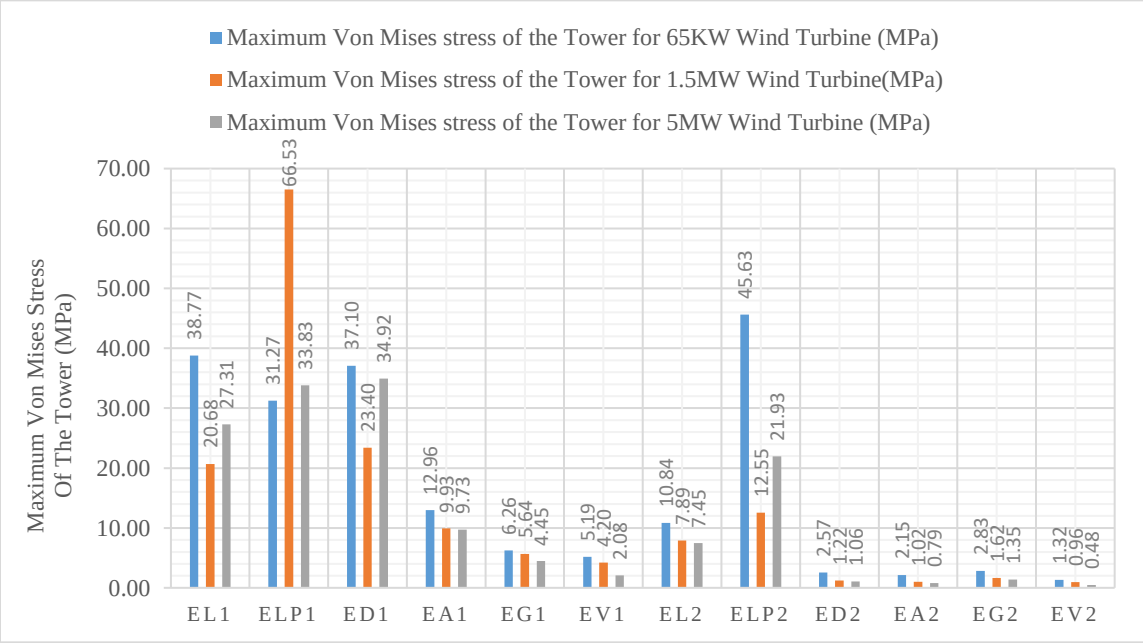

Figure 5.18: Maximum Von Mises stress of the tower when wind speed is 17 m/s for 65kW, 1.5MW and 5MW wind turbines under seismic excitations

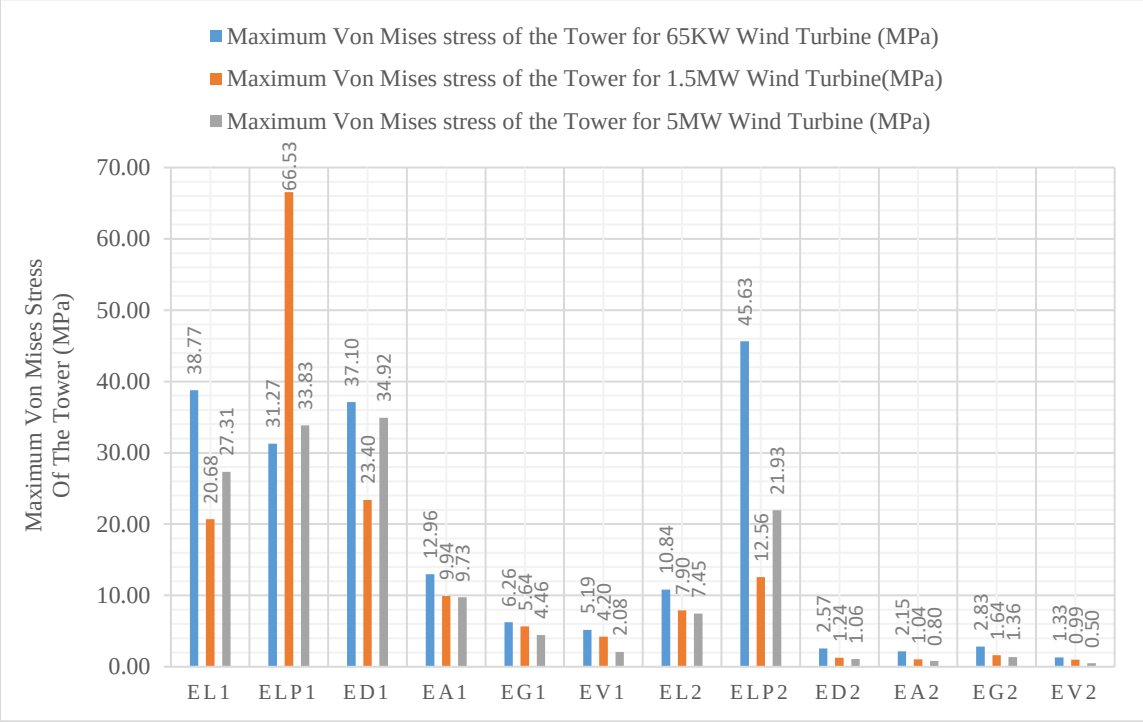

Figure 19: Maximum Von Mises stress of the tower when wind speed is 19 m/s for 65kW, 1.5MW and 5MW wind turbines under seismic excitations

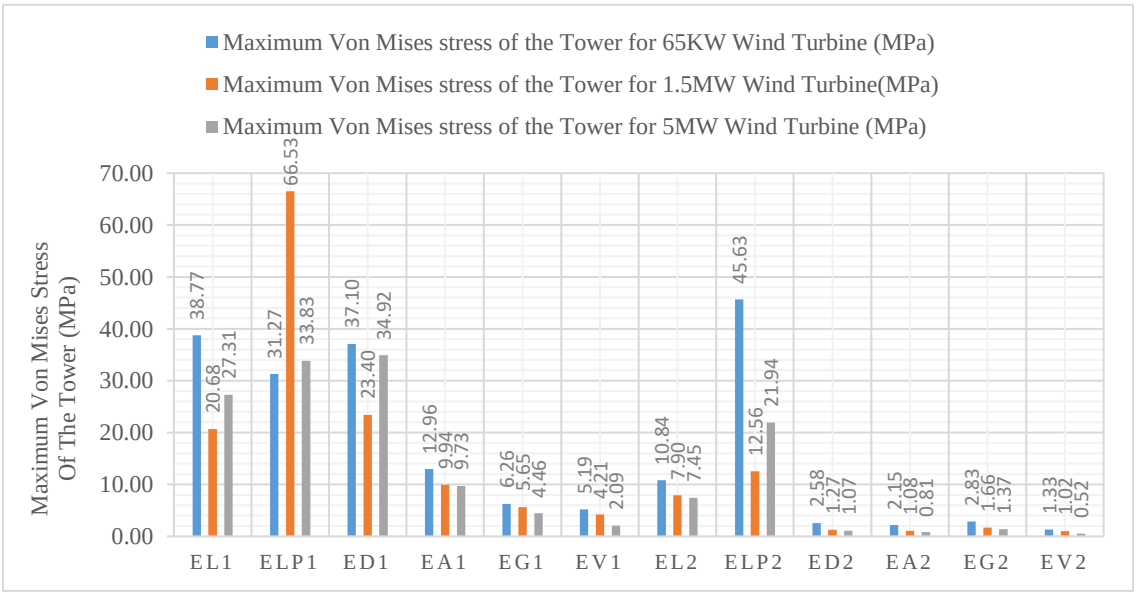

Figure 20: Maximum Von Mises stress of the tower when wind speed is 21 m/s for 65kW, 1.5MW and 5MW wind turbines under seismic excitations

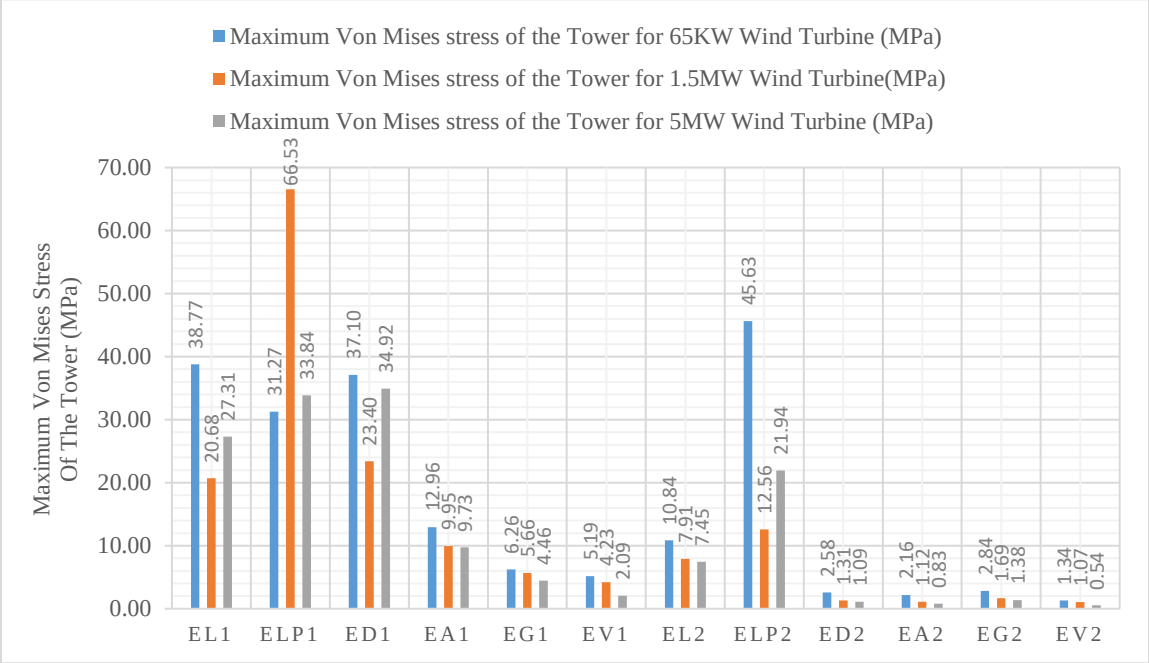

Figure 21: Maximum Von Mises stress of the tower when wind speed is 23 m/s for 65kW, 1.5MW and 5MW wind turbines under seismic excitations

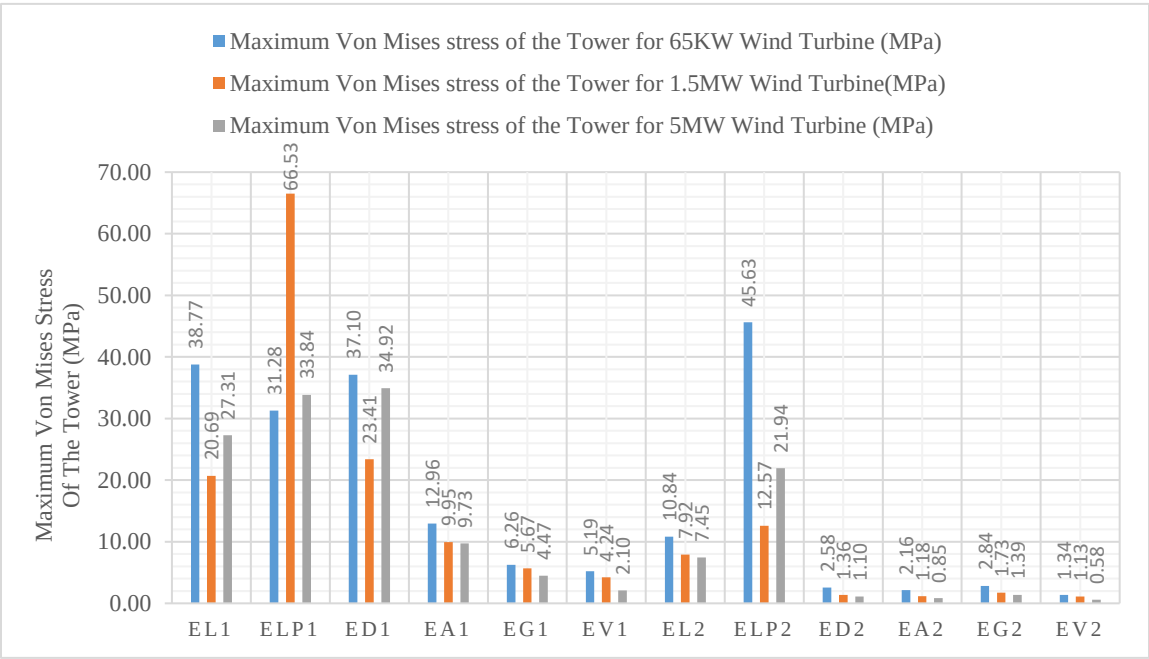

Figure 22: Maximum Von Mises stress of the tower when wind speed is 25 m/s for 65kW, 1.5MW and 5MW wind turbines under seismic excitations